PETROLOGY OF LOW-PRESSURE GRANULITES AND MIGMATITES FROM THE BAVARIAN UNIT, UPPER AUSTRIA

by

Dominik Sorger

Thesis Submitted in Partial Fulfilment

of the Requirements for the Degree of

Master of Science

in the

Institute for Earthsciences

University of Graz

Supervisor

Christoph A. Hauzenberger

Summer 2015

. . . for my parents

and my beloved Julia . . .

Acknowledgement

First of all I would like to express my gratitude to my supervisor Dr. Christoph Hauzenberger, for his guidance and advice through the process of preparing this thesis. Special thanks goes to Dr. Manfred Linner and Dr. Christoph Iglseder from the Geological Survey of Austria for their advice and support in field. I would like to thank Dr. Karl Ettinger for assistance with the electron microprobe and Mr. Jürgen Neubauer for assistance with the scanning electron microscope and furthermore, Mr. Anton Pock for support in the preparation of thinsections. Special gratitude goes to Faculty of Natural Science-University of Graz for a financial grant, which enabled detailed fieldwork and acquisition of new equipment.

I am glad to have Julia Huemer at my side, and I thank her for her love, patience and unyielding support. Last, but not least, I would like to thank my family, friends and fellow students for their support and encouragement.

Zusammenfassung

Die untersuchten niedrig-druck Granulite zählen zum österreichischen Teil des Moldanubikums, welcher durch eine spätvariszische (post 330 Ma, Gerdes et al., 2006) LP–HT Überprägung gebildet wurde. Als Ursache wird eine Delamination von Mantel-Lithosphäre und ein damit verbundener Wärmefluss angenommen (Henk et al., 2000). Die meisten Gesteine wurden dabei partiell aufgeschmolzen und bildeten Meta- und Diatexite. Kalt et al. (1999) und Tropper et al. (2006) bestimmten in früheren Arbeiten Metamorphose Bedingungen von 700–800°C und 0.4–0.5 GPa. Die Proben für diese Arbeit stammen aus dem (1) Donautal (westlich von Linz), aus der (2) Lichtenberg Zone (nördlich von Linz), der (3) Bad Leonfelden Zone (westlich der Rodl Störung) und aus dem (4) Sauwald. Die gesammelten Proben wurden Lichtmikroskopisch untersucht und mineralchemisch, sowohl mit einem Rasterelektronenmikroskop, als auch einer Elektronenstrahlmikrosonde analysiert. Gesamtgesteinsanalysen ausgewählter Proben wurden mittels Röntgenfluoreszenzanalyse (RFA) angefertigt. Durch geothermobarometrische Berechnungen, als auch Berechnung von Pseudosections wurden die Druck und Temperatur Bedingungen über das gesamte Gebiet verteilt bestimmt, sowie ein möglicher P–T Pfad rekonstruiert. Dabei wurde ein abnehmender Temperatur und Druck Gradient von 830–910°C und 0.60–0.66 GPa aus dem Donautal im Süden zu 650–700°C und 0.25–0.45 GPa in den nördlichen Bereichen um Lichtenberg und Bad Leonfelden erkannt. Große Granat Porphyroblasten in Proben aus dem Donautal zeigen eine chemische Zonierung, insbesondere in der Grossular Komponente, was die Rekonstruktion eines P–T Pfades ermöglicht. Eine HP–HT (740–825°C und 1.1–1.3 GPa) Phase wird gefolgt von einer Phase der Exhumation (580–610°C und 0.44–0.54 GPa) und von der bekannten LP–HT Phase (830–910°C und 0.60–0.66 GPa). Proben aus den nördlichen Bereichen zeigen den LP–HT Teil des Pfades bei niedrigeren Bedingungen, eine frühere hochdruck Überprägung ist möglich konnte aber nicht dokumentiert werden.

Abstract

Low pressure granulite facies rocks are commonly found in the Bohemian Massif. Investigated rocks belong to the Austrian part of the Moldanubian zone and were formed during a late Variscan (post 330 Ma, determined by Gerdes et al., 2006) LP–HT overprint due to delamination of mantle lithosphere and asthenospheric upwelling (Henk et al., 2000). Most of these rocks underwent high degrees of melting forming meta- and diatexites. Former work of Kalt et al. (1999) and Tropper et al. (2006) yielded metamorphic conditions of 700–800°C and 0.4–0.5 GPa In this study samples were taken along the (1) Danube valley (west of Linz), from the (2) Lichtenberg area (north of Linz), the (3) Bad Loenfelden area (west of the Rodl Fault) and the (4) Sauwald area (south of the river Danube). Samples were prepared for transmitting-light microscopy as well as selected samples were prepared for mineral chemical analyses with electron microprobe and scanning electron microscope. Furthermore bulk-rock composition of selected samples was analysed using X-ray fluorescence spectroscopy (XRF). Acquired data were used for geothermobarometric calculations as well for calculating pseudosections in order to constrain metamorphic conditions distributed over the investigated area and to reconstruct a possible P–T path. Conspicuous is a decreasing temperature and pressure gradient from 830–910°C and 0.60–0.66 GPa in the Danube valley in the south to 650–700°C and 0.25–0.45 GPa in the northern parts of the Lichtenberg and Bad Leonfelden area. Large garnet porphyroblasts in Danube valley samples shows a chemical zoning especially in grossular component, which allows the reconstruction of a *P–T* path. A first HP–HT stage (740–825°C and 1.1–1.3 GPa) and a subsequently exhumation stage (580–610°C and 0.44–0.54 GPa) are followed by the well-established LP–HT stage (830–910°C and 0.60–0.66 GPa). Samples from northern areas show a LP–HT path as well at lower conditions, a former high pressure overprint is possible but can not be documented.

Table of Content

1 Introduction

1.1 Geographical overview

Upper Austria is with an area of 11,982 km^2 the fourth largest federal state of Austria and with 1.4 million inhabitants the third-most populous. In the north it borders the Czech Republic, Lower Austria in the east, Salzburg and Styria in the south as well as Germany in the west. Traditional it is divided into four quarters: Muehlviertel, Innviertel, Hausruckviertel and Traunviertel besides the capital city Linz and the surrounding district Linz-Land (Figure 1) (Linner et al., 2011).

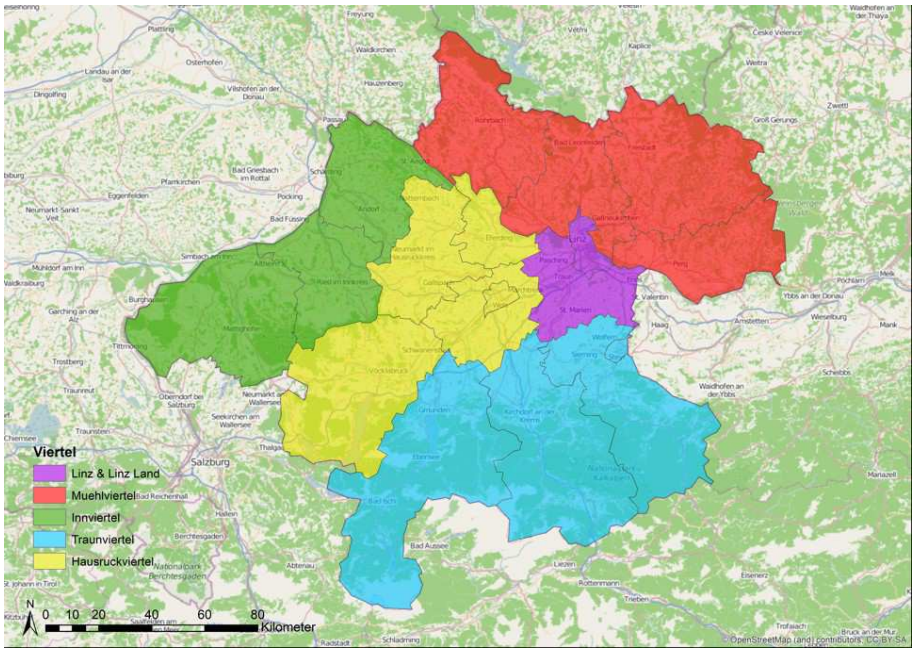

Figure 1: Map of Upper Austria divided in its four quarters modified after cartographic model 1:500000 (Geological Survey of Austria, 2013), (© OpenStreetMap contributors)

Upper Austria has portion of three major land regions: The alpine foreland with a changeover of hill country and largely flat gravel planes, the Alps, including the mountains of the flysh zone and the calcareous Prealps, as well as the rugged mountain of the calcareous Alps and the Bohemian Massif, a densely wooded highland with mountain ranges, mainly located north of the river Danube (Muehlviertel). The investigated area belongs to latter one and reaches from Linz westwards till Schärding and northwards till the border to the Czech Republic (Linner et al., 2011).

1.2 Geological background

The Carboniferous was characterized by the formation of the supercontinent Pangäa and the ultimate closing of the Rheic ocean going along with a collision of Gondwana and Laurussia and the resulting Variscan orogeny. The evolution in the Moldanubian sector of the Bohemian massif (Figure 2) can be distinguished in at least two different stages of tectonometamorphic phases: the Moravo-Moldanubian phase (345–330 Ma) and the Bavarian phase (330–315 Ma) (Finger et al., 2007). The Moravo-moldanubian phase represents the main tectonometamorphic overprint in the Moldanubian zone. It involved the overthrusting of the Moldanubian over the Moravian zone (Suess, 1926; Schulmann, 1990; Fritz and Neubauer, 1993; Schulmann et al., 1991, 2005) as well as the subduction of crustal rocks to mantle depth (Carswell, 1991; Becker and Altherr 1992; Kotková et al. 1997; O'Brien 2000; Vrána and Frýda 2003) followed by rapid exhumation to middle and upper crustal levels, which built up the Gföhl Unit. Apart from that a LP–HT metamorphism in a late stage (335 Ma) (Friedl, 1997) was recorded in large parts of the Moldanubian zone (Petrakakis, 1997; O'Brien, 2000). The LP–HT Bavarian phase represents an independent event of regional metamorphism combined with granitic plutonism. This mainly thermal overprint could be explained by delamination of mantle lithosphere and asthenospheric upwelling (Henk et al., 2000) with a resulting heat pulse which caused widespread lower crustal melting and forming of various anatexites (meta-, diatexites). This late Variscan phase affected the area south of the Pfahl Fault, in Figure 2 this area is designated as Bavarian Terrane (Fiala et al., 1995). Late Variscan monazites ages (post 330 Ma) are known from the Austrian Muehl and Sauwald Zone (Gerdes et al., 2006) as well as from several localities in the southern Bavarian Forest (Grauert et al., 1974; Propach et al., 2000; Gerdes et al., 2006). Former petrological work of samples from the Austrian Sauwald zone(Tropper et al., 2006) and the Bavarian Forest (Kalt et al., 1999) indicates low pressure granulite-facies conditions of 700–800°C and 0.4–0.5 GPa (Figure 2).

Samples of the present study (red rectangle in Figure 2) were taken along the (1) Danube valley west of Linz, from the (2) Lichtenberg area north of Linz and east of the Rodl Fault, the (3) Bad Leonfelden area west of the Rodl Fault and the Sauwald area south of the Danube Fault, near to the village of Schärding. Most of the lithologies in the investigated area are plagioclase + biotite + quartz ± K-feldspar ± cordierite bearing migmatites or anatexites. Exceptions are in southern Lichtenberg area and in the Danube valley where garnet bearing

gneisses (or migmatites) and peraluminous garnet + cordierite + sillimanite migmatites (or restites) have been observed.

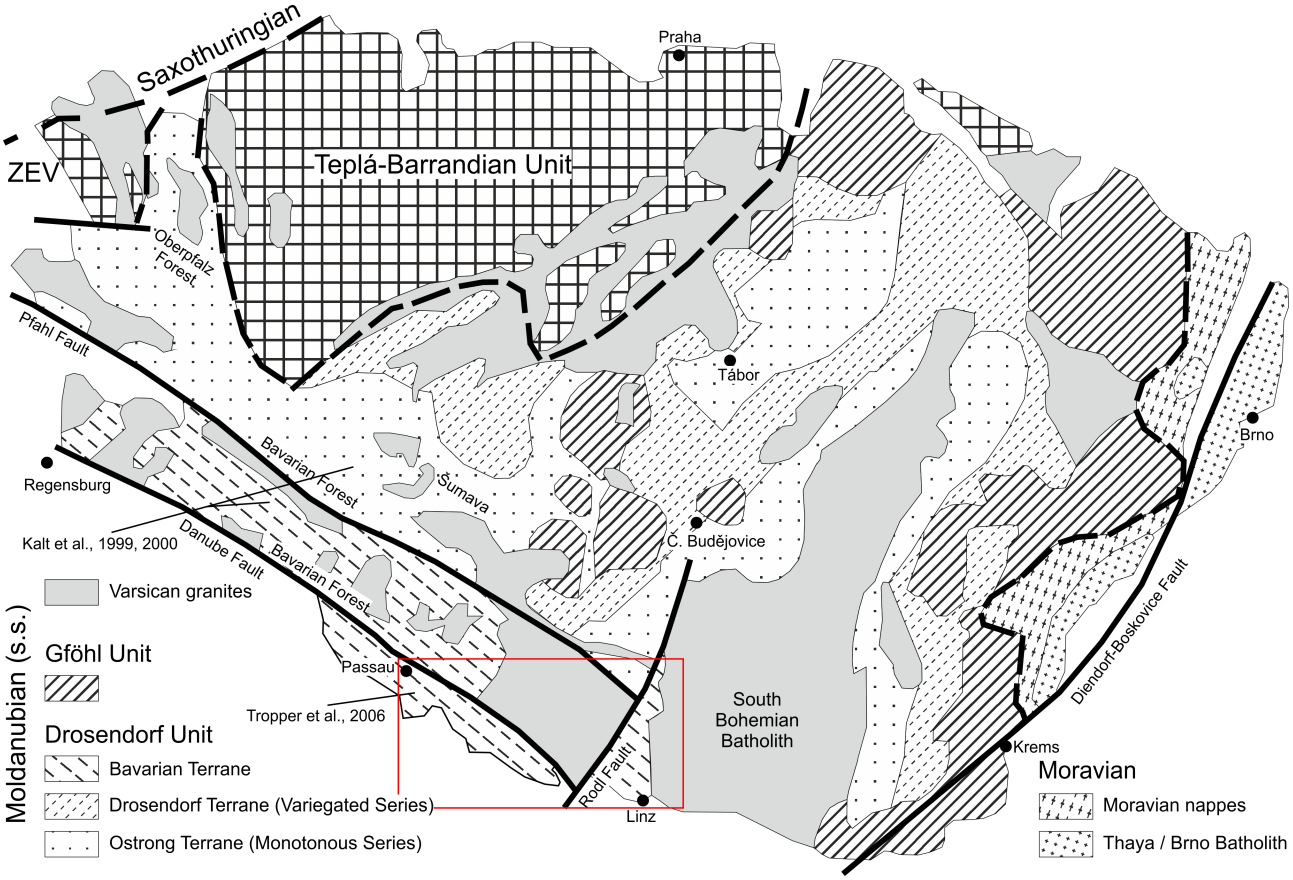

Figure 2: Simplified geological map of the Moldanubian sector of the Bohemian Massif modified after Finger et al. (2007). Variscan granites and rocks of the Gföhl and Drosendorf units distributed according to Dallmeyer et al. (1995) with slightly modifications. Drosendorf Unit is subdivided into Bavarian Terrane, Drosendorf Terrane (Variegated Series) and Ostrong Terrane (Monotonous Series) according to Fiala et al. (1995). The red rectangle marked the investigated area of this work, investigated areas of Kalt et al. (1999, 2000) and Tropper et al. (2006) are distinguished as well.

1.3 Outcrop appearance in field

In the Danube valley, along the river Danube outcrops appear common and in big scale (Figure 3). As well in the Kuernberg forest and the Hainzenbach valley outcrops can be found next to streets and smaller streams (Figure 3). At several spots in the Danube valley garnet and cordierite bearing aluminium-rich metapelites with a well developed migmatite structure can be observed (Figure 3). Temporarily mafic lenses occur within felsic migmatites, for instance the natural monument from Plesching, close to the city of Linz is a famous example (Figure 3).

Figure 3: Photos of large outcrops in the Danube valley area. ***A*** *Next to the River Danube and* ***B*** *next to the road in the Hainzenbach valley, close to the city of Linz.* ***C*** *Migmatitic garnet and cordierite bearing granulite from the Hainzenbach valley.* ***D*** *Schollenmigmatite, natural monument from Plesching. Lenses of amphibolite occur within paragneisses.*

In northern regions especially in the northern Lichtenberg and Bad Leonfelden area outcrops are scarce. Sometimes old stone quarries provide an excellent opportunity to gather samples, but in most cases only small blocks next to roads, or lying around in the forest are the only way to get useful samples Figure 4. Figure 5 shows the sampled locations over the whole investigated area, the legend is shown in Figure 6. 1 shows a list of all taken samples.

Figure 4: Photos of outcrop situation in northern Regions. ***A, B*** *The rare stone quarries are the best way to gather useful samples. In most cases you have to put up with blocks next to the road (****C****) or in forests (****D****).*

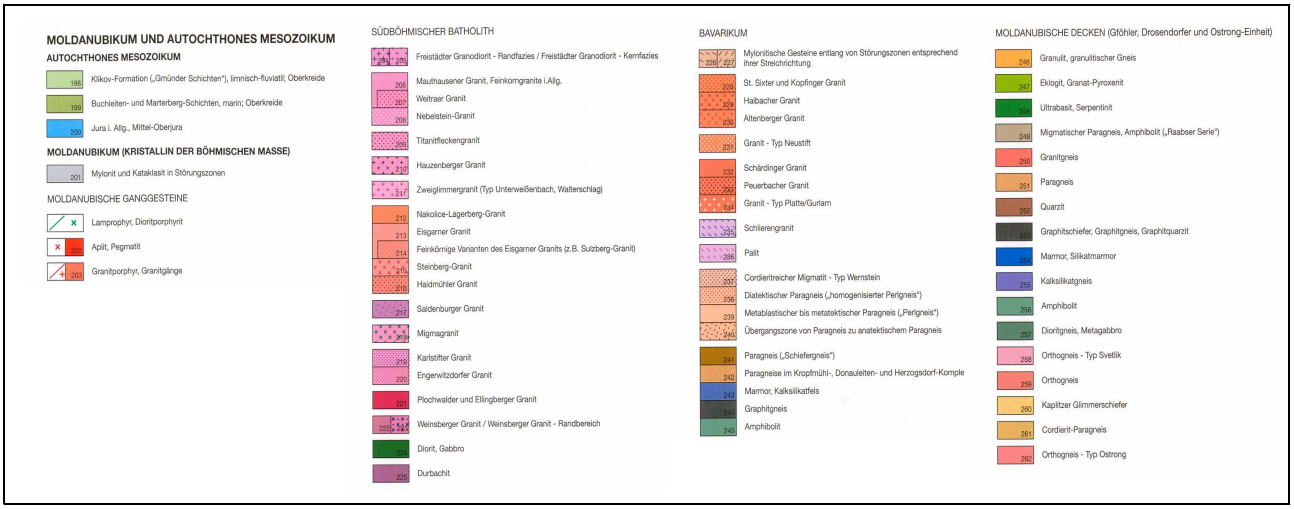

Figure 6: Legend of the Moldanubian sector of geological map of investigated area in Figure 5. Modified after Geological map of Upper Austria (Geological Survey of Austria, 2006)

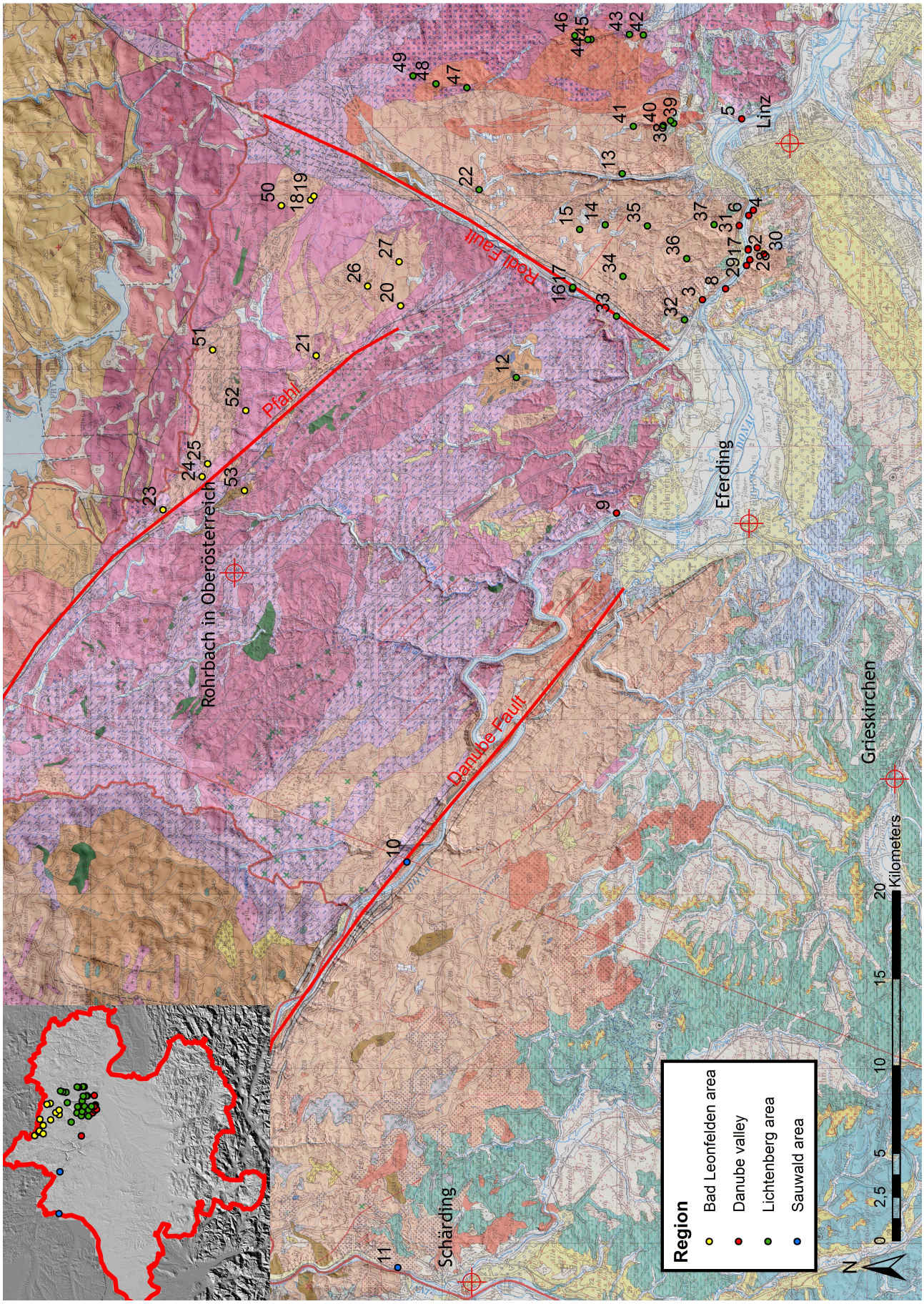

Figure 5: Geological map of investigated area. Numbers of sampled locations listed in 1. Legend is shown in Figure 5. Modified after Geological map of Upper Austria (Geological Survey of Austria, 2006)

1.4 Samples

1 shows the sampled location, the outcrop number in Figure 5, longitude and latitude and the lithology of taken samples.

Table 1: List of samples, with locations, outcrop number in Figure 6, GPS north and east and the lithology.

Sample	Location	Outcrop Nr.	GPS N	GPS E	Lithology
MA-1	Danube valley	**1**	48,3068	14,2361	Al-rich Migmatite/Restite
ML04-6B	Danube valley	**1**	48,3082	14,2663	quartzitic Paragneiss
ML04-8A	Danube valley	**1**	48,3150	14,2667	Migmatite, coarse grained
ML04-11	Danube valley	**1**	48,3058	14,2640	metablastc Grt-Bt-Paragneiss
ML04-14B	Danube valley	**1**	48,3062	14,2618	Crd-Migmatite
ML04-17	Danube valley	**1**	48,3350	14,1901	homogeneous Migmatite
ML04-58	Danube valley	**1**	48,3067	14,2580	Crd-Migmatite
ML04-68	Danube valley	**1**	48,3076	14,2442	Grt-Bt-Paragneiss
ML04-78	Danube valley	**1**	48,3323	14,1913	Grt-Bt-Paragneis, mylonitic
ML04-79B	Danube valley	**1**	48,3718	14,2958	Calcsilicate
ML05-13	Danube valley	**1**	48,3065	14,2350	Grt-Bt-Paragneiss
ML05-15	Danube valley	**1**	48,3066	14,2355	Calcsilicate
ML05-16	Danube valley	**1**	48,3067	14,2361	Al-rich Migmatite/Restite
ML05-17A	Danube valley	**1**	48,3068	14,2362	Al-rich Migmatite/Restite
ML05-17A1/1	Danube valley	**1**	48,3068	14,2362	Al-rich Migmatite/Restite
ML05-17A1/2	Danube valley	**1**	48,3068	14,2363	Al-rich Migmatite/Restite
ML05-17B/1	Danube valley	**1**	48,3068	14,2362	Al-rich Migmatite/Restite
ML05-17B/2	Danube valley	**1**	48,3068	14,2362	Al-rich Migmatite/Restite
ML05-19B	Danube valley	**2**	48,3022	14,2369	Crd-Migmatite
ML07-1A	Danube valley	**3**	48,3307	14,1972	Grt-Crd-Migmatite
ML07-1B	Danube valley	**3**	48,3307	14,1972	Grt-Crd-Migmatite
ML09-16	Danube valley	**4**	48,3040	14,2659	Amphibolite
BA1	Plesching,Gruber Stein	**5**	48,3094	14,3364	Migmatitic Bt-Paragneiss
BA2	Plesching,Gruber Stein	**5**	48,3094	14,3364	Paragneiss
BA3	Plesching,Gruber Stein	**5**	48,3094	14,3364	Paragneiss
BA4	Stone quarry Margarethen	**6**	48,3064	14,2619	Crd-Migmatite
BA5	Stone quarry Margarethen	**6**	48,3064	14,2619	Gneiss
BA6	Stone quarry Margarethen	**6**	48,3064	14,2619	Gneiss, fine grained
BA7	Danube valley/Hainzenbach valley	**7**	48,3069	14,2353	Opx-Grt-Bt-Gneiss
BA8	Danube valley/Hainzenbach valley	**7**	48,3069	14,2353	Grt-Crd-Migmatite
BA9	Danube valley/Hainzenbach valley	**7**	48,3069	14,2353	Grt-Crd-Migmatite
BA10	Danube valley/Hainzenbach valley	**7**	48,3069	14,2353	Grt-Crd-Migmatite
BA11	Danube valley/Hainzenbach valley	**7**	48,3069	14,2353	Grt-Crd-Migmatite
BA12	Danube valley/Hainzenbach valley	**7**	48,3069	14,2353	Grt-Granite/Gneiss

Sample	Location	Outcrop Nr.	GPS N	GPS E	Lithology
BA13	Wilhering	**8**	48.3209	14.3209	Grt-Crd-Gneiss
BA14	Wilhering	**8**	48.3209	14.3209	Crd-Gneiss, fine grained
BA15	Wilhering	**8**	48.3187	14.2055	Bt-Gneiss
BA16	Wilhering	**8**	48.3187	14.2055	Bt-Crd-Gneiss
BA17	Oberlandshaag	**9**	48.3759	14.0330	Granodiorite
BA18	Oberlandshaag	**9**	48.3778	14.0323	Granite
BA19	former stone quarry Rannariedl	**10**	48.4850	14.7643	Paragneiss, mylonitic
BA20	former stone quarry Rannariedl	**10**	48.4850	14.7643	Paragneiss, mylonitic
BA21	former stone quarry Rannariedl	**10**	48.4850	14.7643	Paragneiss/Calcsilicate, mylonitic
BA22	former stone quarry Rannariedl	**10**	48.4850	14.7643	Calcsilicate, mylonitic
BA23	former stone quarry Rannariedl	**10**	48.4850	14.7643	Calcsilicate
BA24	former stone quarry Rannariedl	**10**	48.4850	14.7643	Calcsilicate
BA25	former stone quarry Rannariedl	**10**	48.4850	14.7643	Calcsilicatemarble, coarse grained
BA26	former stone quarry Rannariedl	**10**	48.4850	14.7643	Calcsilicateschist
BA27	former stone quarry Rannariedl	**10**	48.4850	14.7643	Calcsilicate
BA28	former stone quarry Rannariedl	**10**	48.4850	14.7643	Bt-Gneiss, fine grained
BA29	Wernstein	**11**	48.4850	14.7643	Bt-Crd-Migmatite
BA30	Wernstein	**11**	48.4850	14.7643	Migmatite
BA31	Wernstein	**11**	48.4851	14.7643	Migmatite
BA32	Wernstein	**11**	48.4851	14.7643	Migmatite
BA33	Wernstein	**11**	48.4904	36.1170	Migmatite
BA34	Ledermühle	**12**	48.4267	14.1387	migmatitic Bt-Gneiss
BA35	Ledermühle	**12**	48.4267	14.1387	migmatitic Bt-Gneiss
BA36	Ledermühle	**12**	48.4267	14.1387	leucrocratic (granitic) Layer
BA37	Ledermühle	**12**	48.4267	14.1387	migmatitic Bt-Gneiss
BA38	Ledermühle	**12**	48.4267	14.1387	migmatitic Bt-Gneiss
BA39	Ledermühle	**12**	48.4267	14.1387	Bt-Gneiss
BA40	Ledermühle	**12**	48.4267	14.1387	migmatitic Bt-Gneiss
BA41	Ledermühle	**12**	48.4267	14.1387	migmatitic Bt-Gneiss
BA42	Ledermühle	**12**	48.4267	14.1387	migmatitic Bt-Gneiss
BA43	Ledermühle	**12**	48.4267	14.1387	migmatitic Hbl-Gneiss
BA44	Ledermühle	**12**	48.4262	14.1375	Bt-Gneiss
BA45	Ledermühle	**12**	48.4275	14.1385	Granite
BA46	Haselgraben, east side	**13**	48.3711	14.2954	migmatitic Bt-Gneiss
BA47	Haselgraben, east side	**13**	48.3711	14.2954	migmatitic Bt-Gneiss
BA48	Haselgraben, east side	**13**	48.3711	14.2954	Bt-Gneiss
BA49	Haselgraben, east side	**13**	48.3711	14.2954	Bt-Gneiss
BA50	Haselgraben, east side	**13**	48.3711	14.2954	Bt-Gneiss
BA51	Haselgraben, east side	**13**	48.3711	14.2954	migmatitic Bt-Gneiss
BA52	Haselgraben, east side	**13**	48.3711	14.2954	Granite
BA53	Haselgraben, east side	**13**	48.3711	14.2954	Quartzic Calcsilicate
BA54	Giselawarte, parking place	**14**	48.3802	14.2559	Crd-Bt-Migmatite
BA55	Giselawarte, parking place	**14**	48.3802	14.2559	Crd-Bt-Migmatite
BA56	Giselawarte, parking place	**14**	48.3802	14.2559	Crd-Bt-Migmatite
BA57	Giselawarte, parking place	**14**	48.3802	14.2559	Crd-Bt-Migmatite
BA58	Giselawarte, parking place	**14**	48.3802	14.2559	Crd-Grt-Bt-Gneis
BA59	Giselawarte, parking place	**14**	48.3802	14.2559	Gneiss
BA60	Giselawarte, parking place	**14**	48.3802	14.2559	migmatitic Gneiss
BA61	Giselawarte, parking place	**14**	48.3802	14.2559	Grt-And-Dike

Sample	Location	Outcrop Nr.	GPS N	GPS E	Lithology
BA62	Rotes Kreuz (next to the road)	**15**	48,3933	14,2526	Bt-Crd-Migmatite
BA63	Rotes Kreuz (next to the road)	**15**	48,3933	14,2526	Bt-Gneiss
BA64	Rotes Kreuz (next to the road)	**15**	48,3933	14,2526	Bt-Crd-Migmatite
BA65	Rotes Kreuz (next to the road)	**15**	48,3933	14,2526	Bt-Gneiss
BA66	Rotes Kreuz (next to the road)	**15**	48,3933	14,2526	migmatitic Gneiss
BA67	Zimmermeisterbach	**16**	48,3974	14,2067	Grt-Bt-Ms-Phyllonite
BA68	Zimmermeisterbach	**16**	48,3974	14,2067	Qartz-rich Layer
BA69	Zimmermeisterbach	**16**	48,3974	14,2067	Grt-bearing Aplite
BA70	Zimmermeisterbach eastward	**17**	48,3972	14,2079	Gneiss
BA71	Zimmermeisterbach eastward	**17**	48,3972	14,2079	Bt-Fsp-Qz-Gneiss
BA72	Zimmermeisterbach eastward	**17**	48,3975	14,2091	Bt-Gneiss
BA73	Bad Leonfelden	**18**	48,5314	14,2779	migmatitic Gneiss
BA74	Bad Leonfelden	**18**	48,5314	14,2779	Calcsilicate
BA75	Bad Leonfelden	**18**	48,5314	14,2779	Bt-Sil-Gneiss
BA76	Bad Leonfelden	**18**	48,5314	14,2779	Bt-Sil-Gneiss
BA77	Bad Leonfelden	**18**	48,5314	14,2779	Bt-Sil-Gneiss
BA78	Bad Leonfelden	**19**	48,5296	14,2809	Crd-Bt-Gneiss
BA79	Bad Leonfelden	**19**	48,5296	14,2809	Crd-Bt-Gneiss
DS1	Waxenberg – Traberg	**20**	48.48585	14.19521	Granite/Gneiss
DS2	Waxenberg – Traberg	**20**	48.48585	14.19521	Granite/Gneiss
DS3	Road to Burg Piberstein, Ahorn	**21**	48.52943	14.15728	Granite/Gneiss
DS4	Road to Burg Piberstein, Ahorn	**21**	48.52943	14.15728	foliated Bt-Gneiss
DS5	Zwettl an der Rodl, Glasau	**22**	48.44474	14.28436	Bt-Gneiss
DS6	Stone quarry Unterurasch	**23**	48.60890	14.03899	Crd-Bt-Migmatites/Anatexites
DS7	Stone quarry Unterurasch	**23**	48.60890	14.03899	Crd-Bt-Migmatites/Anatexites
DS8	Stone quarry Unterurasch	**23**	48.60890	14.03899	Crd-Bt-Migmatites/Anatexites
DS9	Hörleinsödt, Leitenmühle	**24**	48.58874	14.06434	Bt-Gneiss
DS10	Hörleinsödt, Leitenmühle	**24**	48.58874	14.06434	Bt-Gneiss
DS11	Güterweg Leitenmühle	**25**	48.58589	14.07422	Bt-Gneiss
DS12	Kleintraberg	**26**	48.50261	14.21062	Bt-Gneiss
DS13	Kleintraberg	**26**	48.50261	14.21062	Bt-Gneiss
DS14	Güterweg Waldschlag, Ameschlag	**27**	48.48632	14.22939	Bt-Gneiss
DS15	Kürnberg Forest, Römerturm	**28**	48,3061	14,2276	Crd-Bt-Gneiss
DS16	Kürnberg Forest, Römerturm	**28**	48,3061	14,2276	Crd-Bt-Gneiss
DS17	Kürnberg Forest, Prinzenstieg	**29**	48,3078	14,2233	Crd-Bt-Gneiss
DS18	Kürnberg Forest, Prinzenstieg	**29**	48,3078	14,2233	Crd-Bt-Gneiss
DS19	Kürnberg Forest, West	**30**	48,2987	14,2319	mafic Lens
DS20	Rohrbacher Bundesstraße	**31**	48,3113	14,2542	Bt-Crd-Gneiss
DS21	Rohrbacher Bundesstraße	**31**	48,3113	14,2542	Bt-Crd-Gneiss
DS22	Rohrbacher Bundesstraße	**31**	48,3113	14,2542	Bt-Crd-Gneiss
DS23	Niederottensheim	**32**	48,3400	14,1819	Bt-Crd-Gneiss
DS24	Niederottensheim	**32**	48,3400	14,1819	Bt-Crd-Gneiss
DS25	Lichtenhag	**33**	48,3749	14,1852	Mylonite
DS26	Lichtenhag	**33**	48,3749	14,1852	Mylonite
DS27	Lichtenhag	**33**	48,3749	14,1852	Mylonite
DS28	Türkstetten	**34**	48,3713	14,2160	Bt-Gneiss
DS29	Schmiedgraben	**35**	48,3585	14,2547	Bt-Gneiss
DS30	Schmiedgraben	**35**	48,3585	14,2547	Bt-Gneiss
DS31	Schmiedgraben	**35**	48,3585	14,2547	Bt-Gneiss

Sample	Location	Outcrop Nr.	GPS N	GPS E	Lithology
DS32	Großamberg	**36**	48,3385	14,2291	Granite/Gneiss
DS33	Großamberg	**36**	48,3385	14,2291	Bt-Gneiss
DS34	Pöstlingberg	**37**	48,3242	14,2551	Bt-Gneiss
DS35	Pöstlingberg	**37**	48,3242	14,2551	Grt-Bt-Gneiss
DS36	Pöstlingberg	**37**	48,3242	14,2551	felsic Granite/Gneiss
DS37	Elmbergwerg	**38**	48,3443	14,3337	Crd-Bt-Migmatites/Anatexites
DS38	Elmbergwerg	**38**	48,3443	14,3337	Crd-Bt-Migmatites/Anatexites
DS39	Former stone quarry, Am Elmberg	**39**	48,3459	14,3358	Crd-Bt-Migmatites/Anatexites
DS40	Former stone quarry, Am Elmberg	**39**	48,3459	14,3358	Crd-Bt-Migmatites/Anatexites
DS41	Former stone quarry, Am Elmberg	**39**	48,3459	14,3358	Crd-Bt-Migmatites/Anatexites
DS42	Katzbachgraben, Road	**40**	48,3497	14,3322	Crd-Bt-Migmatites/Anatexites
DS43	Katzbachgraben, Road	**40**	48,3497	14,3322	Crd-Bt-Migmatites/Anatexites
DS44	Katzbachgraben, Road	**40**	48,3497	14,3322	Crd-Bt-Migmatites/Anatexites
DS45	Katzbachgraben, Haslach	**41**	48,3651	14,3318	Bt-Gneiss
DS46	Katzbachgraben, Haslach	**41**	48,3651	14,3318	Bt-Gneiss
DS47	Veitsdorf	**42**	48,3593	14,4022	Granite/Gneiss
DS48	Veitsdorf	**42**	48,3593	14,4022	Granite/Gneiss
DS49	Riedegg Castle	**43**	48,3664	14,4028	Granite/Gneiss, fine grained
DS50	Riedegg Castle	**43**	48,3664	14,4028	Granite/Gneiss, coarse grained
DS51	Former stone quarry, Gusental	**44**	48,3862	14,3994	Granite/Gneiss, Anatexite
DS52	Former stone quarry, Gusental	**45**	48,3879	14,3992	felsic Gneiss
DS53	Former stone quarry, Gusental	**45**	48,3879	14,3992	mafic Gneiss
DS54	Quarry behind a house, Gusental	**46**	48,3945	14,4025	Ms-Bt-Granite
DS55	Affenberg	**47**	48,4503	14,3633	foliated Bt-Gneiss
DS56	Affenberg	**47**	48,4503	14,3633	felsic Granite/Gneiss
DS57	Affenberg	**47**	48,4503	14,3633	mafic Gneiss-Boudin
DS58	Affenberg	**47**	48,4503	14,3633	mafic Gneiss
DS59	Affenberg	**47**	48,4503	14,3633	Bt-Gneiss
DS60	Blocks next to the road, Lichtenstei	**48**	48,4662	14,3667	Bt-Gneiss
DS61	Blocks next to the road, Lichtenstei	**48**	48,4662	14,3667	Bt-Gneiss
DS62	Blocks next to the road, Lichtenstei	**48**	48,4662	14,3667	Crd-Gneiss
DS63	Blocks next to the road, Lichtenstei	**49**	48,4779	14,3731	Bt-Gneiss
DS64	Sternstein, next to Waldschenke	**50**	48,5464	14,2739	Crd-Bt-Gneiss
DS65	Sternstein, next to Waldschenke	**50**	48,5464	14,2739	Bt-Gneiss
DS66	Next to Guglwald	**51**	48,5826	14,1625	Bt-Gneiss
DS67	St. Stefan am Walde, Herrnschlag	**52**	48,5659	14,1152	Bt-Crd-Gneiss
DS68	St. Stefan am Walde, Herrnschlag	**52**	48,5659	14,1152	Bt-Crd-Gneiss
DS69	St. Stefan am Walde, Herrnschlag	**52**	48,5670	14,0532	Bt-Crd-Gneiss
DS70	Haslacher Bezirkstraße	**53**	48,5670	14,0532	Bt-Crd-Gneiss

1.5 Data acquisition

Mineral chemical analyses were performed with a scanning electron microscope JEOL JSM 6310 at the Institute of Earth Sciences, Mineralogy and Petrology, at the University of Graz. Data were obtained with a LINK-ISIS energy dispersive system (EDS) as well as a MICROSPEC wavelength dispersive system (WDS) for Na and F. Chemical mappings as well as selected analyses have been performed using a JEOL JXA 8200 electron microprobe at the Institute of Earth Sciences at the Montanuniversity, Leoben. Measurement conditions were 15 kV acceleration voltage, 5 nA beam current and a beam diameter of ca. 1µm. Systems was calibrated with a range of natural and synthetic mineral standards. Calculation of mineral formula was performed with petrological elementary tools for Mathematica (PET 7) by Dachs (1998). Mineral chemical plots were prepared with GeoChemical Data toolkit (GCDkit) by Janoušek et al. (2006).

Bulk-rock compositions were determined using X-ray fluorescence spectroscopy (XRF) on a Bruker Pioneer S4. Mineral abbreviations after Whitney and Evans (2010) were used and additional “Fe-Crd” for the cordierite iron endmember.

2 Petrography and Mineral Chemistry

2.1 Al-rich Migmatite/Restite type 1

Al-rich migmatite/restite is found mainly along the Danube valley west of Linz (Figure 5). The investigated samples contain the mineral assemblage, garnet + cordierite + olive green or brown spinel + sillimanite + quartz + perthitic K-feldspar + graphite + ilmenite ± plagioclase ± biotite. Large garnet porphyroblasts (up to 1cm in size) display a distinct chemical zoning as well as different mineral inclusions in their cores and rims. In garnet cores the minerals biotite + plagioclase + green spinel + quartz + ilmenite ± rutile ± staurolite ± corundum ± sillimanite are found. Both, in garnet cores and in garnet rims zircon + monazite + apatite + pyrite ± chalcopyrite occur as accessory minerals. The chemical zoning pattern in garnet porphyroblasts and the different mineral assemblages associated with core and rim compositions indicate a poly-phase metamorphic history. The common formation of leucosomes (K-feldspar, plagioclase, quartz) and melanosomes (garnet, cordierite, sillimanite, spinel, ilmenite) indicates high temperature metamorphism related partial melting (Figure 7). Three samples of this type were investigated in detail, ML05-17A1, ML05-17A and MA1.

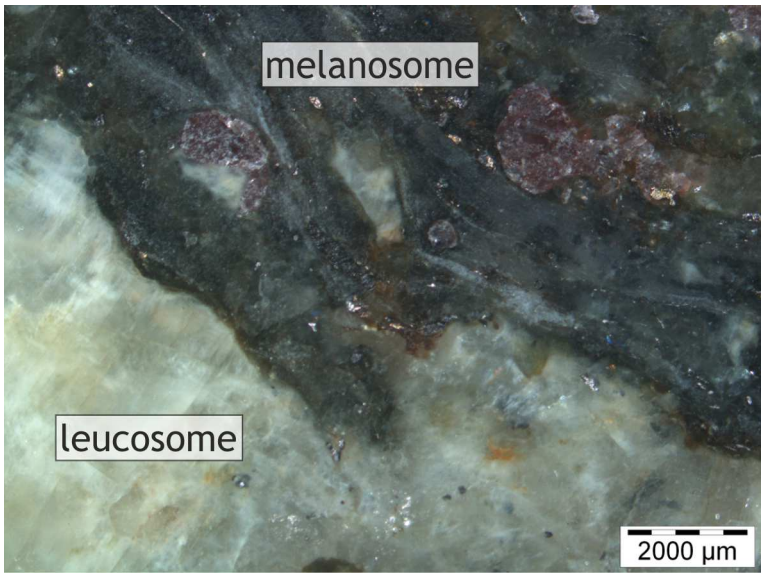

Figure 7: Stereomicroscope Image of Sample ML05-17A1 showing the boundary between the cordierite and garnet-rich melanosome and the quartz and feldspar-rich leucosome

The leucosome is built up by large perthitic K-feldspar grains and smaller plagioclase and quartz grains (up to 1mm). Quartz also occurs as an inclusion in most of the mineral phases, as well as in the melanosome. K-feldspars range in size from 0.5mm up to 2mm, show sometimes a typically microcline grid and clear exsolution lamellae (Figure 8). Two types of exolution lamellae can be recognised, where the finer ones are pure albite and the coarser ones have a small amount of anorthite (up to 4 wt% CaO). Plagioclase is smaller in size (up to 0.5mm) displays polysynthetic twins under crossed nicols but does not show any exsolutions. In sample ML05-17A no plagioclase is found in the leucosome. Cracks and grain boundaries of plagioclase and K-feldspar are affected by sericitization. Sometimes garnet appears in leucosomes (Figure 8), but are smaller in size (1–2mm) compared to garnets from melanosomes (up to 12mm) and show a homogeneous iron-rich chemical composition.

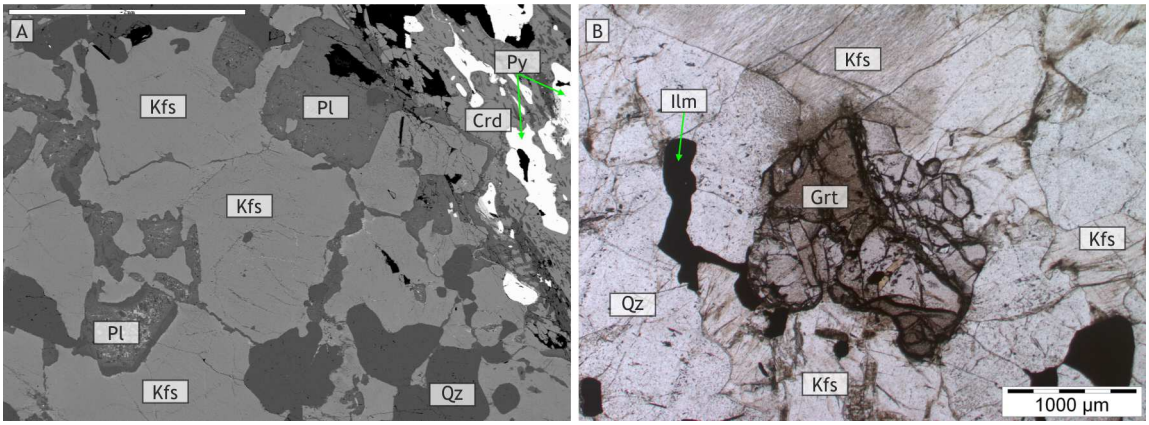

Figure 8: ***A*** *Backscatter electron (BSE) image of the leucosome showing large K-feldspars and smaller plagioclase and quartz grains (the scale bar represents 2mm).* ***B*** *Photomicrograph of leucosome garnet surrounded by K-feldspar and quartz. K-feldspar in both images show clear exsolution lamellae.*

Large garnet porphyroblasts and cordierite are the main components in the melanosomes. Codierite includes large amounts of sillimanite needles (Figure 9), which is common also as inclusions in garnet rims, ilmenite and biotite. Furthermore brown spinel, biotite, ilmenite and small garnet occur as inclusions in large cordierite grains. Spinel is hercynitic in composition with some amounts of ZnO and Cr_2O_3. Depending on the Cr_2O_3 content the colour ranges from green (low Cr_2O_3) to brown (higher Cr_2O_3). Biotites occur as single flakes which are commonly associated with ilmenite (Figure 9). Ilmenite itself is pure $FeTiO_3$, shows sometimes rutile intergrowth (Figure 9) and occurs in variable sizes from µm as garnet inclusions up to 1mm with inclusions of brown spinel and sillimanite. Small garnet has a homogenous almandine-rich chemistry and contains only few inclusions. Based on textural evidence, small garnet

grains as well as sillimanite and quartz enclosed in cordierite is indicative for the following reaction (Figure 9):

$$Grt + Sil + Qz = Crd \qquad (1)$$

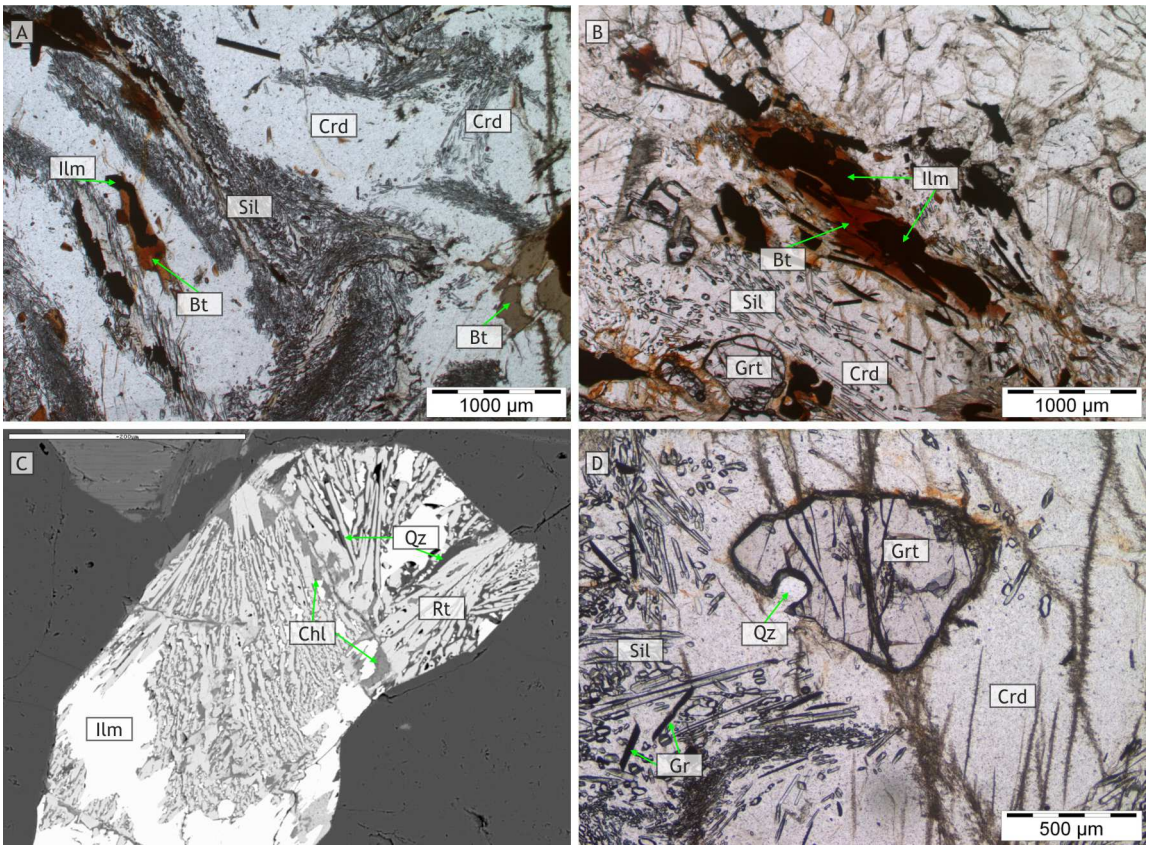

*Figure 9: Photomicrographs and BSE images. **A** Sillimanite is common in all samples and pervade especially the large cordierite grains. **B** Biotite flakes in association with ilmenite. **C** Matrix ilmenite showing intergrowth with rutile. **D** Garnet inclusion in cordierite next to sillimanite and quartz. Sillimanite forms larger needles as well as smaller grains. Next to sillimanite often occur graphite needles.*

Of special interest are the very large (up to 12mm) poly-phase garnet porphyroblasts and their numerous inclusions (Figure 10). Inclusions of biotite and plagioclase differ from their chemical composition of matrix equivalents. Staurolite (100µm) and corundum (20–25µm) occur only as small inclusions in garnet. Conspicuous is the different colour and chemical composition of green spinel inclusion and olive green/brown matrix spinel (Figure 10).

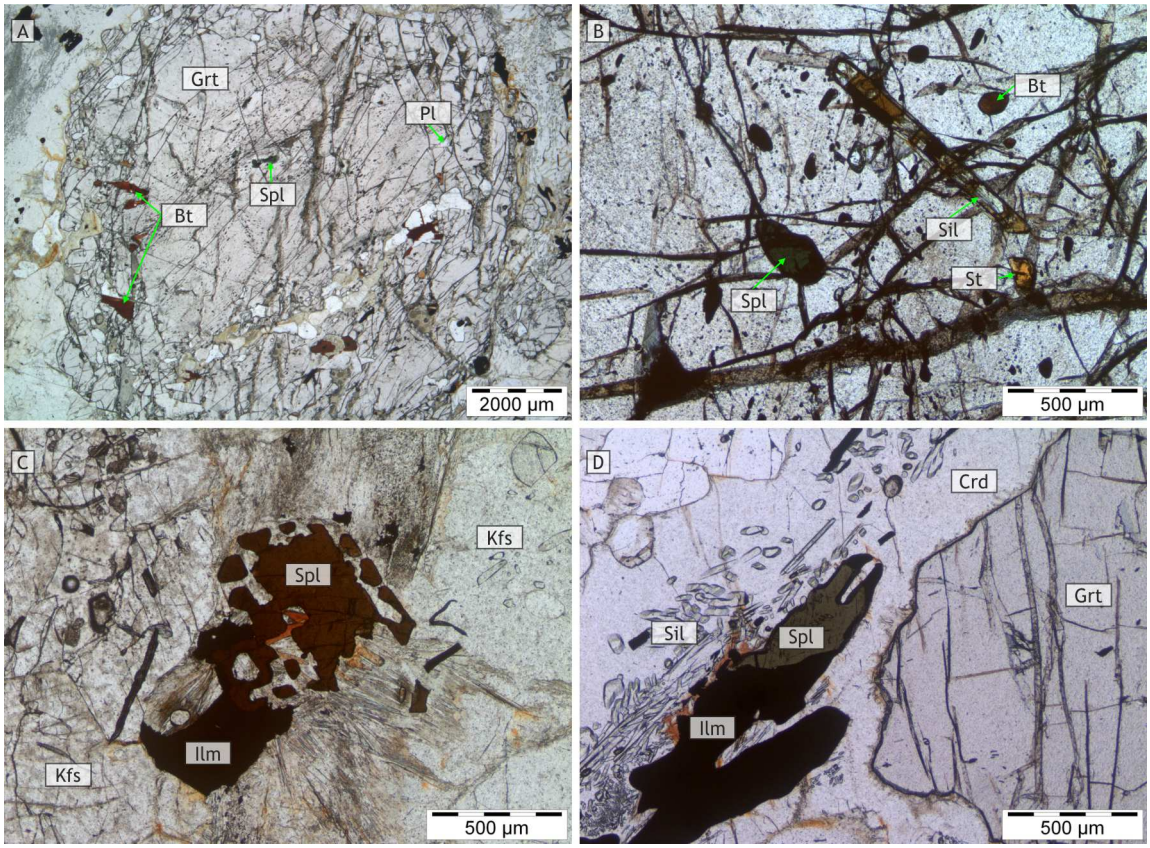

*Figure 10: Photomicrographs of garnet inclusions and different types of spinel **A** a large garnet porphyroblast (12mm) with multiple inclusions such as biotite, plagioclase, spinel, ilmenite and rutile. **B** Inclusions in another large garnet showing a dark green spinel inclusion, furthermore biotite, staurolite and sillimanite. **C, D** The spinels in the matrix have an olive green to brown colour depending on their chromium content. Dark brown spinels contain the highest chromium percentage.*

Most of the garnets show a homogenous iron-rich composition and form generally an almandine-pyrope (X_{alm}=0.78–0.80, X_{prp}=0.16–0.18) solid solution with minor contents of grossular and spessartine (X_{grs}=0.028–0.032, X_{sps}=0.020–0.024) (2). The outermost rims are characterized by a slight increase in almandine and decrease in pyrope component due to retrograde diffusional zoning if in contact with biotite or cordierite. Large poly-phase garnets show an elevated Ca-plateau in the cores (X_{grs}=0.053–0.055) and a slightly increased spessartine component (X_{sps}=0.030–0.035), almandine and pyrope increase continuously from core to rim (X_{alm}=0.75–0.76, X_{prp}=0.14–0.16)(2). A ternary plot (Figure 11) of garnet endmembers shows a clear difference between core and rim but basically no difference between samples.

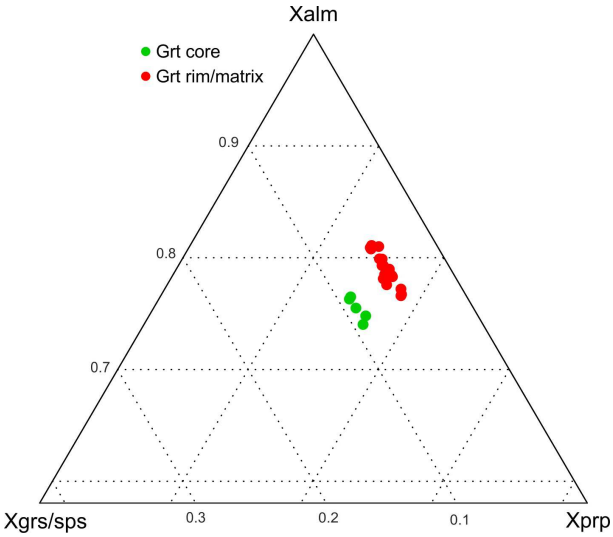

Figure 11: Ternary plot of garnet core (green dots) and rim as well as unzoned matrix garnet (red dots) compositions showing grossular and spessartine-richer cores and almandine and pyrop-richer rims.

Table 2: Representative analyses of garnet. ***A-gt53*** *garnet core (ML05-17A),* ***A-gt54*** *garnet rim (ML05-17A),* ***A1-gt39*** *garnet core (ML05-17A1),* ***A1-gt40*** *garnet rim (ML05-17A1)*

Analysis	**A-gt53**	**A-gt54**	**A1-gt39**	**A1-gt40**
Mineral	grt	grt	grt	grt
SiO2	37.03	37.22	37.68	37.51
Al2O3	20.47	20.72	20.89	20.90
FeO	34.72	35.77	34.10	36.18
MnO	1.44	1.00	1.71	0.97
MgO	3.85	4.06	4.23	4.07
CaO	1.98	1.14	1.88	1.09
Total	**99.49**	**99.91**	**100.49**	**100.72**
Si	2.984	2.987	2.997	2.987
Al	1.944	1.960	1.958	1.962
Fe3	0.088	0.065	0.048	0.064
Fe2	2.252	2.335	2.220	2.346
Mn	0.098	0.068	0.115	0.065
Mg	0.463	0.486	0.502	0.483
Ca	0.171	0.098	0.160	0.093
Sum	**8.000**	**7.999**	**8.000**	**8.000**
Xalm	0.755	0.782	0.741	0.785
Xprp	0.155	0.163	0.168	0.162
Xgrs	0.057	0.033	0.053	0.031
Xsps	0.033	0.023	0.038	0.022

Cordierite has a homogenous chemical composition with approximately same amounts of Fe- and Mg-cordierite (X_{Mg} =0.48–0.52) (4). Only cordierite in sample MA1 shows slightly higher amounts of magnesium (X_{Mg}=0.56–0.58). Cordierite grains typically do not display chemical zoning between core and rim. In some cases a slight increase in magnesium at the rim is seen. The Na content ranges between 0.1 and 0.24 wt%. Cordierite usually contains some H_2O or CO_2 in their crystal structure seen in analytical totals of 97–98 wt% (4).

Table 3: Representative analyses of cordierite. ***A-cd14*** *cordierite core (ML05-17A),* ***A-cd15*** *cordierite rim (ML05-17A),* ***A1-cd23*** *cordierite core (ML05-17A1),* ***A1-cd24*** *cordierite rim (ML05-17A1),* ***ma1cd47*** *cordierite rim (MA1),* ***ma1cd48*** *cordierite core (MA1)*

Analysis	**A-cd14**	**A-cd15**	**A1-cd23**	**A1-cd24**	**ma1cd47**	**ma1cd48**
Mineral	crd	crd	crd	crd	crd	crd
SiO2	47.24	46.86	47.75	47.01	47.97	47.94
Al2O3	32.55	32.46	32.51	33.03	32.27	31.86
FeO	11.22	11.08	11.19	11.06	9.63	9.17
MnO	<0.1	<0.1	<0.1	<0.1	0.16	0.13
MgO	6.53	6.61	6.92	6.94	7.09	6.91
Na2O	0.24	0.11	0.14	0.14	0.12	0.13
K2O	<0.1	<0.1	<0.1	<0.1	<0.1	<0.1
Total	**97.78**	**97.12**	**98.51**	**98.18**	**97.24**	**96.14**
Si	4.962	4.952	4.974	4.916	5.024	5.064
Al	4.029	4.043	3.992	4.070	3.983	3.966
Fe2	0.986	0.979	0.975	0.967	0.843	0.810
Mn	0.000	0.000	0.000	0.000	0.014	0.012
Mg	1.022	1.041	1.075	1.082	1.107	1.088
Na	0.049	0.023	0.028	0.028	0.024	0.027
K	0.000	0.000	0.000	0.000	0.000	0.000
Sum	**11.048**	**11.038**	**11.044**	**11.063**	**10.995**	**10.967**
Xmg	0.509	0.515	0.524	0.528	0.568	0.573

Biotite occurs as flakes in the matrix and as small grains as inclusions in larger garnets. Matrix biotite has an iron-rich composition with an X_{Mg} of 0.36 to 0.41 (4). Conspicuous is the high TiO_2 content (up to 3.95 wt%) at the contact with ilmenite and small amounts of chromium (up to 0.41 wt% Cr_2O_3) in matrix biotite. Fluorine values range from 0.24 to 0.48 wt% while no chlorine was detected in any biotite. Biotite enclosed in garnet cores show higher magnesium content (X_{Mg}=0.50–0.53) and significantly lower values of TiO_2 (1.30–1.82 wt%) and no chromium.

Table 4: Representative analyses of biotite. ***A-bt13*** *matrix biotite core (ML05-17A),* ***A1-bt30*** *matrix biotite core (ML05-17A1),* ***A1-bt33*** *matrix biotite rim (ML05-17A1),* ***A1-bt32*** *inclusion biotite (ML05-17A1),* ***A-bt42*** *inclusion biotite (ML05-17A)*

Analysis	**A-bt13**	**A1-bt30**	**A1-bt33**	**A1-bt32**	**A-bt42**
Mineral	bt	bt	bt	bt	bt
SiO2	36.45	34.12	35.46	35.47	34.69
TiO2	3.95	3.24	2.69	1.30	1.82
Al2O3	19.24	18.66	19.80	20.34	19.31
Cr2O3	0.41	0.37	0.23	<0.1	<0.1
FeO	20.08	20.64	20.34	17.44	19.12
MnO	<0.1	<0.1	<0.1	<0.1	<0.1
MgO	6.33	8.13	7.78	11.17	11.48
CaO	<0.1	<0.1	<0.1	<0.1	<0.1
Na2O	0.19	0.09	0.13	0.17	0.20
K2O	9.50	9.65	9.43	9.49	9.25
F	0.24	0.46	0.28	0.48	0.35
Total	**96.39**	**95.36**	**96.14**	**95.86**	**96.22**
Si	2.75	2.640	2.690	2.667	2.623
Ti	0.224	0.189	0.153	0.074	0.104
Al	1.711	1.702	1.770	1.802	1.721
Cr	0.024	0.023	0.014	0.000	0.000
Fe2	1.267	1.336	1.291	1.097	1.209
Mn	0.000	0.000	0.000	0.000	0.000
Mg	0.712	0.938	0.880	1.252	1.294
Ca	0.000	0.000	0.000	0.000	0.000
Na	0.028	0.014	0.019	0.025	0.029
K	0.914	0.953	0.913	0.910	0.892
F	0.057	0.113	0.067	0.114	0.084
Sum	**7.687**	**7.908**	**7.797**	**7.941**	**7.956**
Xmg	0.360	0.412	0.405	0.533	0.517

Three types of spinel can be distinguished, green, olive green and brown (Figure 10) depending on their chemical composition. All of them are rich in hercynite ($FeAl_2O_4$) component (X_{hc}=0.60–0.80) (5) and minor contents of spinel ($MgAl_2O_4$), gahnite ($ZnAl_2O_4$) and chromite ($FeCr_2O_4$) component and very small amounts of galaxite ($MnAl_2O_4$). Especially the chromium content leads to the different colour variations. The spinel inclusions in garnet cores show the lowest chromium content (up to 0.18 wt% Cr_2O_3) and have a dark green colour. They have the highest spinel component (X_{spl}=0.17–0.20), intermediate gahnite content (0.05–0.09) and a very small content of manganese (up to 0.18 wt% MnO). Olive green spinels occur in the matrix of sample MA1, they have intermediate chromium content (0.87–0.99 wt% Cr_2O_3), the magnesium content is lower than in spinel inclusion in garnet (X_{spl}=0.11–0.12), but

zinc and manganese contents are quite similar. The highest chromium content have brown to dark brown matrix spinels from samples ML05-17A and ML05-17A1 (5.28–11.54 wt% Cr_2O_3). They have the lowest magnesium content (X_{spl}=0.095–0.11), intermediate zinc (X_{ghn}=0.10–0.12) but no manganese. Furthermore, matrix spinel has a small amount of titanium (up to 0.7 wt% TiO_2). A spinel inclusion in a matrix ilmenite shows the highest gahnite component of all measured spinels (X_{ghn}=0.39) and a variation in zinc content from core (12.24 wt% ZnO) to rim (15.71 wt% ZnO) (5). A ternary plot of X_{ghn}, X_{spl} and X_{chr} is shown in Figure 12.

Table 5: Representative analyses of spinel. ***A-sp38*** *matrix spinel core (ML05-17A),* ***A-sp39*** *matrix spinel rim (ML05-17A),* ***A1-sp19*** *ilmenite inclusion spinel core (ML05-17A1),* ***A1-sp20*** *ilmenite inclusion spinel rim (ML05-17A1),* ***A1-sp11*** *garnet inclusion spinel (ML05-17A1),* ***ma1sp51*** *matrix spinel (MA1)*

Analysis	**A-sp38**	**A-sp39**	**A1-sp19**	**A1-sp20**	**A1-sp11**	**ma1sp51**
Mineral	spl	spl	spl	spl	spl	spl
TiO2	0.62	0.70	<0.1	0.72	<0.1	<0.1
Al2O3	52.56	47.17	52.02	50.83	59.74	57.81
Cr2O3	6.46	11.54	5.28	6.08	0.00	0.99
V2O3	<0.1	<0.1	1.00	1.01	<0.1	<0.1
FeO	33.90	34.30	27.75	24.58	33.37	32.70
MnO	<0.1	<0.1	<0.1	<0.1	0.18	0.18
MgO	2.19	1.52	1.87	2.07	4.09	2.74
ZnO	3.95	3.78	12.24	15.71	2.65	4.17
Total	**99.68**	**99.01**	**100.16**	**101.00**	**100.03**	**98.59**
Ti	0.014	0.016	0.000	0.016	0.000	0.000
Al	1.821	1.685	1.815	1.774	1.983	1.973
Cr	0.150	0.277	0.124	0.142	0.000	0.023
V	0.000	0.000	0.024	0.024	0.000	0.000
Fe3	0.001	0.007	0.037	0.028	0.017	0.004
Fe2	0.832	0.863	0.650	0.581	0.769	0.788
Mn	0.000	0.000	0.000	0.000	0.004	0.004
Mg	0.096	0.069	0.083	0.091	0.172	0.118
Zn	0.086	0.085	0.268	0.343	0.055	0.089
Sum	**3.000**	**3.002**	**3.001**	**2.999**	**3.000**	**2.999**
Xspl	0.111	0.094	0.095	0.105	0.173	0.121
Xhc	0.789	0.790	0.598	0.499	0.772	0.787
Xghn	0.100	0.116	0.307	0.396	0.055	0.092
Xchr	0.076	0.141	0.064	0.074	0.000	0.012

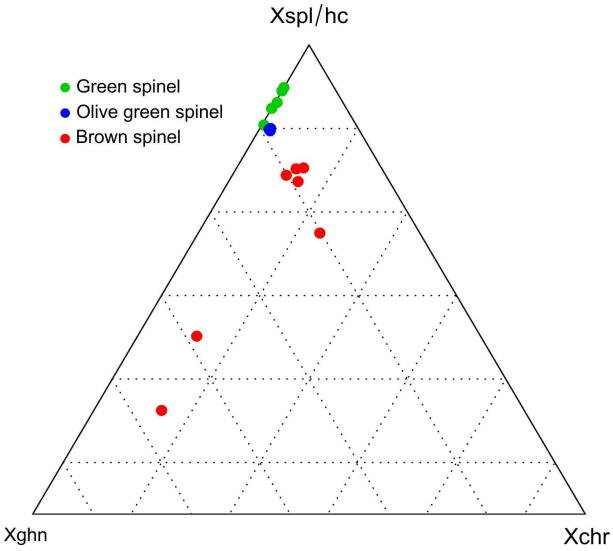

Figure 12: Ternary plot of green spinel (green dots), olive green spinel (blue dots) and brown spinel (red dots)

Two different plagioclase grains were observed. The first group is anorthite-richer matrix plagioclase, they have a X_{an}=0.30–0.34 and show no chemical zoning. The second group is plagioclase inclusions in larger garnet porphyroblasts, which have a lower anorthite content (X_{an}=0.10–0.12) (6). Just very low K-feldspar component is detected in all plagioclase grains (X_{or}=0.15–0.40).

K-feldspar shows albite contents of 8–15 mol% and small amounts of barium (up to 0.66 wt% BaO) (6). K-feldspar usually developed perthitic exsolution lamellae, which are not pure albite but have small amounts of anorthite (X_{an}=0.16–0.18).

Ilmenite occurs as large matrix grains and as small inclusions in several minerals, but without any observable chemical variation. The composition is almost pure ilmenite with small amounts of geikilite (X_{gk}=0.009–0.024) and pyrophanite (X_{pph}=0.004–0.009).

Table 6: Representative analyses of feldspar. **A1-fs16** matrix plagioclase core (ML05-17A1), **ma1fs72** matrix plagioclase rim (MA1), **ma1fs73** matrix plagioclase core (MA1), **A-fs49** inclusion plagioclase (ML05-17A), **A1-fs38** inclusion plagioclase (ML05-17A1), **A-fs29** K-feldspar (ML05-17A), **A-fs27** exsolution lamella (ML05-17A), **A1-fs36** K-feldspar (ML05-17A1), **A1-fs37** exsolution lamella (ML05-17A1)

Analysis	**A-1fs16**	**ma1fs72**	**ma1fs73**	**A-fs49**	**A1-fs38**	**A-fs29**	**A-fs27**	**A1-fs36**	**A1-fs37**
Mineral	pl	pl	pl	pl	pl	kfs	pl	kfs	pl
SiO2	60.42	61.03	61.93	65.52	64.00	64.24	64.27	64.32	65.15
Al2O3	25.78	24.99	24.78	21.79	22.37	18.00	22.53	19.31	22.73
Fe2O3	0.00	<0.1	<0.1	0.68	0.33	<0.1	<0.1	<0.1	<0.1
CaO	5.92	6.73	6.46	2.11	2.29	0.00	3.97	<0.1	3.59
BaO	0.00	<0.1	<0.1	<0.1	<0.1	0.40	0.00	0.64	0.17
Na2O	8.46	7.09	7.24	9.67	10.25	0.94	9.42	1.49	9.94
K2O	0.28	0.25	0.33	0.68	0.10	15.50	0.13	14.73	0.39
Total	**100.86**	**100.09**	**100.74**	**100.45**	**99.34**	**99.08**	**100.32**	**100.49**	**101.97**
Si	2.668	2.705	2.725	2.874	2.839	3.001	2.828	2.959	2.828
Al	1.342	1.306	1.285	1.126	1.169	0.991	1.168	1.047	1.163
Fe3	0.000	0.000	0.000	0.022	0.011	0.000	0.000	0.000	0.000
Ca	0.280	0.320	0.305	0.099	0.109	0.000	0.187	0.000	0.167
Ba	0.000	0.000	0.000	0.000	0.000	0.007	0.000	0.012	0.003
Na	0.724	0.609	0.618	0.822	0.881	0.085	0.804	0.133	0.837
K	0.016	0.014	0.019	0.038	0.006	0.924	0.007	0.865	0.022
Sum	**5.030**	**4.954**	**4.952**	**4.981**	**5.015**	**5.008**	**4.994**	**0.864**	**5.020**
Xab	0.710	0.646	0.656	0.857	0.885	0.084	0.806	0.132	0.813
Xan	0.275	0.339	0.324	0.103	0.109	0.000	0.187	0.000	0.162
Xor	0.016	0.015	0.020	0.040	0.006	0.909	0.007	0.856	0.021
Xcls	0.000	0.000	0.000	0.000	0.000	0.007	0.000	0.012	0.003

2.2 Al-rich Migmatite/Restite type 2

The second type of Al-rich migmatite is similar to the first type (Figure 13) and differ just in a few points. Biotite is more common and larger in size (up to 3mm) and builds up, next to cordierite and garnet, a considerably part of the melanosome. Sillimanite is quite common, but just small amounts of spinel occur in this type of rock. In the leucosome the plagioclase forms larger grains (up to 1mm) and is more common compared to type 1 migmatite/restite. However, K-feldspar is the most abundant constituent of the leucosome. Sample ML05-16 was investigated in detail.

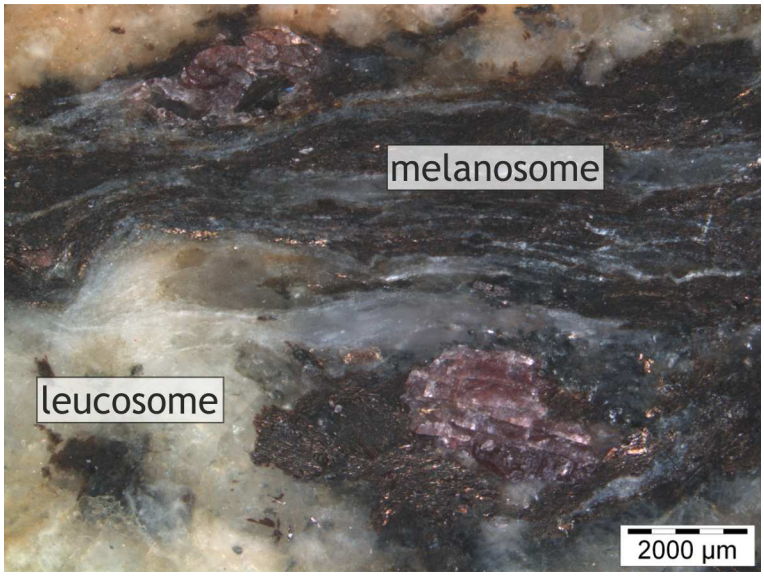

Figure 13: Stereomicroscope Image of Sample ML05-16. The melanosome looks a little bit different to type 1, cause of the higher amounts of biotite it seems shiny.

Plagioclase appears as polysynthetic twins without any exsolutions. K-feldspar are perthitic and range in size between 0.5 and 3mm, sometimes they show a typically microcline grid. Matrix quartz grains are up to 2mm in size and appear also as inclusions in most mineral phases. Biotite occurs to a greater extent in melanosome than in type 1. A possible mineral reaction can be observed in most of the larger biotite grains, which are intergrown with sillimanite needles (Figure 14). Spinel is small and uncommon, but shows a similar chemical composition as in type 1. Garnet ranges in size between 200µm and 6mm, the smaller ones are heavily consumed by cordierite (Figure 14). The larger garnet porphyroblasts have inclusion-rich cores anorthite-rich plagioclase next to biotite, quartz, ilmenite, zircon, monazite and apatite (Figure 14).

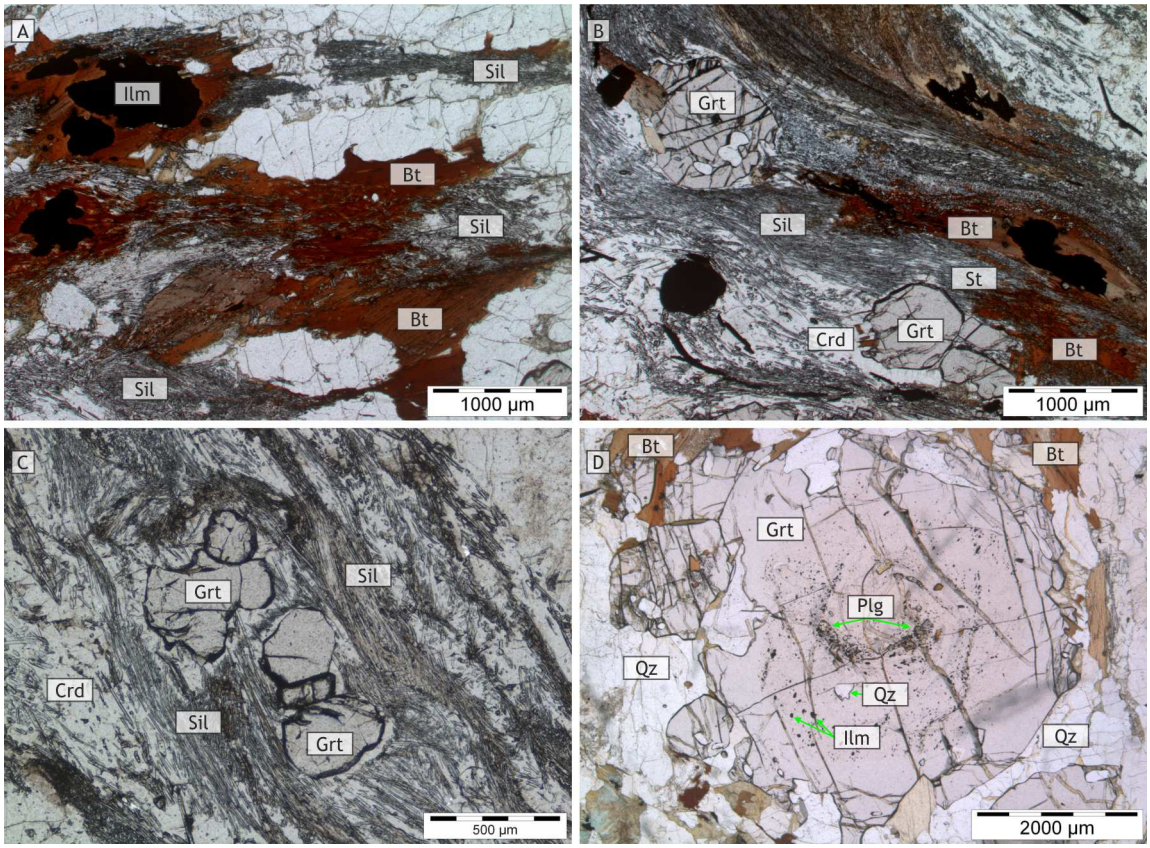

*Figure 14: Photomicrographs **A** Large biotites intergrown with sillimanite, like in type 1 biotites are often connected to ilmenite. **B, C** Garnet and Sillimanite as inclusions in cordierite, garnets are heavily consumed by cordierite. Fine grained sillimanite needles intergrown with biotite occur as well in larger cordierite grains. **D** Large garnet porphyroblast (6mm) with inclusion-rich core, unlike the most larger garnets this one is surrounded by quartz and not by cordierite.*

Garnet has a homogeneous iron-rich composition (X_{alm}=0.80–0.82), with small amounts of pyrope (X_{prp}=0.12–0.14) and minor amounts of grossular (X_{grs}=0.030–0.036) and spessartine (X_{sps}=0.015–0.018) components (8). They also show a slight increase in iron and decrease of magnesium due to retrograde diffusional zoning. But only one single garnet with a conspicuous chemical zoning profile could be observed. The core composition is characterized by high contents of grossular (X_{grs}=0.20–0.23) and spessartine (X_{sps}=0.10–0.12) as well as a lower almandine (X_{alm}=0.61–0.63) and pyrope (X_{prp}=0.035–0.040) components (8).

Table 7: Representative analyses of garnet and spinel. ***516gt40*** *garnet core (ML05-16),* ***516gt41*** *garnet rim (ML05-16),* ***516gt17*** *garnet core (ML05-16),* ***516gt18*** *garnet rim (ML05-16),* ***516sp30*** *brown matrix spinel (ML05-16)*

Analysis	**516gt40**	**516gt41**	**516gt17**	**516gt18**	**516sp30**
Mineral	**grt**	**grt**	**grt**	**grt**	spl
SiO2	37.29	37.07	37.27	37.70	<0.1
TiO2	<0.1	<0.1	<0.1	<0.1	0.24
Al2O3	20.97	21.26	21.48	21.23	51.38
Cr2O3	<0.1	<0.1	<0.1	<0.1	6.24
V2O3	n.d.	n.d.	n.d.	n.d.	<0.1
FeO	27.45	36.65	36.88	36.33	33.79
MnO	4.89	0.78	0.69	0.71	0.11
MgO	1.10	3.20	3.36	3.18	1.03
CaO	8.06	1.12	1.11	1.24	<0.1
ZnO	n.d.	n.d.	n.d.	n.d.	6.46
Total	**99.76**	**100.08**	**100.79**	**100.39**	**99.25**
Si	3.002	2.983	2.975	3.016	0.000
Ti	0.000	0.000	0.000	0.000	0.005
Al	1.990	2.016	2.021	2.002	1.811
Cr	0.000	0.000	0.000	0.000	0.148
V	0.000	0.000	0.000	0.000	0.000
Fe3	0.007	0.017	0.028	0.000	0.031
Fe2	1.841	2.450	2.434	2.431	0.814
Mn	0.333	0.053	0.047	0.048	0.003
Mg	0.132	0.384	0.400	0.379	0.046
Ca	0.695	0.097	0.095	0.106	0.000
Zn	0.000	0.000	0.000	0.000	0.143
Sum	**3.008**	**3.001**	**3.004**	**2.964**	**2.858**
Xalm	0.613	0.821	0.818	0.820	-
Xprp	0.044	0.129	0.134	0.128	-
Xgrs	0.232	0.033	0.032	0.036	-
Xsps	0.111	0.018	0.016	0.016	-
Xspl	-	-	-	-	0.054
Xhc	-	-	-	-	0.778
Xghn	-	-	-	-	0.168
Xchr	-	-	-	-	0.076

Large cordierite grains have a homogeneous composition (X_{Mg}=0.47–0.50) with a slight increase of iron towards the rim (8). Some smaller and partly resorbed grains show cores with high amounts of Mg-cordierite (X_{Mg}=0.89) and rims with intermediate component (X_{Mg}=0.45). Cordierite contains Na_2O ranging from 0.13–0.16 wt%. Some grains additionally show a small manganese content of about 0.15 wt% MnO.

Biotite is larger and richer in annite component (X_{Mg}=0.28–0.30) (8) than biotite in type 1 Al-rich migmatite/restite (4). There is no significant chemical zoning between biotite cores and rims. The titanium content ranges from 2.80 to 3.40 wt% TiO_2 and have small amounts of Na_2O (up to 0.34 wt%). Manganese and calcium values are less than 0.1 wt%, chromium values reach 0.17wt% and fluorine 0.55–0.70 wt%. Biotite inclusions in garnet have a phlogopite-richer composition (X_{Mg}=0.66) (8) with lower values of TiO_2 (2.40 wt%), but higher fluorine content (1.04 wt%).

*Table 8: Representative analyses of cordierite.**516cd37** cordierite core (ML05-16), **516cd39** cordierite rim (ML05-16), **516cd42** cordierite core (ML05-16), **516cd43** cordierite rim (ML05-16)*

Analysis	**516cd37**	**516cd39**	**516cd42**	**516cd43**
Mineral	crd	crd	crd	crd
SiO2	50.16	47.30	47.72	47.63
Al2O3	33.10	31.76	32.49	32.13
FeO	2.58	12.59	11.72	12.03
MnO	<0.1	<0.1	<0.1	<0.1
MgO	12.41	5.82	6.72	6.18
Na2O	0.13	0.15	0.15	0.16
K2O	<0.1	<0.1	<0.1	<0.1
Total	**98.38**	**97.62**	**98.80**	**98.13**
Si	5.027	5.005	4.970	4.999
Al	3.909	3.961	3.988	3.975
Fe2	0.216	1.114	1.021	1.056
Mn	0.000	0.000	0.000	0.000
Mg	1.854	0.918	1.043	0.967
Na	0.025	0.031	0.030	0.033
K	0.000	0.000	0.000	0.000
Sum	**11.031**	**11.029**	**11.052**	**11.030**
Xmg	0.896	0.452	0.505	0.478

Spinel is small and uncommon in this type, but shows a similar hercynite-rich composition. (X_{hc}=0.77–0.80) and occurs only as chromium-rich (up to 6.24 wt%) brown spinel (8). Zinc values are quite high (up to 6.46 wt%) and small amounts of manganese (0.11 wt% MnO) and titanium (0.24 wt% TiO_2) were observed.

Table 9: Representative analyses of biotite. ***516bt20*** *matrix biotite core (ML05-16),* ***516bt21*** *matrix biotite rim (ML05-16),* ***516bt28*** *matrix biotite core (ML05-16),* ***516bt29*** *matrix biotite rim (ML05-16),* ***516bt23*** *inclusion biotite (ML05-16)*

Analysis	**516bt20**	**516bt21**	**516bt28**	**516bt29**	**516bt23**
Mineral	bt	bt	bt	bt	bt
SiO2	33.76	34.59	34.62	34.76	37.28
TiO2	3.38	3.23	2.83	3.26	2.40
Al2O3	18.40	19.02	19.85	19.68	18.42
Cr2O3	0.17	<0.1	<0.1	<0.1	<0.1
FeO	24.23	24.34	23.84	23.53	13.03
MnO	<0.1	<0.1	<0.1	<0.1	<0.1
MgO	5.43	5.36	5.73	5.38	14.55
CaO	<0.1	<0.1	<0.1	<0.1	<0.1
Na2O	0.18	0.17	0.16	0.16	0.34
K2O	9.33	9.45	9.43	9.58	8.97
F	0.68	0.56	0.56	0.66	1.04
Total	**95.56**	**96.72**	**97.02**	**97.01**	**96.03**
Si	2.656	0.614	2.659	2.670	2.745
Ti	0.200	0.325	0.163	0.188	0.133
Al	1.706	3.000	1.797	1.782	1.599
Cr	0.011	0.000	0.000	0.000	0.000
Fe2	1.594	2.724	1.531	1.512	0.802
Mn	0.000	0.000	0.000	0.000	0.000
Mg	0.637	1.069	0.656	0.616	1.597
Ca	0.000	0.000	0.000	0.000	0.000
Na	0.027	0.044	0.024	0.024	0.049
K	0.936	1.613	0.924	0.939	0.843
F	0.169	0.237	0.136	0.160	0.242
Sum	**7.936**	**9.626**	**7.890**	**7.891**	**8.010**
Xmg	0.286	0.282	0.300	0.289	0.666

Matrix plagioclase has low anorthite content (X_{an}=0.19–0.24) and shows a slight chemical zoning with albite-richer cores and anorthite-richer rims (10). Plagioclase inclusions in large garnet porphyroblasts display the highest anorthite contents ($X_{an=}$0.83–0.90) measured in all felsic samples. K-feldspar component in plagioclase is usually low (X_{or}=up to 0.020).

K-feldspar has an albite content between 12–15 mol% and barium values less than 0.1 wt% (10). Most K-feldspar shows perthitic exsolution lamellae consisting of pure albite. Samples from type 1 and type 2 were plotted together in the feldspar triangle (Figure 15). Conspicuous are albite-rich plagioclase inclusions in garnet in type 1 and anorthite-rich inclusions in garnet in type 2 Al-rich migmatite/restite.

Table 10: Representative analyses of feldspar. ***516fs34*** *matrix plagioclase core (ML05-16),* ***516fs35*** *matrix plagioclase rim (ML05-16),* ***516fs5*** *inclusion plagioclase (ML05-16),* ***516fs6*** *inclusion plagioclase (ML05-16),* ***516fs10*** *K-feldspar core (ML05-16),* ***516fs8*** *K -feldspar rim (ML05-16)*

Analysis	**516fs34**	**516fs35**	**516fs5**	**516fs6**	**516fs10**	**516fs8**
Mineral	pl	pl	pl	pl	kfs	kfs
SiO2	63.29	63.31	47.15	46.03	65.56	65.22
Al2O3	22.90	23.64	34.52	35.55	19.10	18.76
Fe2O3	0.00	0.00	0.26	0.37	<0.1	<0.1
CaO	3.95	4.33	16.56	17.75	<0.1	<0.1
BaO	<0.1	<0.1	<0.1	<0.1	<0.1	<0.1
Na2O	9.04	8.07	1.76	1.14	1.36	1.67
K2O	0.24	0.32	<0.1	<0.1	14.41	14.05
Total	**99.42**	**99.67**	**100.25**	**100.84**	**100.89**	**99.88**
Si	2.810	2.797	2.155	2.099	2.979	2.991
Al	1.198	1.231	1.859	1.910	1.023	1.014
Fe3	0.000	0.000	0.009	0.013	0.000	0.000
Ca	0.188	0.205	0.811	0.867	0.000	0.000
Ba	0.000	0.000	0.000	0.000	0.000	0.000
Na	0.778	0.691	0.156	0.101	0.120	0.148
K	0.014	0.018	0.000	0.000	0.835	0.822
Sum	**4.988**	**4.942**	**4.990**	**4.990**	**4.957**	**4.975**
Xab	0.794	0.756	0.161	0.104	0.126	0.153
Xan	0.192	0.224	0.839	0.896	0.000	0.000
Xor	0.014	0.020	0.000	0.000	0.874	0.847
Xcls	0.000	0.000	0.000	0.000	0.000	0.000

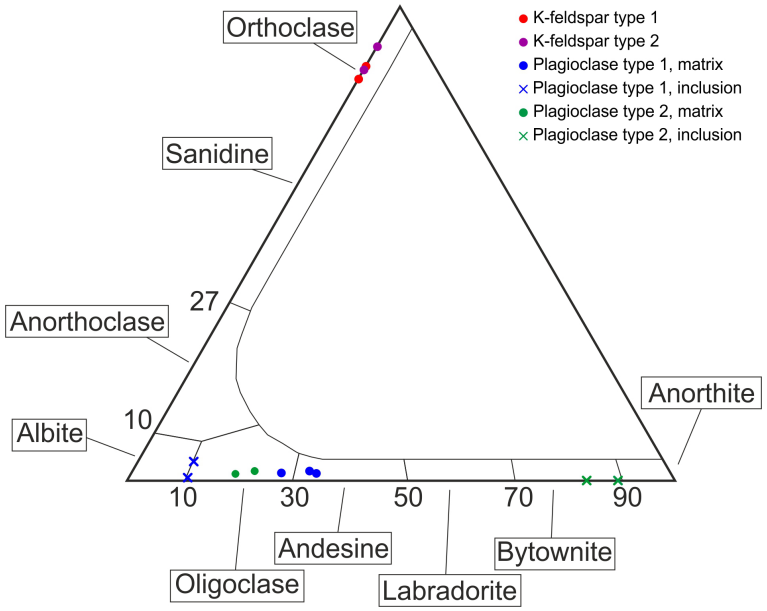

Figure 15: Feldspar triangle showing different compositions of feldspars in type 1 and type 2 Al-rich migmatite/restite. Especially different compositions of plagioclases, both in the matrix and enclosed in garnets.

2.3 Grt-Crd-Migmatite

Grt-Crd-migmatite is a commonly found along the Danube valley west of Linz (Figure 5). These samples contain the mineral assemblage, cordierite + garnet + biotite + perthitic K-feldspar + plagioclase + quartz +sillimanite and the accessory minerals monazite + zircon + pyrite. There is no well developed migmatitic structure (Figure 16) (leucosome/melanosome) as in Al-rich migmatite/restite type 1 and 2. Large cordierite and K-feldspar grains (several mm) build up the main part of the rock, smaller plagioclase and quartz (1–2mm) grains form the rest of the matrix. Sample ML07-1B was investigated in detail.

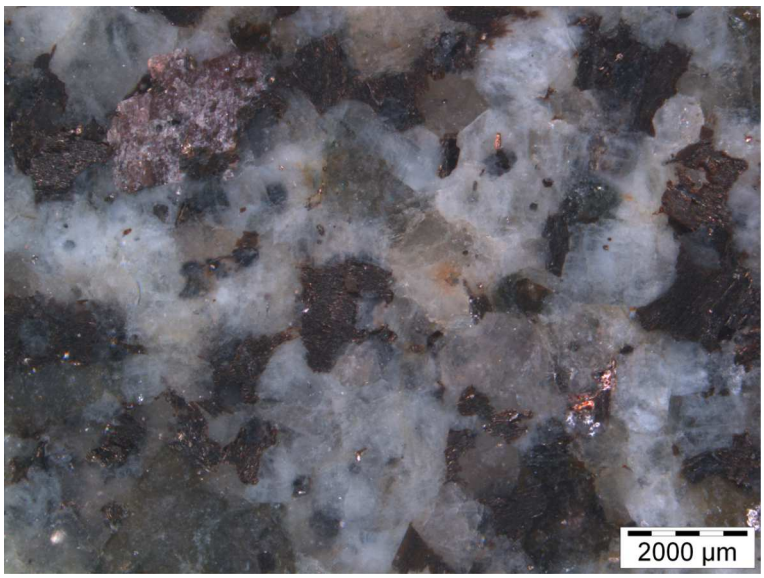

Figure 16: Stereomicroscope Image of Sample ML07-1B

Perthitic K-feldspar is the main component of the felsic matrix minerals. The grains range in size from 1–4mm and have inclusions of quartz and monazite and show exsolution lamellae (Figure 17). Plagioclase is smaller in size (0.5–1mm), displays polysynthetic twins without any exsolutions. Quartz is also a common matrix phase (0.5–2mm) but is also found as inclusions in several minerals. Garnets are usually small (0.5–1mm) and consumed by cordierite by a mineral reaction with sillimanite and quartz (Figure 17). Sometimes small garnet grains are enclosed in biotite or in plagioclase (Figure 17).

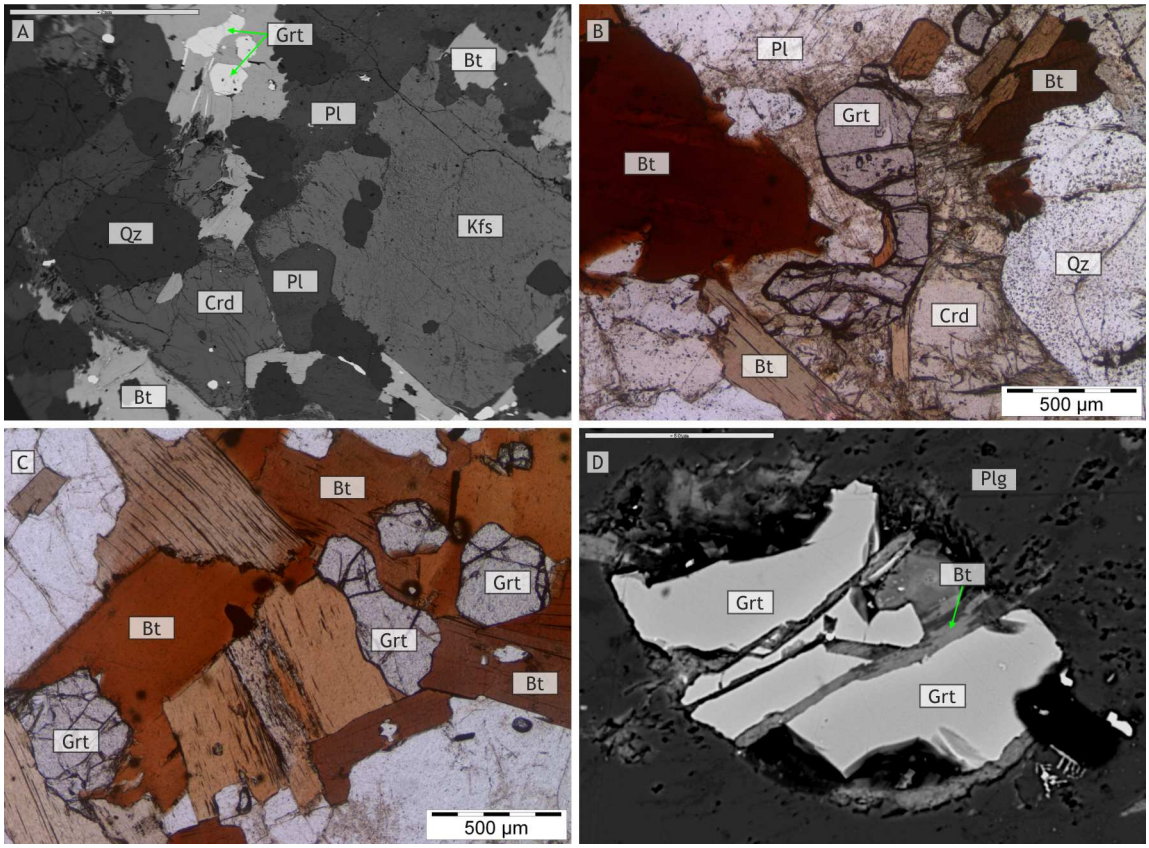

*Figure 17: Backscatter elecctron images (BSE) and Photomicrographs of **A** Large perthitic K-feldspar next to plagioclase and quartz.(the scale bar represents 2mm) **B** Resorbed garnet grain next to cordierite representing a mineral chemical reaction between this two phases, whereat cordierite grows and garnet is consumed. **C** Small garnet grains (250–500µm) occurring within biotites. **D** Garnet inclusion in a large plagioclase grain. (the scale bar represents 50µm)*

Biotite is common in this rock type and occurs as single flakes (1–2mm) often next to cordierite or as aggregates of multiple grains with several mm in size (0.5–1mm per single grain). Biotite quartz symplectites (Figure 18) indicate partial melting. Cordierite occurs as large grains (up to 5mm), with several inclusions like biotite, quartz, small garnet, monazite (up to 200µm in size) plagioclase and K-feldspar, but very rare are inclusions of sillimanite (Figure 18). At grain boundaries and in cracks most of the cordierite grains are affected by pinitisation (Figure 18).

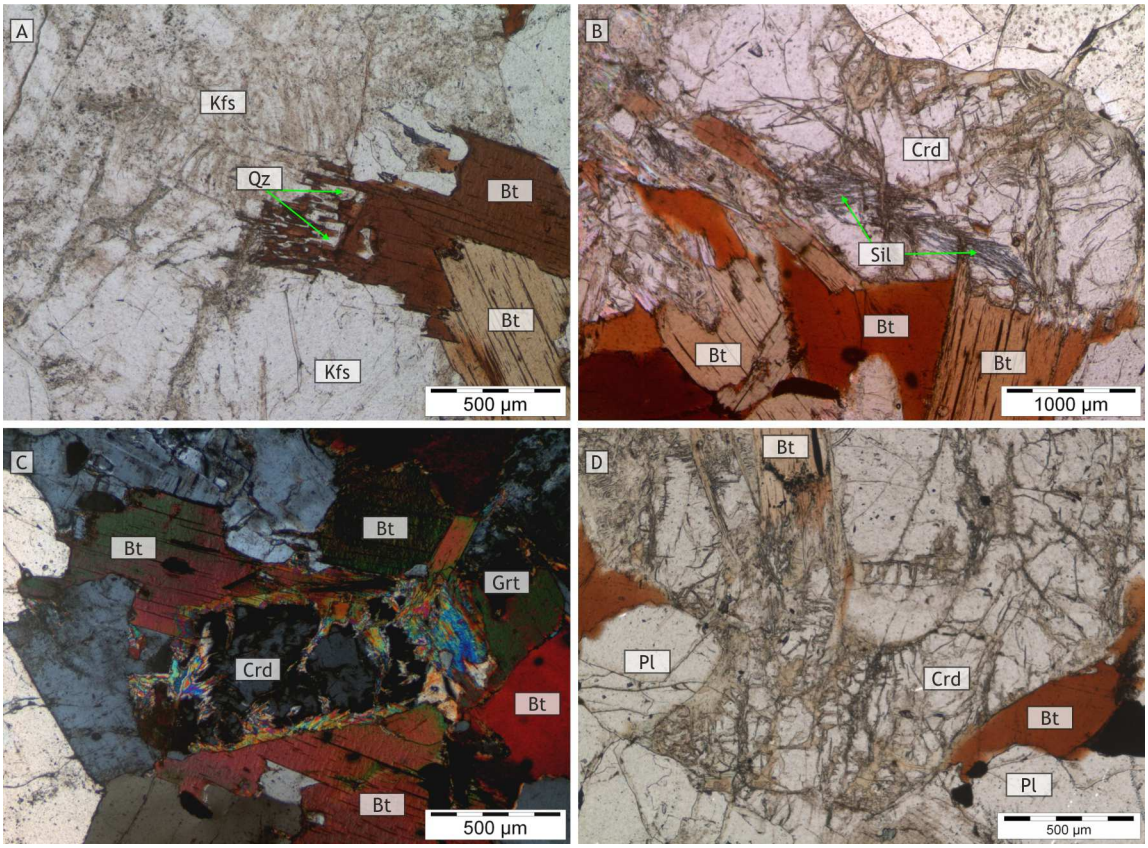

*Figure 18: Photomicrographs of **A** Biotite quartz symplectites are common in this rock type. **B** Sillimanite is uncommon but occurs sometimes as inclusion in cordierite. **C (crossed nicols)**, **D** Most of the cordierites are affected of pinitisation, especially in cracks and at grain boundaries.*

Garnet has an iron-rich composition (X_{alm}=0.72–0.76) with minor amounts of pyrope (X_{prp}=0.09–0.13) and grossular (X_{grs}=0.024–0.027) (11). The small garnet grains are enriched in spessartine component (X_{sps}=0.09–0.12) and are usually consumed by cordierite. Garnet inclusions in biotite, cordierite or plagioclase show quite similar compositions, but a small inclusion in plagioclase shows the highest manganese content (X_{sps}=0.16). Garnet compositions were plotted together with garnets from Al-rich migmatite/restite type 1 and type 2 (Figure 19).

Cordierite is magnesium-richer (X_{Mg}=0.56–0.65) than cordierite in the Al-rich migmatite/restite (4). Sometimes they show a slight chemical zoning with magnesium-richer cores and iron-richer rims. Furthermore when in contact to garnet they have slightly elevated amounts of manganese (up to 0.45 wt% MnO). Sodium values range from 0.10–0.18 wt% Na_2O (12).

Table 11: Representative analyses of garnet. ***7-1bgt46*** *garnet core (ML07-1B),* ***7-1bgt49*** *garnet rim (ML07-1B),* ***7-1bgt32*** *garnet inclusion in plagioclase (ML07-1B),* ***7-1bgt33*** *garnet inclusion in biotite (ML07-1B)*

Analysis	**7-1bgt46**	**7-1bgt49**	**7-1bgt32**	**7-1bgt33**
Mineral	grt	grt	grt	grt
SiO2	36.96	36.46	36.55	36.79
Al2O3	20.71	20.50	20.45	21.11
FeO	36.06	34.66	33.67	34.74
MnO	4.15	4.57	7.22	4.68
MgO	3.01	2.89	1.32	3.14
CaO	0.93	0.88	0.83	0.85
Total	**101.82**	**99.96**	**100.04**	**101.31**
Si	2.941	2.954	2.990	2.935
Al	1.942	1.958	1.972	1.985
Fe3	0.175	0.134	0.048	0.145
Fe2	2.225	2.215	2.256	2.173
Mn	0.280	0.314	0.500	0.316
Mg	0.357	0.349	0.161	0.373
Ca	0.079	0.076	0.073	0.073
Sum	**7.999**	**8.000**	**8.000**	**8.000**
Xalm	0.757	0.750	0.755	0.740
Xprp	0.121	0.118	0.054	0.127
Xgrs	0.027	0.026	0.024	0.025
Xsps	0.095	0.106	0.167	0.108

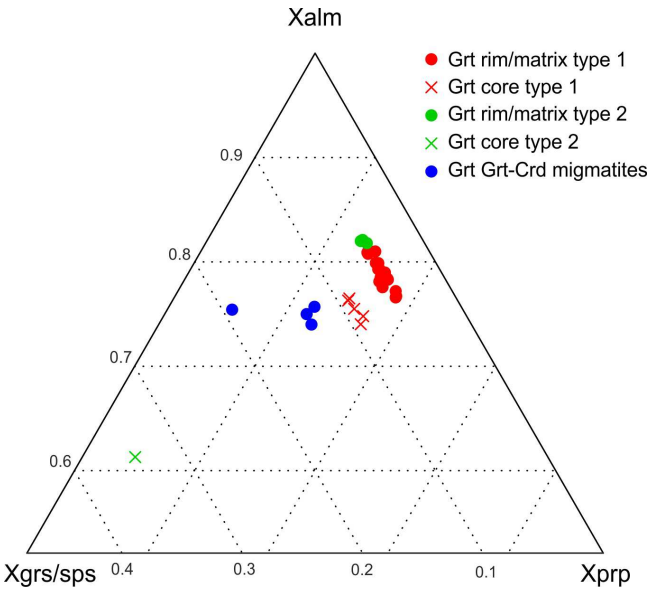

Figure 19: Ternary plot of garnet core (crosses) and rim and unzoned matrix garnet (dots) compositions. Conspicuous is the spessartine-richer composition of garnets from Grt-Crd-migmatite.

Table 12: Representative analyses of cordierite. ***7-1bcd57*** *cordierite core (ML07-1B),* ***7-1bcd58*** *cordierite rim (ML07-1B),* ***7-1bcd60*** *cordierite core (ML07-1B),* ***7-1bcd59*** *cordierite rim (ML07-1B)*

Analysis	**7-1bcd57**	**7-1bcd58**	**7-1bcd60**	**7-1bcd59**
Mineral	crd	crd	crd	crd
SiO2	48.32	48.27	48.66	48.19
Al2O3	32.84	32.24	32.71	32.86
FeO	9.28	9.52	8.74	9.68
MnO	0.19	0.36	0.29	0.34
MgO	7.90	7.71	8.60	7.65
Na2O	0.13	0.18	0.12	0.14
K2O	<0.1	<0.1	<0.1	<0.1
Total	**98.66**	**98.28**	**99.12**	**98.86**
Si	4.984	5.009	4.987	4.974
Al	3.992	3.943	3.951	3.997
Fe2	0.800	0.826	0.749	0.836
Mn	0.017	0.032	0.025	0.030
Mg	1.215	1.193	1.314	1.177
Na	0.026	0.036	0.024	0.028
K	0.000	0.000	0.000	0.000
Sum	**11.034**	**11.039**	**11.050**	**11.042**
Xmg	0.603	0.591	0.637	0.585

Biotite has a slightly more iron-rich composition (X_{Mg}=0.40–0.45), without any chemical zoning but with slightly increased magnesium values when in contact with garnet or cordierite (13). Small amounts of sodium (0.10–0.30 wt% Na_2O) and chromium (up to 0.14 wt % Cr_2O_3) and manganese (0.10–0.24 wt% MnO) were detected. Fluorine values range from 0.60–0.80 wt% and titanium values from 2.80–4.18 wt% TiO_2 which is similar to Al-rich migmatite/restite.

Plagioclase is rich in albite component (X_{ab}=0.69–0.75) with small amounts of K-feldspar (X_{or}=0.008–0.021). Values of barium and ferric iron are below 0.1 wt%. K-feldspars have albite contents ranging from 9–12 mol% and some celsian contents of up to 1.3 mol%.

Table 13: Representative analyses of biotite. ***7-1bbt29*** *matrix biotite core (ML07-1B),* ***7-1bbt30*** *matrix biotite rim (ML07-1B),* ***7-1bbt34*** *matrix biotite next to garnet inclusion (ML07-1B),* ***7-1bbt38*** *matrix biotite next to cordierite (ML01-1B)*

Analysis	**7-1bbt29**	**7-1bbt30**	**7-1bbt34**	**7-1bbt38**
Mineral	bt	bt	bt	bt
SiO2	34.79	34.55	34.56	35.97
TiO2	3.61	3.33	2.83	3.17
Al2O3	18.69	19.30	19.27	19.08
Cr2O3	<0.1	<0.1	0.13	<0.1
FeO	21.31	21.22	21.28	20.08
MnO	<0.1	<0.1	<0.1	<0.1
MgO	8.08	8.08	8.32	9.19
CaO	<0.1	<0.1	<0.1	<0.1
Na2O	0.20	0.29	0.15	0.20
K2O	9.39	9.47	9.37	9.31
F	0.86	0.65	0.67	0.78
Total	**96.93**	**96.89**	**96.58**	**97.78**
Si	2.656	2.633	2.641	2.69
Ti	0.207	0.191	0.163	0.178
Al	1.681	1.733	1.736	1.682
Cr	0.000	0.000	0.008	0.000
Fe2	1.360	1.352	1.360	1.256
Mn	0.000	0.000	0.000	0.000
Mg	0.920	0.918	0.948	1.025
Ca	0.000	0.000	0.000	0.000
Na	0.030	0.043	0.022	0.029
K	0.914	0.921	0.914	0.888
F	0.208	0.157	0.162	0.185
Sum	**7.976**	**7.948**	**7.954**	**7.933**
Xmg	0.404	0.404	0.411	0.449

Table 14: Representative analyses of feldspar. ***7-1bfs64*** *matrix plagioclase core (ML07-1B),* ***7-1bfs63*** *matrix plagioclase rim (ML07-1B),* ***7-1bfs65*** *matrix plagioclase core (ML07-1B),* ***7-1bfs66*** *matrix plagioclase rim(ML07-1B),* ***7-1bfs10*** *K-feldspar (ML07-1B),* ***7-1bfs16*** *K-feldspar (ML07-1B)*

Analysis	**7-1bfs64**	**7-1bfs63**	**7-1bfs65**	**7-1bfs66**	**7-1bfs10**	**7-1bfs16**
Mineral	pl	pl	pl	pl	kf	kf
SiO2	62.54	62.80	61.92	61.78	64.60	64.38
Al2O3	24.02	24.29	24.36	24.47	19.12	18.99
Fe2O3	<0.1	<0.1	<0.1	<0.1	<0.1	<0.1
CaO	5.20	5.36	5.67	5.75	0.00	0.10
BaO	<0.1	<0.1	<0.1	<0.1	0.65	0.64
Na2O	8.40	8.22	7.76	8.18	1.38	1.03
K2O	0.22	0.16	0.36	0.14	14.94	15.21
Total	**100.38**	**100.83**	**100.07**	**100.32**	**100.69**	**100.35**
Si	2.758	2.755	2.741	2.731	2.968	2.970
Al	1.248	1.256	1.271	1.275	1.035	1.033
Fe3	0.000	0.000	0.000	0.000	0.000	0.000
Ca	0.246	0.252	0.269	0.272	0.000	0.005
Ba	0.000	0.000	0.000	0.000	0.012	0.012
Na	0.718	0.699	0.666	0.701	0.123	0.092
K	0.012	0.009	0.020	0.008	0.876	0.895
Sum	**4.982**	**4.971**	**4.967**	**4.987**	**5.014**	**5.007**
Xab	0.736	0.728	0.697	0.715	0.122	0.092
Xan	0.252	0.263	0.282	0.277	0.000	0.005
Xor	0.012	0.009	0.021	0.008	0.866	0.891
Xcls	0.000	0.000	0.000	0.000	0.012	0.012

2.4 Opx-Grt-Bt-Gneiss

Orthopyroxene bearing-Grt-Bt gneiss is an uncommon rock type which appears along the danube valley west of Linz (Figure 5), next to the rock types described above. Samples of this rock type contains the mineral assemblage biotite + garnet + orthopyroxene + plagioclase + quartz + ilmenite and the accessory minerals zircon + apatite + magnetite + monazite. The rocks show dark biotite, garnet and orthopyroxene-rich layers, with fine grained quartz and plagioclase and leucocratic layers with coarser grained quartz and plagioclase (Figure 20). Sample BA7 was investigated in detail.

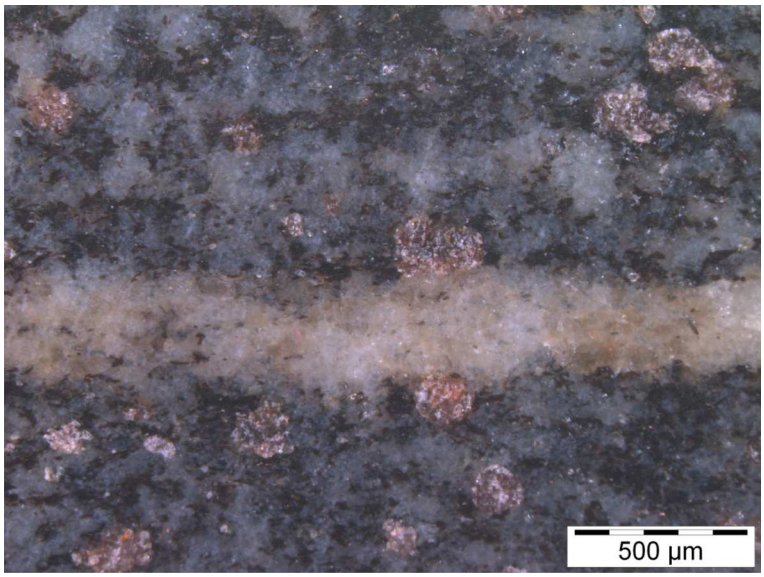

Figure 20: Stereomicroscope Image of Sample BA7 showing two different layers within the rock.

Plagioclase ranges in size between 0.5–1mm. The grains usually show polysynthetic twinning and in some cases small inclusions of K-feldspar (Figure 21). The Plagioclase is anorthite-richer compared to felsic samples (X_{an}=0.47–0.64). However, some grains have anorthite-poorer cores (X_{an}=0.51) and anorthite-richer rims (X_{an}=0.64) (15). K-feldspars is only found as small inclusions in plagioclase grains. Quartz develops two different fractions of grain sizes, where the smaller one (100–500µm) occurs in the melanocratic layers and the larger one (up to 1.5mm) in the leucocratic layers (Figure 21). Quartz also occurs as inclusions in garnet, plagioclase and biotite.

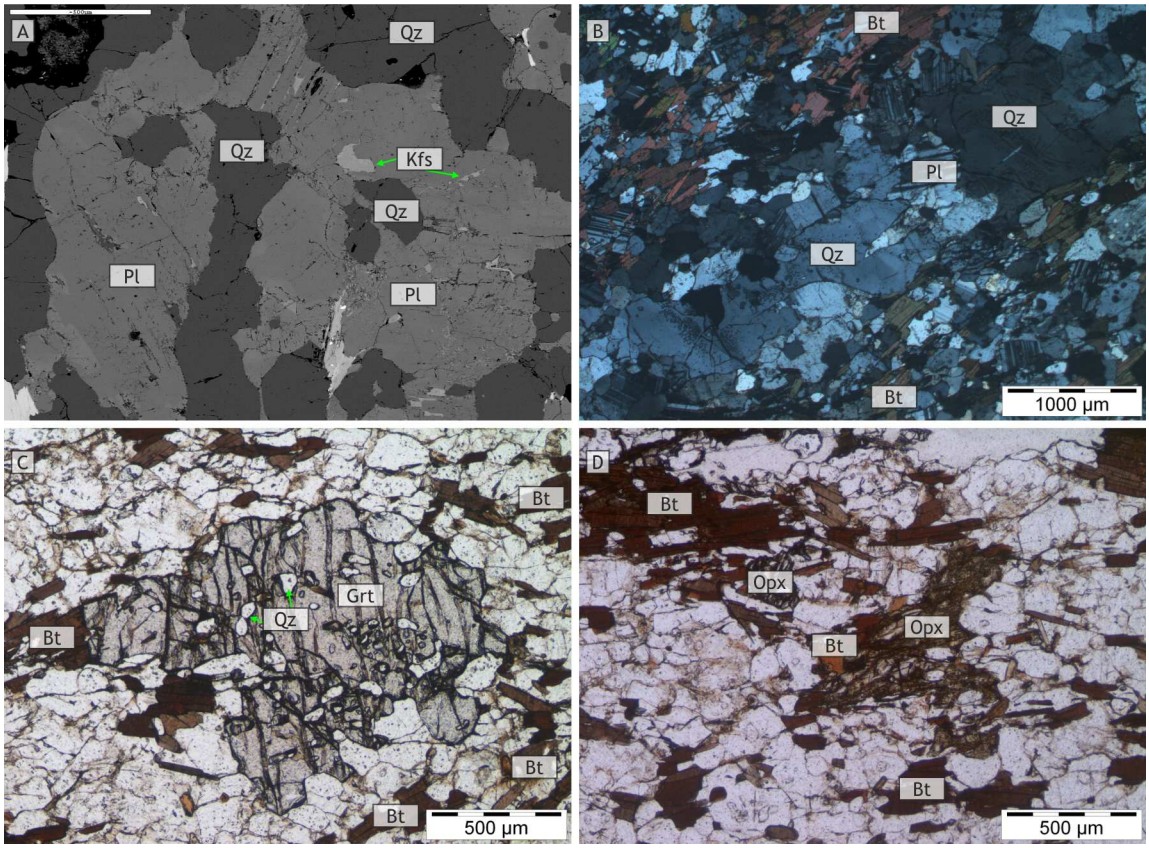

*Figure 21: Backscatter elecctron images (BSE) and Photomicrographs of **A** Plagioclase with inclusions of K-feldspar and quartz.(the scale bar represents 2mm) **B (crossed nicols)** Large quartz grains in the leucocratic layers and finer grained in the biotite-rich layers. **C** A ca.1mm sized garnet porphyroblast with numerous inclusions of quartz. **D** Orthopyroxene occurs in most cases intergrown with biotite.*

Garnet is common in the darker layers, range in size from 0.5–1mm and occurs together with biotite (Figure 21). The garnets have a homogeneous iron-rich composition (X_{alm}=0.66–0.70) without any chemical zoning. Again, only a slight increase in iron is seen towards the rims due to retrograde diffusional zoning. Pyrope and grossular components are slightly higher than in other samples (X_{prp}=0.17–0.20, X_{grs}=0.067–0.088) (16).

Orthopyroxene occurs mostly next to biotite. The grains have a size up to 0.5mm, appear to be resorbed and show no visible cleavage (Figure 21). The composition is slightly richer in enstatite component (X_{Mg}=0.52–0.54), with small amounts of aluminium (up to 2.70 wt% Al_2O_3), calcium (0.20–0.28 wt% CaO) and manganese (0.40–0.70 wt% MnO). Sometimes orthopyroxene also contains some TiO_2 (up to 0.20 wt%) (17).

Table 15: Representative analyses of feldspar. ***ba7fs23*** *matrix plagioclase core (BA7),* ***ba7fs24*** *matrix plagioclase rim (BA7),* ***ba7fs25*** *matrix plagioclase core (BA7),* ***ba7fs26*** *matrix plagioclase rim(BA7),* ***ba7fs27*** *K-feldspar in plagioclase (BA7)*

Analysis	**ba7fs23**	**ba7fs24**	**ba7fs25**	**ba7fs26**	**ba7fs27**
Mineral	plag	plag	plag	plag	kfs
SiO2	55,63	52,49	53,21	51,97	64,48
Al2O3	27,83	29,74	29,27	30,20	18,14
Fe2O3	<0.1	<0.1	<0.1	<0.1	<0.1
CaO	10,42	12,86	12,40	12,90	<0.1
BaO	<0.1	<0.1	<0.1	<0.1	<0.1
Na2O	5,52	3,94	4,32	4,03	0,60
K2O	<0.1	0,09	0,10	<0.1	15,65
Total	**99,43**	**99,12**	**99,30**	**99,10**	**98,87**
Si	2,514	2,397	2,423	2,375	3,006
Al	1,482	1,600	1,571	1,627	0,997
Fe3	0,000	0,000	0,000	0,000	0,000
Ca	0,505	0,629	0,605	0,632	0,000
Ba	0,000	0,000	0,000	0,000	0,000
Na	0,484	0,349	0,381	0,357	0,054
K	0,000	0,005	0,006	0,000	0,931
Sum	**4,501**	**4,626**	**4,599**	**4,634**	**0,997**
Xab	0,489	0,355	0,384	0,361	0,055
Xan	0,511	0,640	0,610	0,639	0,000
Xor	0,000	0,005	0,006	0,000	0,945
Xcls	0,000	0,000	0,000	0,000	0,000

Table 16: Representative analyses of garnet. ***ba7gt1*** *garnet core (BA7),* ***ba7gt2*** *garnet rim (BA7),* ***ba7gt10*** *garnet core (BA7),* ***ba7gt11*** *garnet rim (BA7)*

Analysis	**ba7gt1**	**ba7gt2**	**ba7gt10**	**ba7gt11**
Mineral	grt	grt	grt	grt
SiO2	37.79	38.19	37.73	37.59
Al2O3	20.51	20.78	21.03	20.45
FeO	31.13	32.11	32.04	32.61
MnO	2.39	2.58	2.40	2.28
MgO	5.02	4.49	4.61	4.49
CaO	3.11	2.63	2.38	2.42
Total	**99.95**	**100.78**	**100.19**	**99.84**
Si	2.998	3.018	2.995	3.002
Al	1.918	1.935	1.968	1.925
Fe3	0.086	0.028	0.041	0.072
Fe2	1.979	2.094	2.086	2.106
Mn	0.161	0.173	0.161	0.154
Mg	0.594	0.529	0.546	0.535
Ca	0.264	0.223	0.202	0.207
Sum	**8.000**	**8.000**	**7.999**	**8.001**
Xalm	0.660	0.694	0.696	0.702
Xprp	0.198	0.175	0.182	0.178
Xgrs	0.088	0.074	0.067	0.069
Xsps	0.054	0.057	0.054	0.051

Table 17: Representative analyses of orthopyroxene. ***ba7px19*** *matrix orthopyroxene core (BA7),* ***ba7px20*** *matrix orthopyroxene rim (BA7),* ***ba7px21*** *matrix orthopyroxene core (BA7),* ***ba7px22*** *matrix orthopyroxene rim (BA7)*

Analysis	**ba7px19**	**ba7px20**	**ba7px21**	**ba7px22**
Mineral	opx	opx	opx	opx
SiO2	53.43	53.99	53.35	52.97
TiO2	<0.1	0.17	0.12	0.20
Al2O3	1.73	1.76	1.47	2.69
FeO	26.42	24.96	26.03	25.79
MnO	0.70	0.62	0.48	0.38
MgO	16.67	17.73	17.68	16.69
CaO	0.24	0.21	0.21	0.25
Total	**99.19**	**99.44**	**99.34**	**98.97**
Si	2.033	2.032	2.023	2.011
Ti	0.000	0.005	0.003	0.006
Al	0.078	0.078	0.066	0.120
Fe2	0.841	0.786	0.825	0.819
Mn	0.023	0.020	0.015	0.012
Mg	0.945	0.995	0.999	0.945
Ca	0.010	0.008	0.009	0.010
Sum	**3.930**	**3.924**	**3.940**	**3.923**
Xmg	0.529	0.559	0.548	0.536

Biotite is very common in dark layers and occurs as single flakes or aggregates of multiple grains. Most of the biotite flakes have a preferred orientation, which distinguishes this rock type from the migmatitic types. Biotite has a X_{Mg} ranging from 0.48–0.53 and small amounts of barium (up to 0.34 wt% BaO) were found in some grains. Titanium values are quite high (up to 4.87 wt% TiO_2), fluorine range from 0.40– 0.52 wt% (18), but no chlorine was found.

Table 18: Representative analyses of biotite. ***ba7bt3*** *matrix biotite core (BA7),* ***ba7bt4*** *matrix biotite rim (BA7),* ***ba7bt15*** *matrix biotite core (BA7), ba7bt16 matrix biotite rim (BA7),*

Analysis	**ba7bt3**	**ba7bt4**	**ba7bt15**	**ba7bt16**
Mineral	bt	bt	bt	bt
SiO2	36.27	36.72	36.62	36.33
TiO2	4.87	4.22	3.32	3.69
Al2O3	15.88	16.05	16.08	15.83
Cr2O3	<0.1	<0.1	<0.1	<0.1
FeO	19.18	17.97	18.92	18.35
MnO	<0.1	<0.1	0.00	0.00
MgO	10.27	11.22	11.21	11.59
CaO	<0.1	<0.1	<0.1	<0.1
BaO	0.22	0.20	0.34	0.00
Na2O	0.10	<0.1	0.28	0.15
K2O	9.82	9.67	8.83	9.26
F	0.42	0.50	0.52	0.41
Total	**96.85**	**96.34**	**96.00**	**95.44**
Si	2.738	2.763	2.774	2.759
Ti	0.276	0.239	0.189	0.211
Al	1.413	1.424	1.435	1.417
Cr	0.000	0.000	0.000	0.000
Fe2	1.211	1.131	1.198	1.165
Mn	0.000	0.000	0.000	0.000
Mg	1.156	1.259	1.266	1.312
Ca	0.000	0.000	0.000	0.000
Ba	0.007	0.006	0.010	0.000
Na	0.015	0.000	0.041	0.022
K	0.946	0.928	0.853	0.897
F	0.100	0.119	0.125	0.098
Sum	**6.816**	**6.822**	**6.913**	**6.886**
Xmg	0.488	0.527	0.514	0.530

2.5 Grt-Crd-Bt-Gneiss

This rock type describes the cordierite and garnet bearing gneiss in the Lichtenberg area, to the north of Linz and to the east from the Rodl fault (Figure 5). They show no migmatitic structure or clear foliation (Figure 22) and have the mineral assemblage cordierite + garnet + biotite + plagioclase + K-feldspar + quartz ± spinel ± sillimanite and the accessory minerals apatite + monazite + zircon + ilmenite + magnetite. In the main part of the rock biotites have no preferred orientation, but in zones with relatively small grains (<1mm) plagioclase, cordierite and biotite seems to define a foliation (Figure 23). Furthermore, cordierite contains inclusions of spinel and sillimanite in these zones. Sample BA58 was investigated in detail.

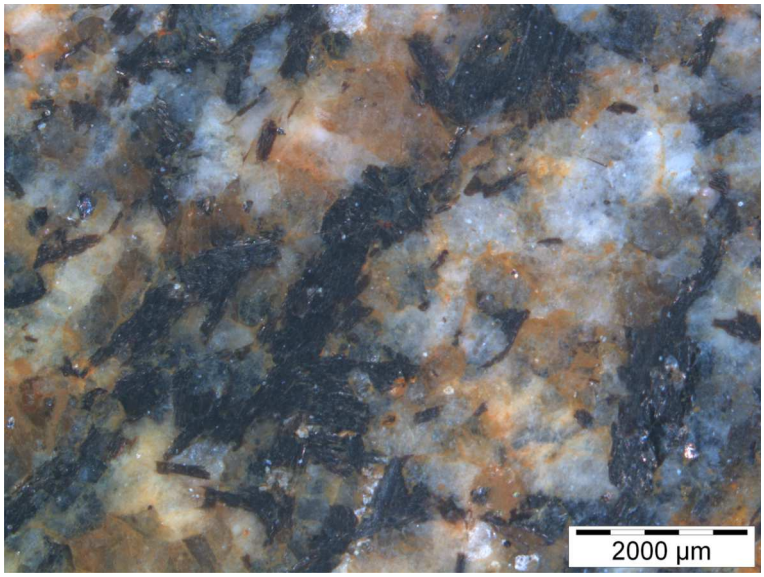

Figure 22: Stereomicroscope Image of Sample BA58

Plagioclase (1.5–2mm) and quartz (~1mm) build up most of the felsic matrix. Plagioclase shows polysynthetic twinning but no exsolution lamellae. Near the fine grained zones plagioclase displays myrmekitic intergrowth of quartz (Figure 23). The chemistry of plagioclase is albite-rich (X_{ab}=0.60–0.75) with sometimes anorthite-richer cores. K-feldspar components are very low (up to X_{or}=0.29), single grains also show a barium content of up to 0.18 wt% BaO (19).

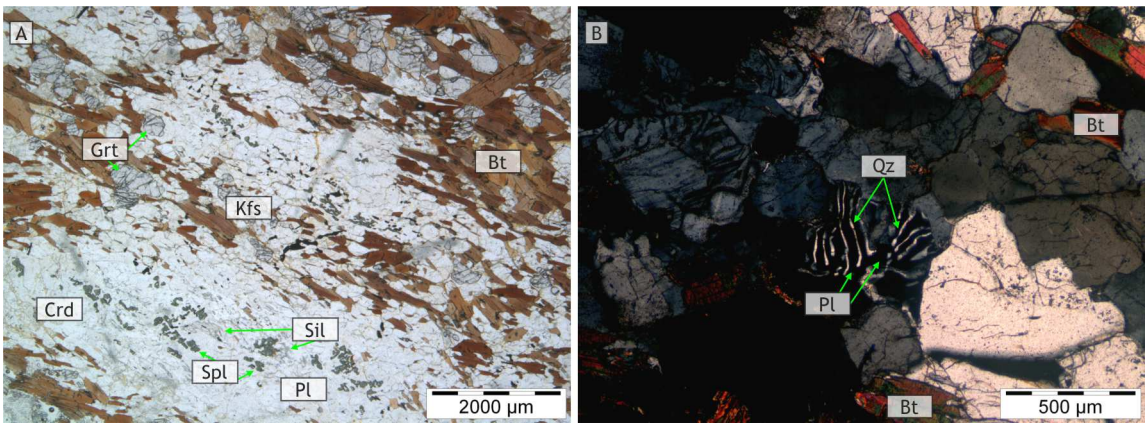

*Figure 23: Photomicrographs of **A** fine grained zone with orientated biotite, plagioclase and cordierite with inclusions of spinel and sillimanite. **B (crossed nicols)** Myrmekites occur often in small grained plagioclases*

K-feldpar is small (0.5–1mm) and uncommon. In the coarser grained zone K-feldspar occurs together with plagioclase, in the fine grained zone no K-feldspar was found. The composition varies with X_{ab} from 0.04–0.39, probably due to very fine exsolution lamellae of albite which were analysed together with the hosting K-feldspar. The barium content is high with values of up to 1.57 wt% BaO (19).

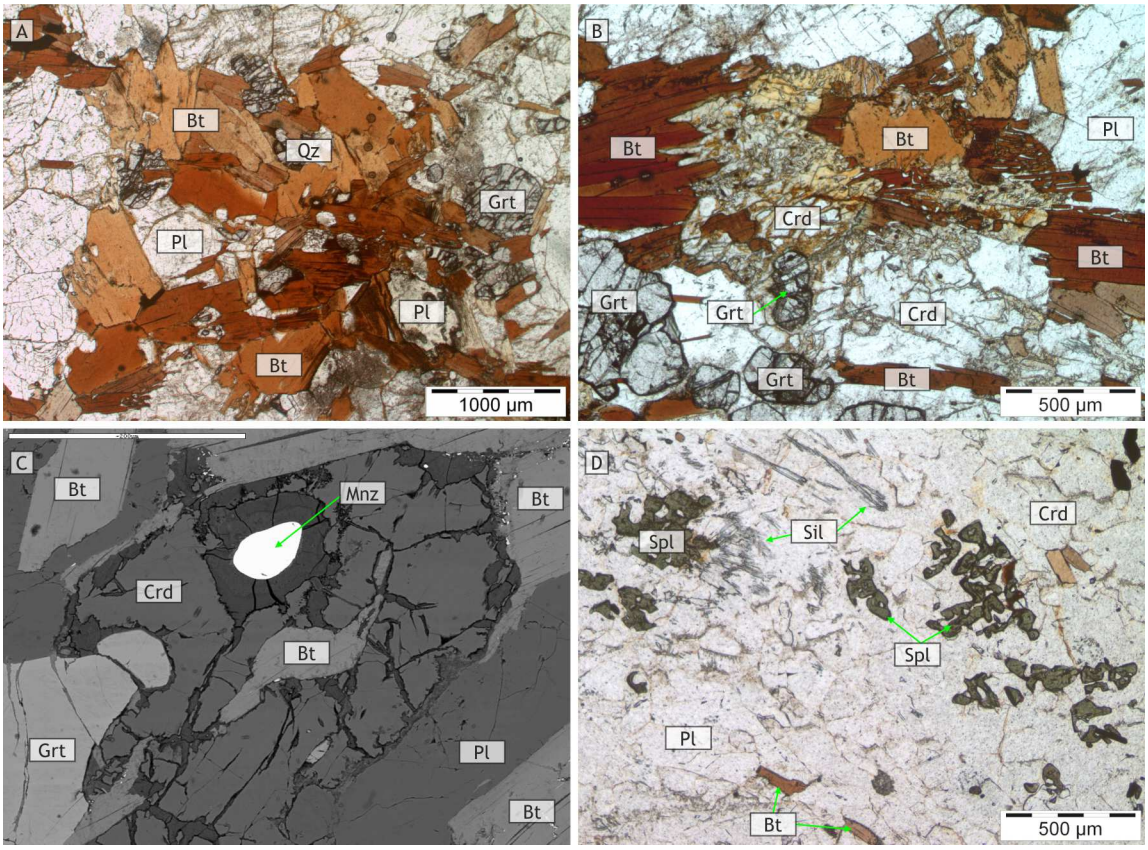

*Figure 24: Photomicrographs and Backscatter elecctron images (BSE) of **A** Biotite aggregate with small garnets. **B** Small garnet consumed by cordierite, the cordierite themselves is consumed by biotite. **C** Monazite inclusion in cordierite destroying the crystal structure due to radioactive radiation.(the scale bar represents 200µm) **D** Olive green spinel nest to sillimanite as inclusion in cordierite.*

Table 19: Representative analyses of feldspar. ***ba58fs6*** *plagioclase core (BA58),* ***ba58fs7*** *plagioclase rim (BA58),* ***ba58fs17*** *K-feldspar core (BA58),* ***ba58fs19*** *K-feldspar rim (BA58)*

Analysis	**ba58fs6**	**ba58fs7**	**ba58fs17**	**ba58fs19**
Mineral	pl	pl	kfs	kfs
SiO2	62.86	63.12	65.16	64.68
Al2O3	24.09	24.03	18.59	18.70
Fe2O3	<0.1	<0.1	<0.1	0.14
CaO	5.04	5.11	<0.1	<0.1
BaO	<0.1	0.13	0.83	1.57
Na2O	8.32	8.55	1.28	1.18
K2O	0.26	0.14	14.74	14.63
Total	**100.57**	**101.08**	**100.60**	**100.90**
Si	2.764	2.765	2.993	2.979
Al	1.248	1.241	1.006	1.015
Fe3	0.000	0.000	0.000	0.005
Ca	0.237	0.240	0.000	0.000
Ba	0.000	0.002	0.015	0.028
Na	0.709	0.726	0.114	0.105
K	0.015	0.008	0.864	0.860
Sum	**4.973**	**4.982**	**4.992**	**4.992**
Xab	0.738	0.744	0.115	0.106
Xan	0.247	0.246	0.000	0.000
Xor	0.016	0.008	0.870	0.866
Xcls	0.000	0.002	0.015	0.028

Garnet grains are small (up to 1mm) and in most cases they look resorbed either by biotite or by cordierite (Figure 24). They are homogeneous in composition and belong to an almandine-pyrope solid solution (X_{alm}=0.72–0.74, X_{prp}=0.19–0.22), with minor amounts of grossular (X_{grs}=0.025–0.030) and spessartine (X_{sps}=0.035–0.040) (20).

Cordierite is uncommon, has grain sizes ranging from 0.2–1mm, and often grows around small garnet grains. Cordierite is frequently affected by pinitisation or is consumed by biotite (Figure 24).Inclusions of monazite (50–100µm) produce radiation damage in cordierite which is seen in a heavily pinitised zone around the inclusion (Figure 24). Cordierite in the fine grained zone is usually fresh and has inclusions of olive green spinel and sillimanite (Figure 24). The Mg-cordierite component is higher compared to other samples with X_{Mg} of 0.65–0.67. Small contents of manganese (up to 0.19 wt% MnO) and sodium (0.05–0.10 wt% Na_2O) were found (21).

Table 20: Representative analyses of garnet. ***ba58gt25*** *garnet core (BA58),* ***ba58gt26*** *garnet rim (BA58),* ***ba58gt27*** *garnet core (BA58),* ***ba58gt28*** *garnet rim (BA58)*

Analysis	**ba58gt25**	**ba58gt26**	**ba58gt27**	**ba58gt28**
Mineral	grt	grt	grt	grt
SiO2	37.65	38.19	38.10	38.42
Al2O3	20.87	20.77	20.92	21.19
FeO	33.30	33.06	32.85	32.46
MnO	1.59	1.52	1.67	1.77
MgO	4.94	5.00	5.35	5.38
CaO	1.04	0.98	0.87	0.96
Total	**99.39**	**99.52**	**99.76**	**100.18**
Si	3.014	3.044	3.028	3.033
Al	1.969	1.951	1.960	1.972
Fe3	0.002	0.000	0.000	0.000
Fe2	2.228	2.204	2.184	2.143
Mn	0.108	0.103	0.112	0.118
Mg	0.590	0.594	0.634	0.633
Ca	0.089	0.084	0.074	0.081
Sum	**8.000**	**7.980**	**7.992**	**7.980**
Xalm	0.739	0.738	0.727	0.720
Xprp	0.196	0.199	0.211	0.213
Xgrs	0.030	0.028	0.025	0.027
Xsps	0.036	0.035	0.037	0.040

Table 21: Representative analyses of cordierite. ***ba58cd50*** *cordierite core (BA58),* ***ba58cd51*** *cordierite rim (BA58),* ***ba58cd52*** *cordierite core (BA58),* ***ba58cd50*** *cordierite rim (BA58)*

Analysis	**ba58cd50**	**ba58cd51**	**ba58cd52**	**ba58cd53**
Mineral	crd	crd	crd	crd
SiO2	48.95	49.27	48.36	49.05
Al2O3	32.90	32.66	32.71	32.60
FeO	7.79	7.67	7.77	7.55
MnO	0.19	<0.1	<0.1	0.12
MgO	8.23	8.56	8.44	8.82
Na2O	0.08	0.09	0.05	0.08
K2O	<0.1	<0.1	<0.1	<0.1
Total	**98.14**	**98.25**	**97.33**	**98.22**
Si	5.032	5.052	5.012	5.034
Al	3.986	3.947	3.996	3.943
Fe2	0.670	0.658	0.673	0.648
Mn	0.017	0.000	0.000	0.010
Mg	1.261	1.309	1.304	1.350
Na	0.016	0.018	0.010	0.016
K	0.000	0.000	0.000	0.000
Sum	**10.982**	**10.984**	**10.995**	**11.001**
Xmg	0.653	0.665	0.660	0.676

Table 22: Representative analyses of biotite. ***ba58bt35*** *biotite core (BA58),* ***ba58bt36*** *biotite rim (BA58),* ***ba58bt37*** *biotite core (BA58),* ***ba58bt35*** *biotite rim (BA58)*

Analysis	**ba58bt35**	**ba58bt36**	**ba58bt37**	**ba58bt38**
Mineral	bt	bt	bt	bt
SiO2	37.09	35.25	36.34	36.10
TiO2	3.37	3.15	2.92	3.24
Al2O3	18.41	18.10	18.56	18.18
Cr2O3	<0.1	0.14	<0.1	<0.1
FeO	17.56	17.99	17.32	17.22
MnO	<0.1	<0.1	<0.1	<0.1
MgO	10.73	10.71	11.22	10.15
CaO	<0.1	<0.1	<0.1	<0.1
Na2O	0.19	0.20	0.09	0.11
K2O	9.53	9.65	9.79	9.64
F	0.39	0.37	0.31	0.30
Total	**97.27**	**95.56**	**96.55**	**94.94**
Si	2.743	2.679	2.711	2.739
Ti	0.187	0.180	0.164	0.185
Al	1.605	1.621	1.632	1.625
Cr	0.000	0.008	0.000	0.000
Fe2	1.086	1.143	1.081	1.092
Mn	0.000	0.000	0.000	0.000
Mg	1.183	1.213	1.248	1.148
Ca	0.000	0.000	0.000	0.000
Na	0.027	0.029	0.013	0.016
K	0.899	0.935	0.932	0.933
F	0.091	0.089	0.073	0.072
Sum	**7.821**	**7.897**	**7.854**	**7.810**
Xmg	0.521	0.515	0.536	0.513

Biotite is common and occurs as aggregates of multiple single grains (Figure 24) with a size ranging from 0.5–2mm. Biotite seems to be growing at the expanse of garnet as well at the expanse of cordierite (Figure 24). The occurrence of biotite-quartz symplectites indicate interaction with a melt phase. The phlogopite content (X_{Mg}) of biotite ranges from 0.50 to 0.53 (22) and decreases in some cases towards the rim. The titanium content is ranging from 2.90–3.40 wt% TiO_2, chromium values are low (up to 0.14 wt% Cr_2O_3) and fluorine content is up to 0.45 wt%. In some grains small amounts of sodium (0.10–0.20 wt% Na_2O) were detected.

Olive green spinel occurs as inclusion in cordierite next to sillimanite in the fine grained zone (Figure 24). The composition is iron-rich (X_{hc}=0.74–0.77) with small amounts of chromium (0.13–0.17 wt% Cr_2O_3) and some zinc (2.40–3.76 wt% ZnO) (23).

Table 23: Representative analyses of spinel. ***ba58sp40*** *spinel inclusion in cordierite (BA58),* ***ba58sp41*** *spinel inclusion in cordierite (BA58),* ***ba58sp42*** *spinel inclusion in cordierite (BA58)*

Analysis	**ba58sp40**	**ba58sp41**	**ba58sp42**
Mineral	spl	spl	spl
SiO2	0.20	0.40	<0.1
TiO2	<0.1	<0.1	<0.1
Al2O3	57.93	57.73	57.74
Cr2O3	0.13	0.17	0.15
V2O3	<0.1	<0.1	<0.1
FeO	33.51	32.28	33.57
MnO	0.15	0.15	0.14
MgO	4.16	4.14	4.33
ZnO	2.41	3.76	2.52
Total	**98.49**	**98.63**	**98.45**
Si	0.006	0.011	0.000
Ti	0.000	0.000	0.000
Al	1.956	1.951	1.950
Cr	0.003	0.004	0.003
V	0.000	0.000	0.000
Fe3	0.029	0.023	0.046
Fe2	0.773	0.751	0.758
Mn	0.004	0.004	0.003
Mg	0.178	0.177	0.185
Zn	0.051	0.080	0.053
Sum	**2.994**	**2.990**	**2.998**
Xspl	0.178	0.176	0.186
Xhc	0.771	0.744	0.760
Xghn	0.051	0.080	0.053
Xchr	0.002	0.002	0.002

2.6 Crd-Bt-Migmatite/Anatexite type 1

Cordierite and biotite bearing migmatite is very common and occur all over the working area. The investigated samples are from (1) the Lichtenberg area (BA62) north of Linz, (2) the Bad Leonfelden area (BA76, DS66) west of the Rodl fault and from (3) the Sauwald area (BA31) next to Schärding (Figure 5). The rocks have the mineral assemblage cordierite + biotite + plagioclase + perthitic K-feldspar + quartz + sillimanite + ilmenite ± rutile ± muscovite and the accessory minerals zircon + apatite + magnetite + monazite+ pyrite ± sphalerite ± chalcopyrite. These rocks are rich in plagioclase and have a dark colour due to high amounts of biotite (Figure 25). These rocks are the product of intensive melting (anatexite). The samples BA62, BA76, DS66 and BA31 were investigated in detail.

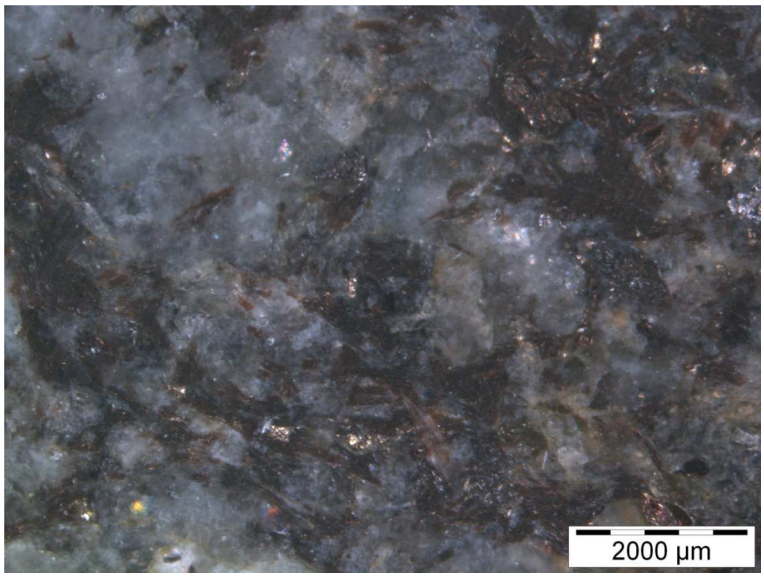

Figure 25: Stereomicroscope Image of Sample DS66

The felsic matrix of these rocks is composed of large plagioclase, K-feldspar and quartz (1–3mm) grains. Plagioclase seldom shows polysynthetic twinning and sometimes a kind of K-feldspar exsolution around quartz inclusions. Larger plagioclase is overgrown by biotite and sillimanite (Figure 26) and have multiple inclusions. They have an albite-rich composition with elevated anorthite content in the cores (rim: X_{an}=0.18–0.23, core: X_{an}=0.20–0.26) (24).

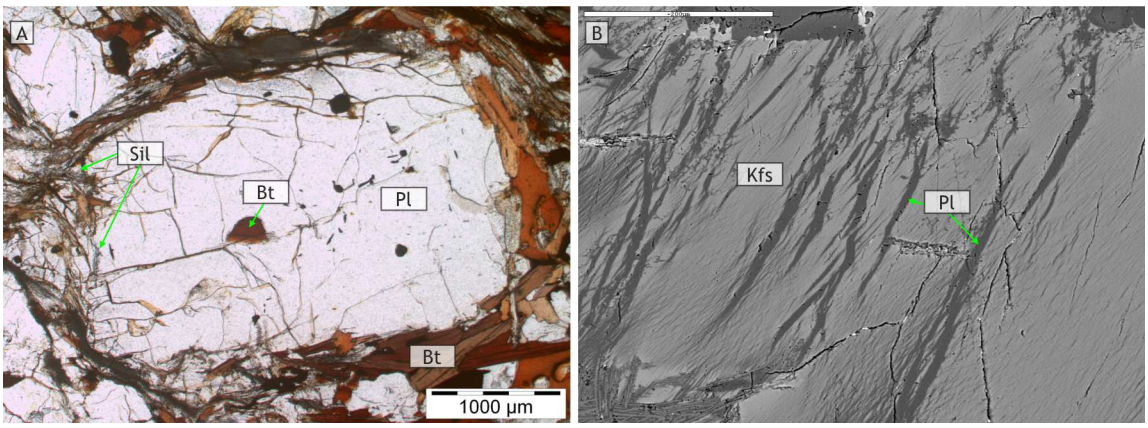

*Figure 26: Photomicrographs and Backscatter elecctron images (BSE) of **A** Large matrix plagioclase surrounded by biotite and sillimanite, with inclusions of biotite, pyrite and ilmenite. **B** K-feldspar shows large perthitic exsolution lamellae. (the scale bar represents 500µm)*

Most of the larger K-feldspar grains show clear exsolution lamellae (Figure 26) of almost pure albite (X_{ab}=0.97–0.98). They contain 8–11 mol% albite, have a very low CaO content of 0.1 wt %. Barium contents range from 0.33–0.52 wt% BaO (24).

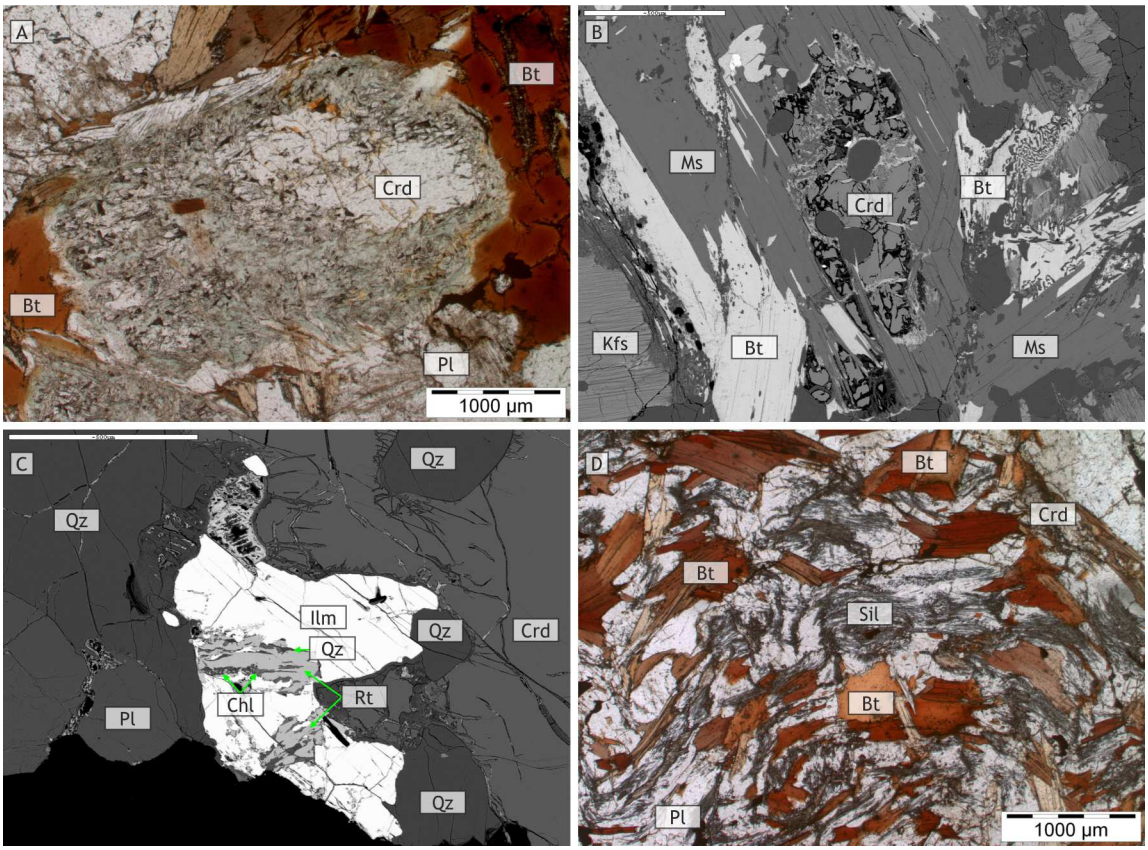

*Figure 27: Photomicrographs and Backscatter elecctron images (BSE) of **A** Most cordierites are heavily or completely pinitised. **B** Sample BA76 contain large muscovite grains grown around consumed cordierites. (the scale bar represents 500µm) **C** The large ilmenites are often intergrown with rutile. (the scale bar represents 500µm) **D** Sillimanite is common in sample DS66 and seems to have grown together with biotite.*

Table 24: Representative analyses of feldspar. ***ds66fs5*** *plagioclase core (DS66),* ***ds66fs5*** *plagioclase rim (DS66),* ***76fs25*** *plagioclase core (BA76),* ***76fs26*** *plagioclase rim (BA76),* ***76fs19*** *K-feldspar (BA76),* ***ds66fs14*** *K-feldspar (DS66)*

Analysis	**ds66fs5**	**ds66fs6**	**76fs25**	**76fs26**	**76fs19**	**ds66fs14**
Mineral	pl	pl	pl	pl	kfs	kfs
SiO2	61.69	63.43	63.29	64.33	64.73	64.18
Al2O3	24.30	23.80	23.66	23.28	18.51	18.57
Fe2O3	<0.1	<0.1	0.00	0.00	<0.1	<0.1
CaO	5.06	4.42	4.24	3.72	<0.1	<0.1
BaO	<0.1	<0.1	0.14	<0.1	0.52	0.49
Na2O	7.87	8.22	8.76	9.11	1.14	0.98
K2O	0.34	0.25	0.24	<0.1	15.09	15.01
Total	**99.27**	**100.12**	**100.33**	**100.44**	**99.99**	**99.22**
Si	2.748	2.791	2.787	2.818	2.991	2.987
Al	1.276	1.234	1.228	1.202	1.008	1.018
Fe3	0.000	0.000	0.000	0.000	0.000	0.000
Ca	0.241	0.208	0.200	0.175	0.000	0.000
Ba	0.000	0.000	0.002	0.000	0.009	0.009
Na	0.680	0.701	0.748	0.774	0.102	0.088
K	0.019	0.014	0.013	0.000	0.890	0.891
Sum	**4.964**	**4.948**	**4.978**	**4.969**	**5.000**	**4.993**
Xab	0.723	0.759	0.777	0.816	0.102	0.089
Xan	0.256	0.225	0.208	0.184	0.000	0.000
Xor	0.020	0.015	0.013	0.000	0.889	0.902
Xcls	0.000	0.000	0.002	0.000	0.009	0.009

Cordierite grains range in size from 0.5–2mm, but in several samples they are heavily affected by pinitisation (Figure 27). In samples BA62 and DS66 cordierite is usually surrounded by, or occurs together with larger biotite grains. In sample BA76 large muscovite grains also occur next to biotite (Figure 27). The cordierite composition varies from sample to sample (X_{Mg}=0.50–0.70), but is relatively constant within each sample (25). Manganese content range from 0.20–0.80 wt% MnO, sodium values from 0.12–0.26 wt% Na_2O.

Biotite grains have up to several mm in size. The composition of matrix biotite is relatively iron-rich (X_{Mg}=0.42–0.47), inclusions in plagioclase and fine grained biotite in cordierite alterations are richer in magnesium content (up to X_{Mg}=0.55). The titanium content ranges from 0.11 wt% in pinites to 3.90 wt% TiO_2 in matrix biotite. Small amounts of manganese (0.11–0.23 wt% MnO) and chromium were detected as well (26).

Table 25: Representative analyses of cordierite. ***ds66cd1*** *cordierite core (DS66),* ***ds66cd1*** *cordierite rim (DS66),* ***76cd1*** *cordierite core (BA76),* ***76cd2*** *cordierite rim (BA76)*

Analysis	**ds66cd1**	**ds66cd2**	**76cd1**	**76cd2**
Mineral	crd	crd	crd	crd
SiO2	47.67	47.63	48.29	47.83
Al2O3	32.79	32.08	32.00	32.27
FeO	9.16	9.84	10.56	10.53
MnO	0.30	0.47	0.46	0.46
MgO	7.83	7.27	6.43	6.53
Na2O	0.12	0.19	0.25	0.22
K2O	<0.1	<0.1	<0.1	<0.1
Total	**97.86**	**97.49**	**97.99**	**97.84**
Si	4.960	4.996	5.048	5.010
Al	4.020	3.966	3.942	3.984
Fe2	0.797	0.863	0.923	0.922
Mn	0.026	0.042	0.041	0.041
Mg	1.214	1.136	1.002	1.020
Na	0.025	0.039	0.051	0.045
K	0.000	0.000	0.000	0.000
Sum	**11.042**	**11.042**	**11.007**	**11.022**
Xmg	0.604	0.568	0.521	0.525

Ilmenite is almost pure $FeTiO_3$ but with small amounts of manganese (0.97–2.37 wt% MnO) and magnesium (0.67–1.05 wt% MgO). Sometimes ilmenite is intergrown with rutile, chlorite and quartz (Figure 27), this probably shows the rutile forming reaction:

$$\text{Ilm} + \text{Silicate (e.g. Crd, Bt)} + H_2O = \text{Rt} + \text{Chl} \qquad (2)$$

Sillimanite is relatively uncommon in most samples, however, in sample DS66 it occurs in high amounts and seems to have grown together with biotite (Figure 27).

Table 26: Representative analyses of biotite. ***ds66bt19*** *biotite core (DS66),* ***ds66bt20*** *biotite rim (DS66),* ***76bt15*** *biotite core (BA76),* ***76bt16*** *biotite rim (BA76),* ***ds66bt21*** *biotite inclusion in plagioclase (DS66),* ***62bt11*** *fine grained pinite biotite (BA62)*

Analysis	**ds66bt19**	**ds66bt20**	**76bt15**	**76bt16**	**ds66bt21**	**62bt11**
Mineral	bt	bt	bt	bt	bt	bt
SiO2	35.11	35.81	35.47	35.18	36.55	35.48
TiO2	3.90	2.82	2.49	2.40	3.20	0.11
Al2O3	18.81	19.70	19.85	20.01	19.33	21.24
Cr2O3	0.17	<0.1	<0.1	<0.1	<0.1	<0.1
FeO	19.88	18.96	20.49	20.23	18.28	16.51
MnO	0.11	0.16	0.23	0.19	0.11	0.17
MgO	9.95	9.14	8.73	8.53	10.11	11.63
CaO	<0.1	<0.1	<0.1	<0.1	<0.1	0.11
Na2O	0.11	0.15	0.15	0.12	0.19	0.25
K2O	9.56	9.16	9.54	9.27	9.50	9.39
F	0.44	0.45	0.49	0.50	0.42	0.38
Total	**98.05**	**96.35**	**97.44**	**96.43**	**97.68**	**95.27**
Si	2.622	2.692	2.666	2.666	2.702	2.667
Ti	0.219	0.160	0.141	0.137	0.178	0.006
Al	1.656	1.746	1.758	1.787	1.684	1.882
Cr	0.010	0.000	0.000	0.000	0.000	0.000
Fe2	1.242	1.192	1.288	1.282	1.130	1.038
Mn	0.007	0.010	0.015	0.012	0.007	0.011
Mg	1.107	1.024	0.978	0.964	1.114	1.303
Ca	0.000	0.000	0.000	0.000	0.000	0.009
Na	0.016	0.022	0.022	0.018	0.027	0.036
K	0.911	0.879	0.915	0.896	0.896	0.901
F	0.104	0.106	0.116	0.120	0.098	0.090
Sum	**7.894**	**7.831**	**7.783**	**7.762**	**7.836**	**7.853**
Xmg	0.471	0.462	0.432	0.429	0.496	0.557

2.7 Crd-Bt-Migmatite/Anatexite type 2

This special type of migmatite occurs just north of the Bad Leonfelden area, near the border to the Czech Republic (Figure 5). The mineral assemblage is quite similar to type 1 but the rocks look completely different. Large plagioclase and cordierite porphyroblasts occur in a fine grained recrystallized plagioclase, quartz and biotite matrix (Figure 28). The samples DS6 and DS8 were investigated in detail.

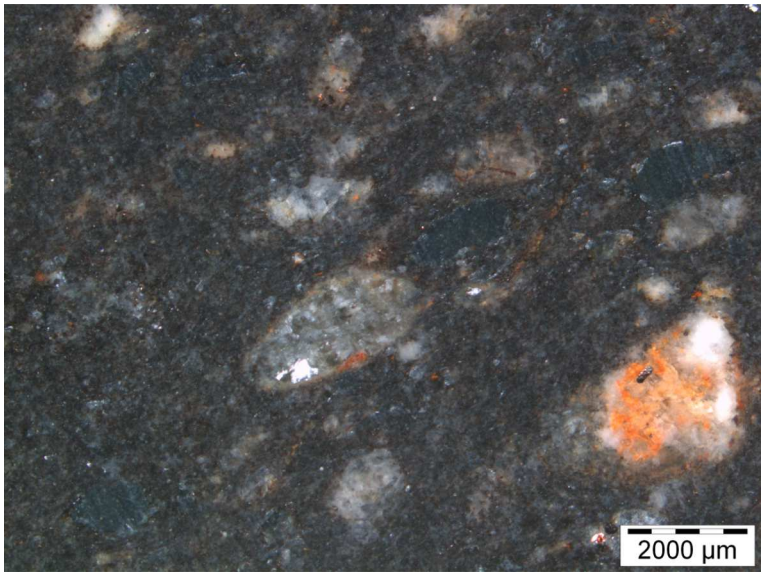

Figure 28: Stereomicroscope Image of Sample DS6

Plagioclase occurs in two different types, first as small grains (100–200µm) in the matrix and second as large (3–4mm) porphyroblasts. Both have an albite-rich composition (X_{ab}=0.73–0.75), only some grains show chemical zoning (Figure 29) with higher amounts of anorthite component in the core (X_{ab}=0.66) (27). Furthermore all of the larger plagioclase grains have multiple inclusions of biotite, quartz, sillimanite and very uncommon even garnet (Figure 29). Enclosed quartz grains in plagioclase cores are surrounded by thin rim of K-feldspar (Figure 29). K-feldspar occurs as 1–2mm large grains, whereas larger grains show typically perthitic exsolution lamellae. K-feldspar in the matrix has albite contents of X_{ab}=0.09–0.17. The thin K-feldspar rims around quartz which are enclosed in plagioclase, have lower albite values (X_{ab}=0.03–0.06). Barium values range from 0.43–0.60 wt% BaO (27).

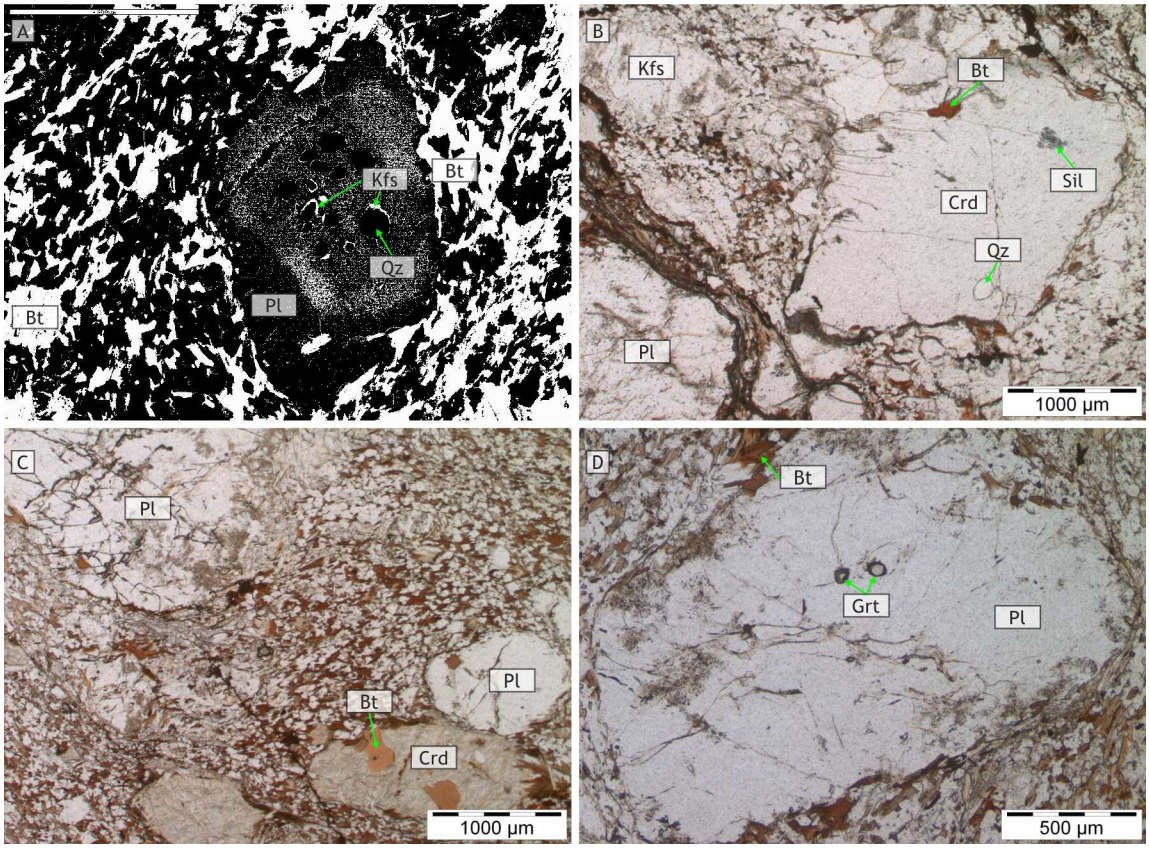

*Figure 29: Photomicrographs and Backscatter elecctron images (BSE) of **A** Chemical zoned plagioclase, with quartz inclusions surrounded by K-feldspar. (high contrast, the scale bar represents 500µm) **B** Cordierite with inclusions of biotite, quartz and sillimanite. **C** Large plagioclase porphyroblasts and pinitised cordierite in a fine grained biotite and plagioclase matrix. **D** Some of the large plagioclase porphyroblasts show inclusions of small garnets.*

Cordierite grains range in size from 1–3mm and have inclusions of biotite, sillimanite and quartz (Figure 29). Most of the cordierite grains are affected by pinitisation, smaller grains are completely pinitised (Figure 29). The composition is similar to type 1 Crd-Bt-migmatite/anatexite (X_{Mg}=0.56–0.63). Sometimes a slightly increase in magnesium towards the rim can be observed. The sodium content is slightly higher (0.18–0.44 wt% Na_2O) in type 2 samples. Manganese values values range from 0.28–0.46 wt% MnO, (28).

Biotite occurs as fine grained recrystallized matrix grains (100–200µm), as well as inclusions in plagioclase and cordierite (up to 500µm). Matrix biotite has a higher X_{Mg}=0.43–0.45 compared to inclusions (X_{Mg}=0.33–0.42), other elements do not show any differences between matrix and inclusion biotite. Chromium (up to 0.16 wt% Cr_2O_3), manganese (0.13–0.28 wt% MnO) and sodium (0.07–0.13 wt% Na_2O) (29) contents are similar to samples from type 1 (26).

Table 27: Representative analyses of feldspar. ***ds6fs6*** *plagioclase core (DS6),* ***ds6fs7*** *plagioclase rim (DS6),****ds8fs13*** *plagioclase core (DS8),* ***ds8fs12*** *plagioclase rim (DS8),* ***ds6fs9*** *matrix K-feldspar (DS6),* ***ds8fs14*** *K-feldspar inclusion in plagioclase (DS8)*

Analysis	**ds6fs6**	**ds6fs7**	**ds8fs13**	**ds8fs12**	**ds6fs9**	**ds8fs14**
Mineral	pl	pl	pl	pl	kfs	kfs
SiO2	63.04	62.25	60.80	62.60	63.90	64.63
Al2O3	23.70	24.60	25.07	23.28	18.62	18.48
Fe2O3	<0.1	<0.1	<0.1	0.10	<0.1	<0.1
CaO	4.86	5.38	6.36	4.96	<0.1	<0.1
BaO	<0.1	<0.1	<0.1	<0.1	0.43	0.76
Na2O	8.57	8.51	7.26	8.11	1.42	0.48
K2O	0.36	0.20	0.32	0.19	14.75	15.29
Total	**100.53**	**100.94**	**99.81**	**99.24**	**99.12**	**99.64**
Si	2.775	2.734	2.703	2.786	2.978	2.998
Al	1.230	1.273	1.313	1.221	1.023	1.010
Fe3	0.000	0.000	0.000	0.003	0.000	0.000
Ca	0.229	0.253	0.303	0.236	0.000	0.000
Ba	0.000	0.000	0.000	0.000	0.008	0.014
Na	0.731	0.725	0.626	0.700	0.128	0.043
K	0.020	0.011	0.018	0.011	0.877	0.905
Sum	**4.985**	**4.996**	**4.963**	**4.957**	**5.014**	**4.970**
Xab	0.746	0.733	0.661	0.739	0.126	0.045
Xan	0.234	0.256	0.320	0.249	0.000	0.000
Xor	0.020	0.011	0.019	0.012	0.866	0.941
Xcls	0.000	0.000	0.000	0.000	0.008	0.015

Table 28: Representative analyses of cordierite. ***ds6cd1*** *cordierite core (DS6),* ***ds6cd2*** *cordierite rim (DS6),* ***ds6cd4*** *cordierite core (DS6),* ***ds6cd5*** *cordierite rim (DS6)*

Analysis	**ds6cd1**	**ds6cd2**	**ds6cd4**	**ds6cd5**
Mineral	crd	crd	crd	crd
SiO2	48.74	48.05	47.62	48.56
Al2O3	31.97	32.64	32.64	32.14
FeO	9.84	9.11	9.98	8.72
MnO	0.29	0.40	0.28	0.46
MgO	7.36	7.09	7.12	8.30
Na2O	0.24	0.18	0.23	0.44
K2O	<0.1	<0.1	<0.1	<0.1
Total	**98.44**	**97.47**	**97.87**	**98.62**
Si	5.051	5.014	4.973	5.011
Al	3.905	4.014	4.017	3.909
Fe2	0.853	0.795	0.872	0.753
Mn	0.025	0.035	0.025	0.040
Mg	1.137	1.103	1.108	1.277
Na	0.048	0.036	0.047	0.088
K	0.000	0.000	0.000	0.000
Sum	**11.019**	**10.997**	**11.042**	**11.078**
Xmg	0.571	0.581	0.560	0.629

Table 29: Representative analyses of biotite. ***ds6bt15*** *matrix biotite (DS6),* ***ds8bt22*** *matrix biotite (DS8),* ***ds6bt14*** *biotite inclusion in plagioclase (DS6),* ***ds8bt10*** *biotite inclusion in plagioclase (DS8)*

Analysis	**ds6bt15**	**ds8bt22**	**ds6bt14**	**ds8bt10**
Mineral	bt	bt	bt	bt
SiO2	35.21	34.70	36.36	34.13
TiO2	2.85	2.82	3.36	3.45
Al2O3	19.30	18.42	19.81	17.52
Cr2O3	0.12	0.12	0.14	0.10
FeO	19.46	20.38	19.20	22.14
MnO	0.15	0.24	0.17	0.28
MgO	8.53	9.15	8.09	6.21
CaO	<0.1	<0.1	<0.1	<0.1
ZnO	<0.1	0.11	<0.1	<0.1
Na2O	0.10	0.07	0.13	0.05
K2O	9.77	9.76	9.90	9.66
F	0.58	0.41	0.50	0.41
Total	**96.07**	**96.18**	**97.66**	**93.95**
Si	2.682	2.658	2.709	2.706
Ti	0.163	0.162	0.188	0.206
Al	1.733	1.663	1.739	1.637
Cr	0.007	0.007	0.008	0.006
Fe2	1.240	1.305	1.196	1.468
Mn	0.010	0.016	0.011	0.019
Mg	0.969	1.045	0.898	0.734
Ca	0.000	0.000	0.000	0.000
Zn	0.000	0.006	0.000	0.000
Na	0.015	0.010	0.019	0.008
K	0.949	0.954	0.941	0.977
F	0.140	0.099	0.118	0.103
Sum	**7.768**	**7.826**	**7.709**	**7.761**
Xmg	0.439	0.445	0.429	0.333

Very uncommon are small garnet inclusions (50–100µm) in plagioclase porhpyroblasts (Figure 29), however no garnets were found in the matrix of the Crd-Bt-migmatite/anatexite. The composition is iron-rich (X_{alm}=0.75–0-77) with minor amounts of magnesium (X_{prp}=0.09–0.12) and calcium (X_{grs}=0.022–0.026). Conspicuous is the relatively high manganese value (X_{sps}=0.10–0.11) (30).

Ilmenite is common and enriched in manganese composition (up to 5.22 wt% MnO).

Table 30: Representative analyses of garnet. ***Ds8gt1–ds8gt4*** *garnet inclusion in plagioclase (DS8)*

Analysis	**ds8gt1**	**ds8gt2**	**ds8gt3**	**ds8gt4**
Mineral	grt	grt	grt	grt
SiO2	36.77	37.64	37.20	37.27
Al2O3	20.32	20.48	19.96	20.15
FeO	33.08	33.05	32.73	32.97
MnO	4.32	4.45	4.26	4.49
MgO	2.97	2.37	2.67	2.39
CaO	0.75	0.82	0.88	0.82
Total	**98.21**	**98.81**	**97.70**	**98.09**
Si	3.022	3.066	3.066	3.064
Al	1.968	1.966	1.939	1.952
Fe3	0.000	0.000	0.000	0.000
Fe2	2.274	2.252	2.256	2.267
Mn	0.301	0.307	0.297	0.313
Mg	0.364	0.288	0.328	0.293
Ca	0.066	0.072	0.078	0.072
Sum	**7.995**	**7.951**	**7.964**	**7.961**
Xalm	0.757	0.771	0.762	0.770
Xprp	0.121	0.099	0.111	0.099
Xgrs	0.022	0.025	0.026	0.024
Xsps	0.100	0.105	0.100	0.106

Table 31: Representative analyses of garnet. ***ba67gt1*** *garnet core (BA67),* ***ba67gt2*** *garnet rim (BA67)*

Analysis	**ba67gt1**	**ba67gt2**
Mineral	grt	grt
SiO2	36.81	36.99
Al2O3	21.11	20.70
FeO	32.58	33.45
MnO	5.93	4.20
MgO	2.50	3.21
CaO	1.90	1.38
Total	**100.83**	**99.93**
Si	2.953	2.984
Al	1.996	1.968
Fe3	0.098	0.065
Fe2	2.088	2.191
Mn	0.403	0.287
Mg	0.299	0.386
Ca	0.163	0.119
Sum	**8.000**	**8.000**
Xalm	0.707	0.734
Xprp	0.101	0.129
Xgrs	0.055	0.040
Xsps	0.136	0.096

2.8 Mylonite (Rodl fault)

Mylonite occurs along the NNE–SSW running Rodl shear zone in the west of the Lichtenberg zone (Figure 5) and contain the mineral assemblage quartz + biotite + muscovite + chlorite ± plagioclase ± K-feldspar ± garnet ± ilmenite ± allanite. They show a typical mylonitic texture (Figure 30) with recrystallized quartz and feldspar grains. Sample BA67 and DS25 were investigated.

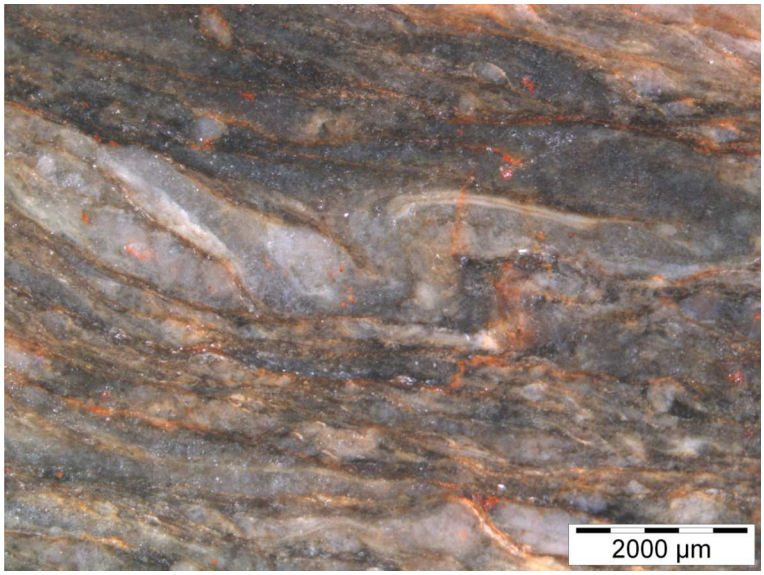

Figure 30: Stereomicroscope Image of Sample DS25

Quartz, plagioclase as well as K-feldspar have grain sizes ranging from very fine recrystallized grains (50µm) up to 1mm. The larger ones appear in most cases as σ-clasts (Figure 31). Under crossed nicols the recrystallisation is well observable (Figure 31).

Garnets are common in sample BA67, are surrounded by chloritized biotite and have a size ranging from 1–2mm (Figure 31). No chemical zoning was observed. The chemical composition is X_{alm}=0.70–0.74, X_{prp}=0.10–0.13, X_{grs}=0.040–0.055 and X_{sps}=0.09–0.14 (31).

Allanite a rare earth element bearing sorosilicate which is sometimes seen next to muscovite and chloritized biotite (Figure 31).

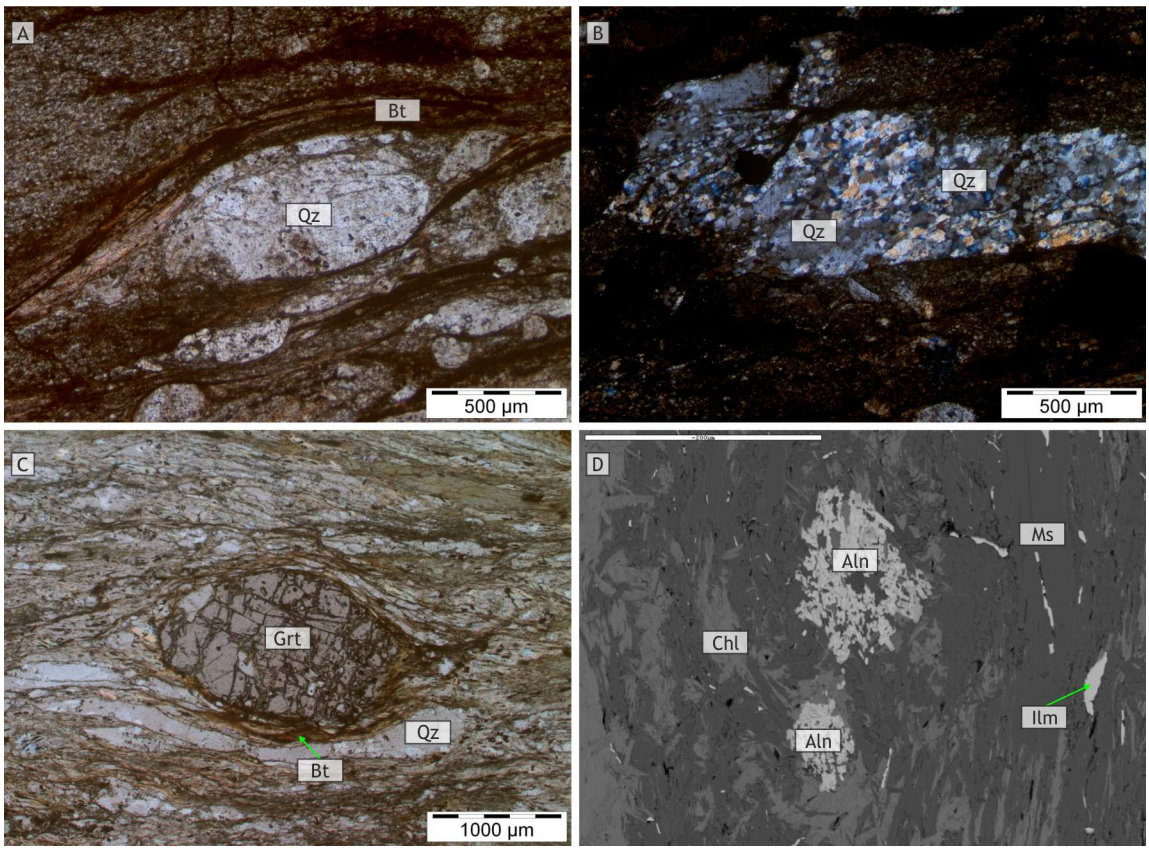

*Figure 31: Photomicrographs and Backscatter elecctron images (BSE) of **A** A large quartz grain forming a σ-clast. **B (crossed nicols)** Fine grained recrystallized quartz grains. **C** Garnet grain surrounded by biotite. **D** Allanite is occurs uncommon in sample BA67. (the scale bar represents 200µm)*

2.9 Mafic Lenses

Mafic lenses of different mineralogical compositions occur predominantly in the danube valley (Figure 5) within the felsic migmatites. They have a generally dark and fine grained appearance (Figure 32) with the mineral assemblage plagioclase + quartz + clinopyroxene + hornblend ± orthopyroxene ± garnet ± biotite ± sphene ± ilmenite ± spinel and the accessory minerals zircon + apatite + monazite+ pyrite ± scheelite. The samples ML09-16 and DS19 were investigated.

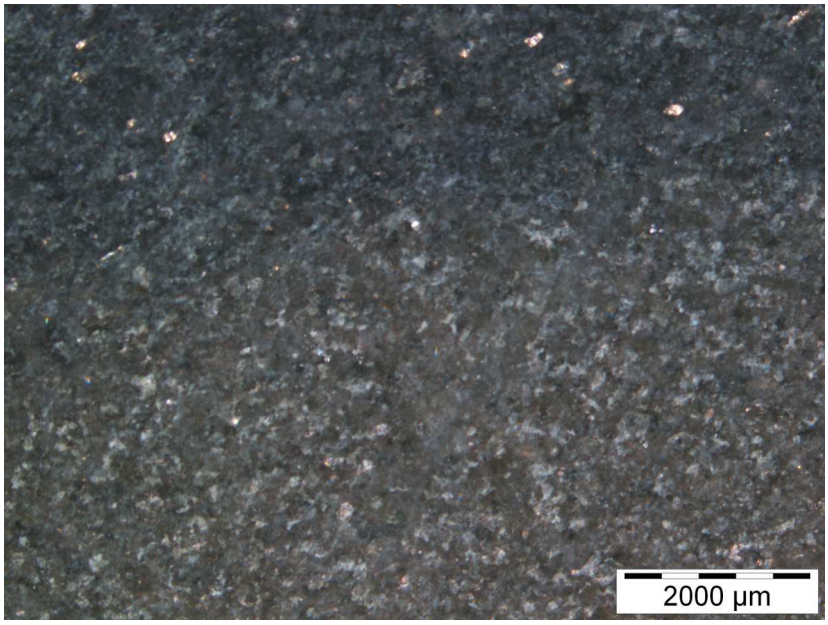

Figure 32: Stereomicroscope Image of Sample DS19

The matrix of these mafic rocks is built up by calcium-rich plagioclase (X_{an}=0.88–0.95) and quartz. The grain size ranges from 0.2–1mm. Plagioclase has a small amount of K-feldspar (up to X_{or}=0.040) and celsian (up to X_{cls}=0.004) component (32).

Clinopyroxene is common and appears as small grains (up to 500µm), in fine grained rock types it is also part of the matrix (Figure 33). Their composition is very variable from sample to sample (X_{Mg}=0.38–0.76), but relatively consistent within each sample (7).

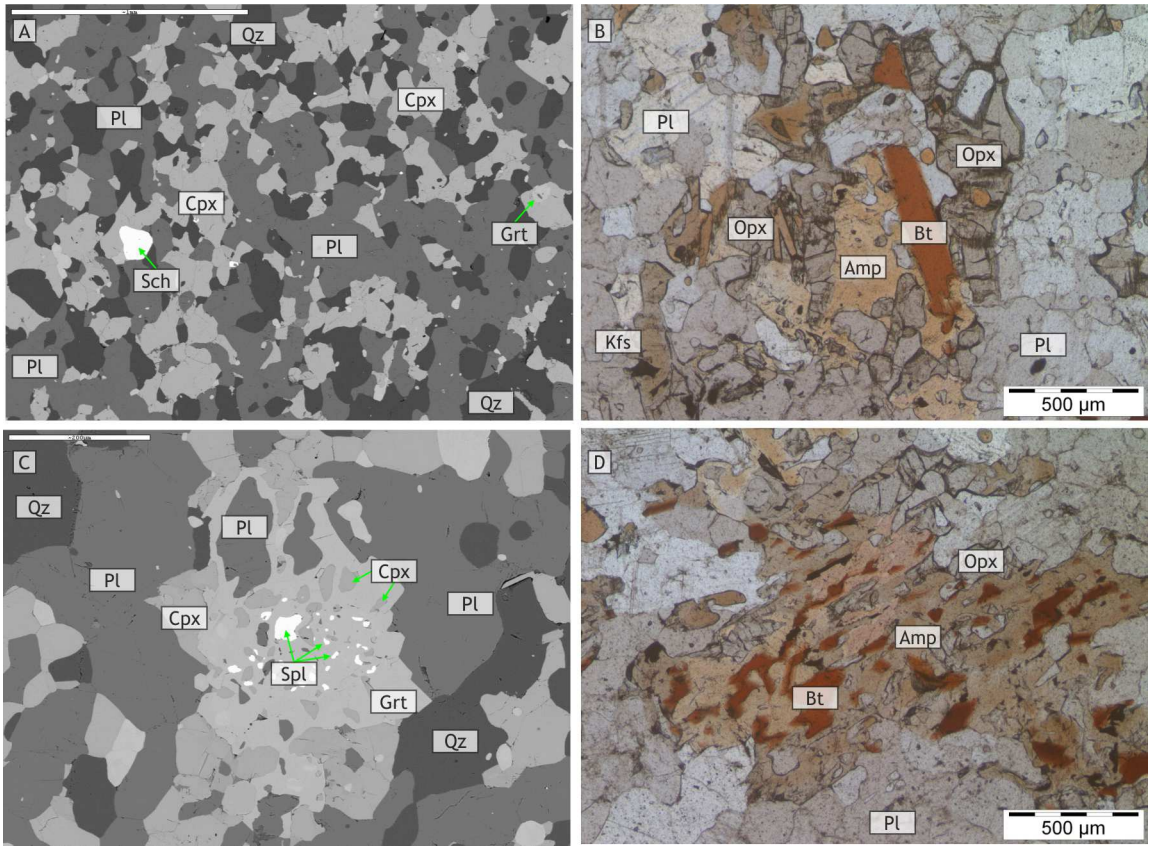

*Figure 33: Photomicrographs and Backscatter elecctron images (BSE) of **A** Fine grained matrix with plagioclase, quartz and clinopyroxene (the scale bar represents 1mm) **B** Orthopyroxene occurs often together with biotite and amphibole. **C** Small garnet with inclusions of clinopyroxene, plagioclase and chromium-rich spinel (the scale bar represents 200µm) **D** Reaction texture of orthopyroxene, biotite and amphibole*

Orthopyroxene is commonly found and has a grain size ranging from 0.5–1mm, but is often altered and intergrown with amphibole and biotite (Figure 33). The composition is magnesium-rich (X_{Mg}=0.58–0.63) with small amounts of calcium (0.70–0.93 wt% CaO), manganese (0.59–0.72 wt% MnO) and aluminium (up to 0.18 wt% Al_2O_3) (7).

Biotite is magnesium-rich with a relatively high variation in the composition (X_{Mg}=0.56–0.68) between different samples. High titanium values (4.40–4.99 wt% TiO_2) and small amounts of chromium (0.26–0.35 wt% Cr_2O_3) were also found.

Garnet is scarce and the grains are small (250–500µm) with multiple inclusions of plagioclase, clinopyroxene and chromium-rich (up to 45 wt% Cr_2O_3) spinel (Figure 33). The composition of garnet is rich in almandine component (X_{alm}=0.48–0.54) with also relatively high amounts of grossular (X_{grs}=0.12–0.25) and spessartine (X_{sps}=0.17–0.21) and minor amounts of pyrope (X_{prp}=0.03–0.07). Within garnet cores slightly elevated Cr_2O_3 values of up to 2.56 wt% were detected (34).

Table 34: Representative analyses of garnet. ***19gt24*** *garnet core (DS19),* ***19gt25*** *garnet rim (DS19),* ***19gt19*** *garnet core (DS19),* ***19gt20*** *garnet rim (DS19)*

Analysis	**19gt24**	**19gt25**	**19gt19**	**19gt20**
Mineral	grt	grt	grt	grt
SiO2	38.19	38.35	37.23	37.83
TiO2	<0.1	<0.1	0.12	<0.1
Al2O3	20.03	20.70	19.11	20.12
Cr2O3	0.56	0.15	2.56	<0.1
FeO	24.50	24.19	22.15	23.01
MnO	7.70	7.94	9.20	8.83
MgO	1.26	1.66	1.32	1.21
CaO	8.39	8.40	8.77	8.25
Total	**100.63**	**101.39**	**100.46**	**99.25**
Si	3.048	3.029	2.992	3.055
Ti	0.000	0.000	0.007	0.000
Al	1.884	1.927	1.810	1.915
Cr	0.035	0.009	0.163	0.000
Fe3	0.000	0.006	0.029	0.000
Fe2	1.636	1.591	1.460	1.554
Mn	0.521	0.531	0.626	0.604
Mg	0.150	0.195	0.158	0.146
Ca	0.718	0.711	0.755	0.714
Sum	**6.603**	**6.562**	**6.461**	**6.524**
Xalm	0.541	0.525	0.487	0.515
Xprp	0.050	0.064	0.053	0.048
Xgrs	0.210	0.228	0.128	0.237
Xsps	0.172	0.175	0.209	0.200
Xuv	0.027	0.007	0.124	0.000

Table 32: Representative analyses of plagioclase. ***19Fs6–19fs7*** *matrix plagioclase (DS19),* ***916pl4–916pl3*** *matrix plagioclase (ML09-16)*

Analysis	**19fs6**	**19fs7**	**916pl4**	**916pl3**
Mineral	pl	pl	pl	pl
SiO2	44.51	45.00	46.05	45.77
Al2O3	35.80	34.94	33.79	34.42
Fe2O3	<0.1	0.26	<0.1	<0.1
CaO	18.82	18.64	17.78	17.80
Na2O	0.46	0.53	1.37	1.32
K2O	<0.1	<0.1	<0.1	<0.1
Total	99.59	99.37	98.99	99.48
Si	2.059	2.086	2.139	2.117
Al	1.952	1.909	1.850	1.876
Fe3	0.000	0.009	0.000	0.012
Ca	0.933	0.926	0.885	0.882
Na	0.041	0.048	0.123	0.118
K	0.000	0.000	0.000	0.000
Sum	**4.985**	**4.978**	**0.885**	**0.882**
Xab	0.042	0.049	0.122	0.118
Xan	0.958	0.951	0.878	0.882
Xor	0.000	0.000	0.000	0.000
Xcls	0.000	0.000	0.000	0.000

Table 33: Representative analyses of pyroxene. ***19Px3–19px4*** *clinopyroxene(DS19)* ***916px5–916px6*** *clinopyroxene (ML09-16),* ***916px1–916px2*** *orthopyroxene (ML09-16)*

Analysis	**19px3**	**19px4**	**916px5**	**916px6**	**916px1**	**916px2**
Mineral	cpx	cpx	cpx	cpx	opx	opx
SiO2	50.95	50.38	52.92	52.40	52.65	52.87
TiO2	<0.1	<0.1	0.26	0.27	0.16	<0.1
Al2O3	0.41	0.92	0.81	0.69	0.54	0.52
FeO	18.93	19.07	8.13	8.63	23.76	24.65
MnO	1.52	1.63	0.24	0.33	0.59	0.64
MgO	6.93	6.60	14.24	14.17	21.60	21.01
CaO	21.09	20.63	22.29	22.16	0.93	0.91
Na2O	0.07	0.14	0.15	0.12	<0.05	<0.05
Total	**99.9**	**99.37**	**99.04**	**98.77**	**100.23**	**100.6**
Si	2.001	1.991	1.985	1.977	1.969	1.978
Ti	0.000	0.000	0.007	0.008	0.004	0.000
Al	0.019	0.043	0.036	0.031	0.024	0.023
Cr	0.000	0.000	0.000	0.009	0.030	0.022
Fe2	0.622	0.630	0.255	0.264	0.713	0.749
Mn	0.051	0.055	0.008	0.011	0.019	0.020
Mg	0.406	0.389	0.796	0.797	1.204	1.172
Ca	0.888	0.874	0.896	0.896	0.037	0.036
Na	0.005	0.011	0.011	0.009	0.000	0.000
Sum	**3.992**	**3.993**	**3.994**	**4.002**	**3.963**	**3.964**
Xmg	0.395	0.382	0.757	0.751	0.628	0.610

2.10 Summary of Mineral Chemistry

A ternary feldspar diagram displays the composition of feldspars from all lithologies (Figure 34). K-feldspar shows similar composition between all samples with just small variation in sodium content. Plagioclase mainly shows an albite-rich composition in felsic samples (only inclusions in garnet porphyroblasts may have high anorthite values = blue crosses). Plagioclase in orthopyroxene bearing gneiss has an intermediate composition and in mafic lenses are very anorthite-rich.

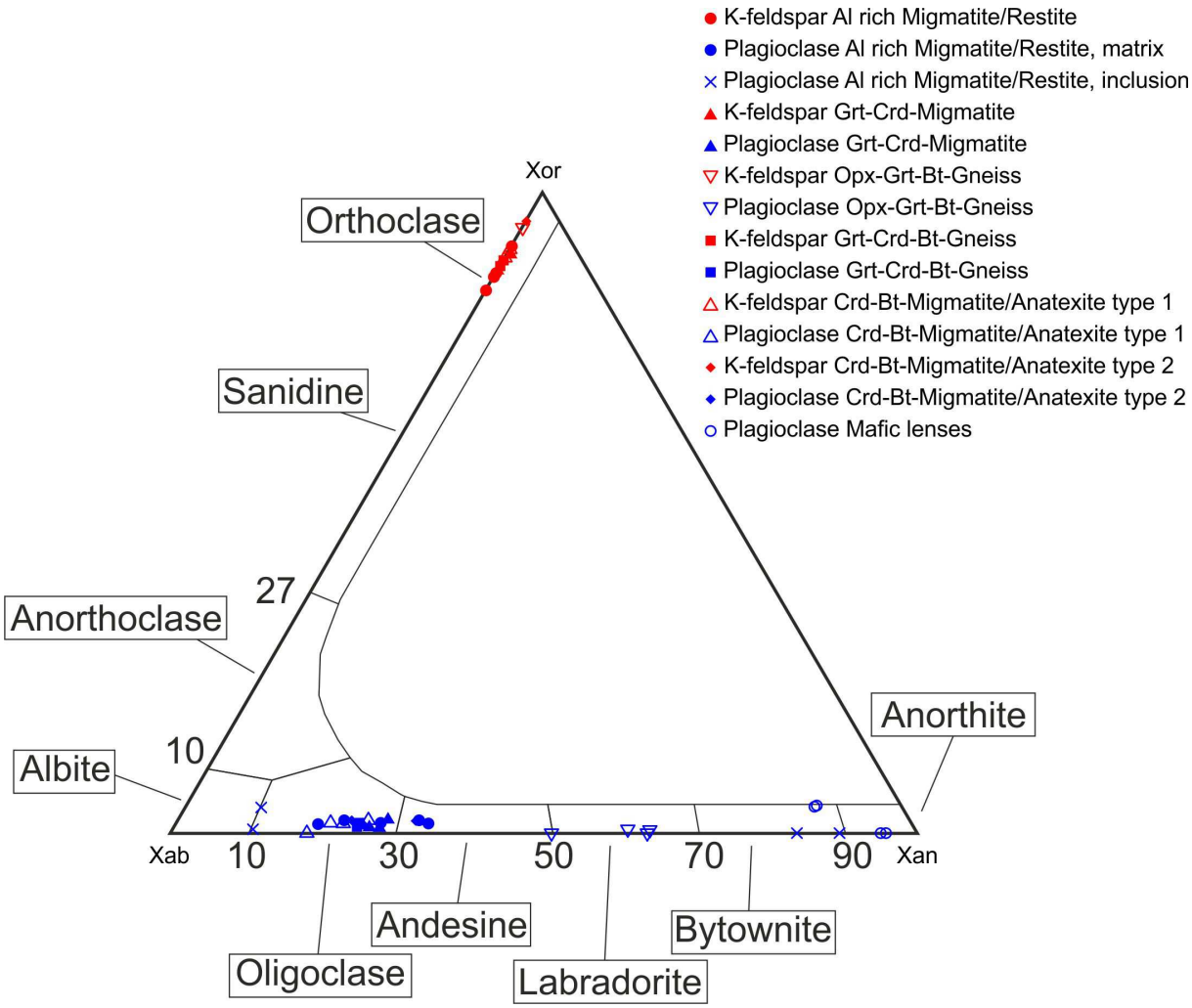

Figure 34: Feldspar triangle showing different compositions of feldspars in all lithologies. K-feldspar show quite similar composition, whereas plagioclase composition show a widespread variety.

A ternary plot of garnet shows the variation in composition between different lithologies (Figure 35). In general, garnet is almandine-rich, with the exception of garnet occurring in mafic lenses. Garnet from orthopyroxene bearing gneiss shows higher pyrope and grossular contents. In samples where garnet is uncommon and small it contains higher amounts of manganese (Mylonites, Grt-Crd-migmatite).

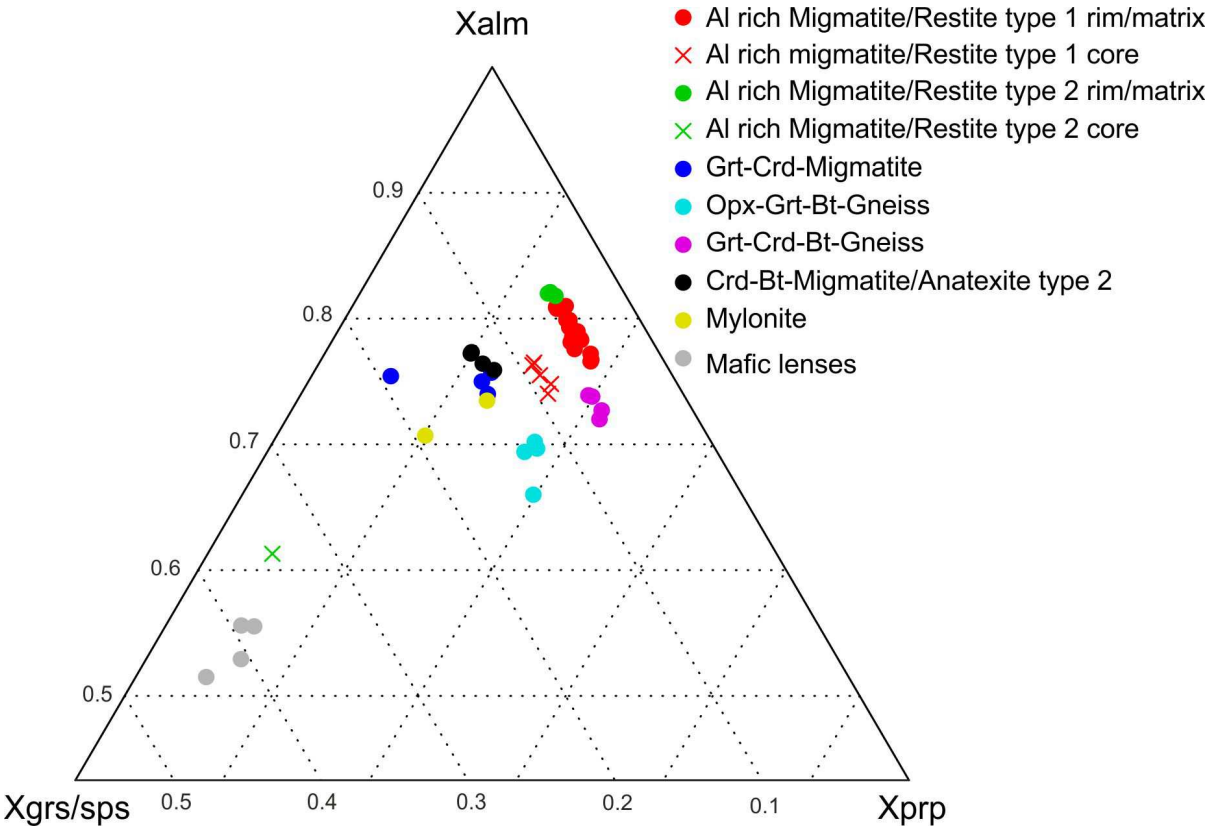

Figure 35: Ternary plot of garnet compositions from several lithologies showing the chemical variation within different samples.

A binary plot X_{Mg} versus Na (a.p.f.u.) in cordierite shows a linear correlation: the higher the Xmg the lower the sodium content (Figure 36). The highest X_{Mg} values were obtained in Grt-Crd-Bt-gneiss, the highest sodium values in in Crd-Bt-migmatite/anatexite. Al-rich migmatite/restite shows a shallower trend (trend 1) with smaller variation in sodium. Other lithologies show a steeper trend with higher variations in X_{Mg} and sodium content.

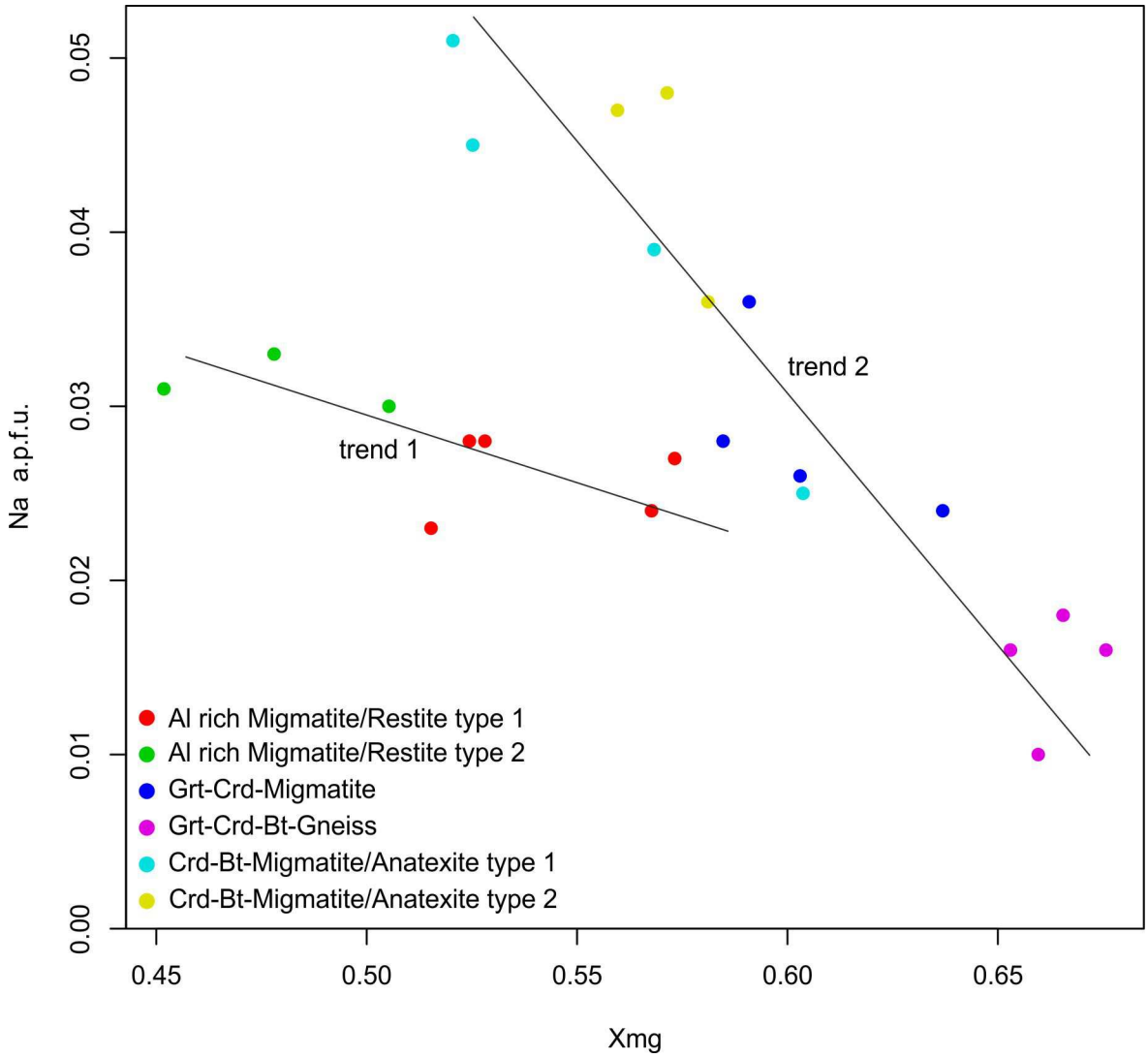

Figure 36: Binary plot of magnesium vs. sodium content in cordierites of several lithologies.

3 Garnet Profiles

3.1 Al-rich Migmatite/Restite type 1

Large garnet porphyroblasts (Figure 37) in Al-rich migmatite/restite show a characteristic chemical zoning (Figure 38), which is found in several samples. Figure 39 shows a detailed profile through a garnet porphyroblast from core to rim. The innermost core (Core 1) has the highest grossular (X_{grs}=0.050–0.055) and spessartine (X_{sps}=0.030–038), but the lowest almandine (X_{alm}=0.74–0.76) content. Pyrope component is approximately at the same level as in the rim zone (X_{prp}=0.15–0.17). Grossular forms a relatively constant plateau which may represents the first stage of garnet growth. About 2mm towards the rim grossular decreases to a very low level (X_{grs}=0.010–0.014), whereas almandine and pyrope increase. This sector marks the second stage of garnet growth (Core 2). Spessartine decreases more or less continuously towards the rim. The rim zone (Rim) represents the latest stage, which is probably a different metamorphic event. Almandine increases at the innermost part of the rim after a small zone of decrease at the end of core 2 and reaches high values (X_{alm}=0.78–0.80) which are generally similar in unzoned garnet grains. Grossular increases again (X_{grs}=0.030–0.033) and reaches values which are between core 1 and core 2. Pyrope decreases again after the increase in outer core to similar values as in core 1 (X_{prp}=0.14–0.17). The outermost rim shows diffusional zoning (decrease in pyrope and increase in almandine component) if in contact with biotite or cordierite.

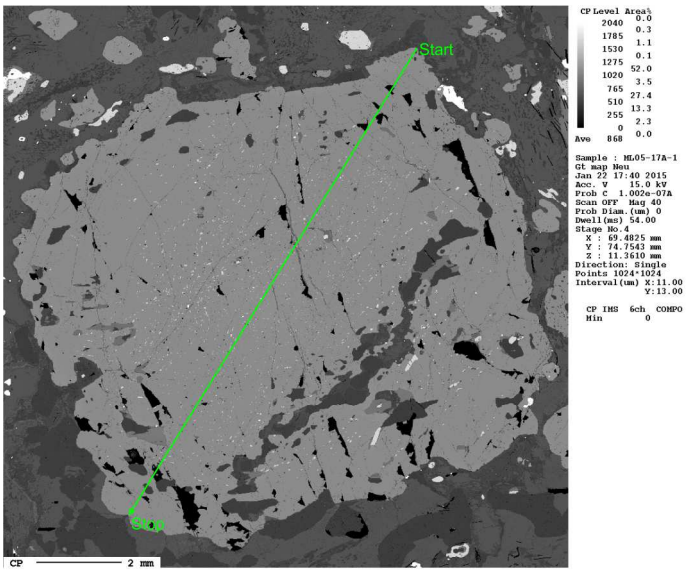

Figure 37: Backscatter electron (BSE) image of a ca. 12mm large garnet porphyroblast. (ML05-17A1). (the scale bar represents 2mm)

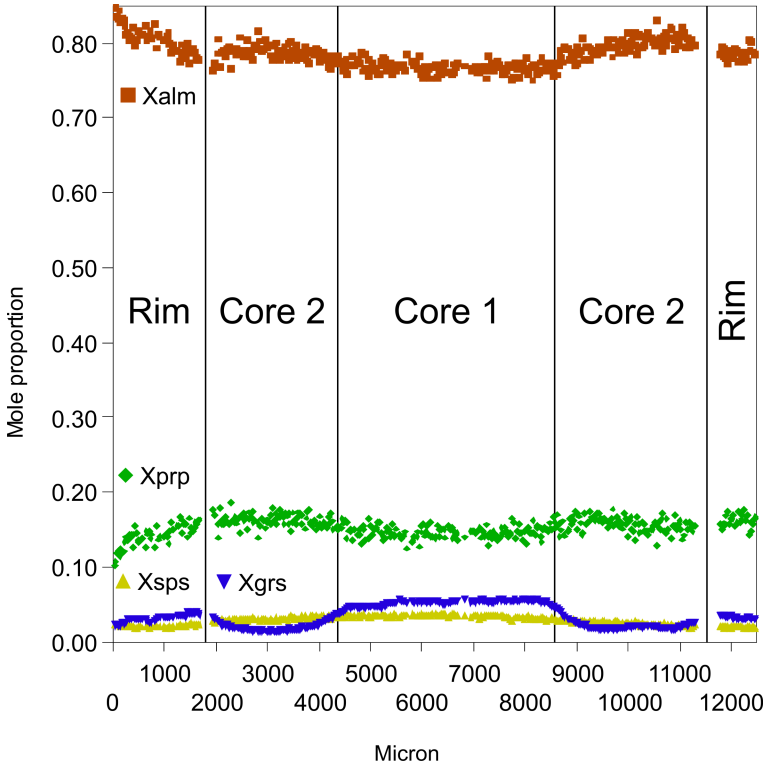

Figure 38: Profile trough the garnet porphyroblast (ML05-17A1) in Figure 37, showing the characteristic zoning.

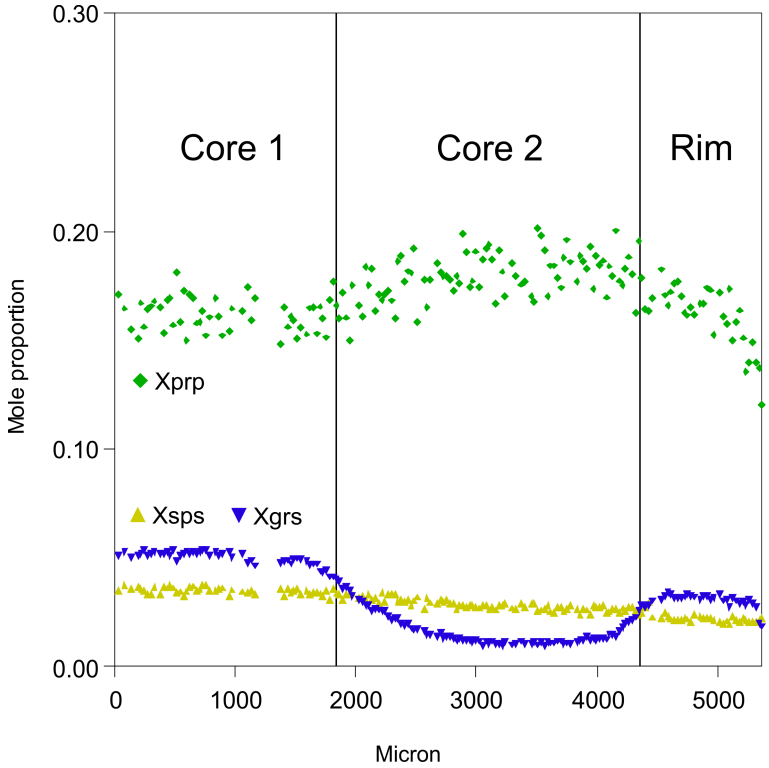

Figure 39: Detailed profile through the same garnet porphyroblast (ML05-17A1) from core to rim. The almandine component is out of the range of this plot and is shown in Figure 38.

Element distribution mapping of the above mentioned garnet was prepared and is shown in Figure 40. The Ca-rich composition is clearly seen in the inner core, a calcium poorer outer core and a rim with intermediate calcium content. The other main elements iron and magnesium do not show observable zoning. Manganese reveals a slight decrease from core to rim. The trace elements yttrium and phosphorus show chemical zoning. Yttrium is enriched in the inner core of garnets, whereas phosphorus is depleted. Since garnet is the mineral where Y is mainly incorporated, the rock is usually depleted after initial garnet crystallization and rims display lower concentrations. Phosphorus is enriched in the outer core zone, which is probably related to the breakdown of a phosphate phase such as apatite or monazite. At the outermost rim phosphorus decreases again

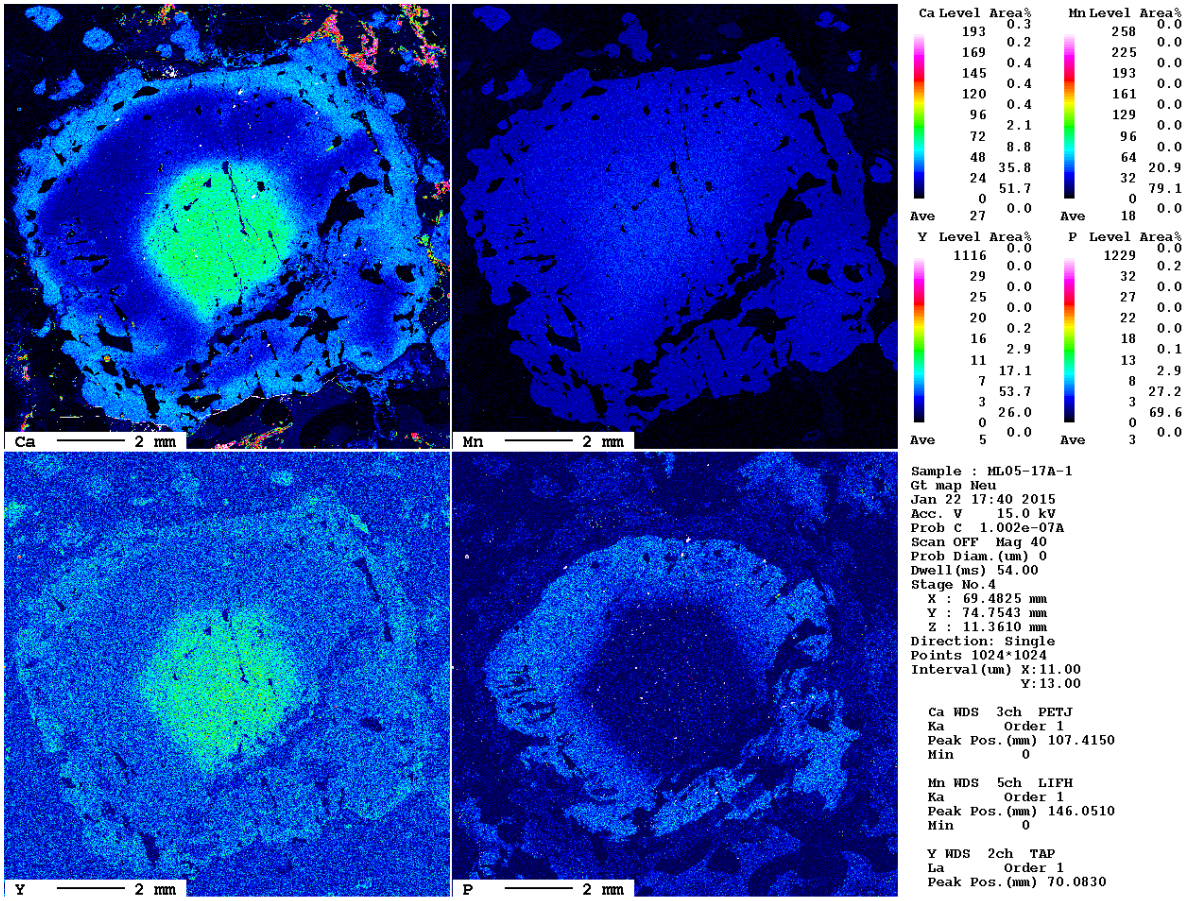

Figure 40: Element distribution mappings of calcium, manganese, yttrium and phosphorus of the ca 12mm large garnet porphyroblast in Fehler: Referenz nicht gefunden. Especially calcium shows distinctly the three phases of garnet growth. (the scale bar represents 2mm)

3.2 Al-rich Migmatite/Restite type 2

A large (6mm) garnet porphyroblast (Figure 41) in an Al-rich migmatite/restite type 2 shows a conspicuous chemical zoning profile (Figure 42), which was observed only at one single garnet grain. The profile displays the highest grossular (X_{grs}=0.23) and spessartine (X_{sps}=0.12) contents, which was obtained from all felsic samples. Towards the rim both decrease continuously to values of X_{grs}=0.03 and X_{sps}=0.02. Almandine and pyrope components are lower in the core (X_{alm}=0.60, X_{prp}=0.03) compared to the typical iron-rich garnets (X_{alm}=0.80). Both components increase towards the rim up to the common values of X_{alm}=0.85 and X_{prp}=0.10. An element distribution mapping displays the similar conspicuous calcium-rich core and the distinct decrease toward the rim (Figure 43). However, no discontinuous zoning pattern was observed in this sample.

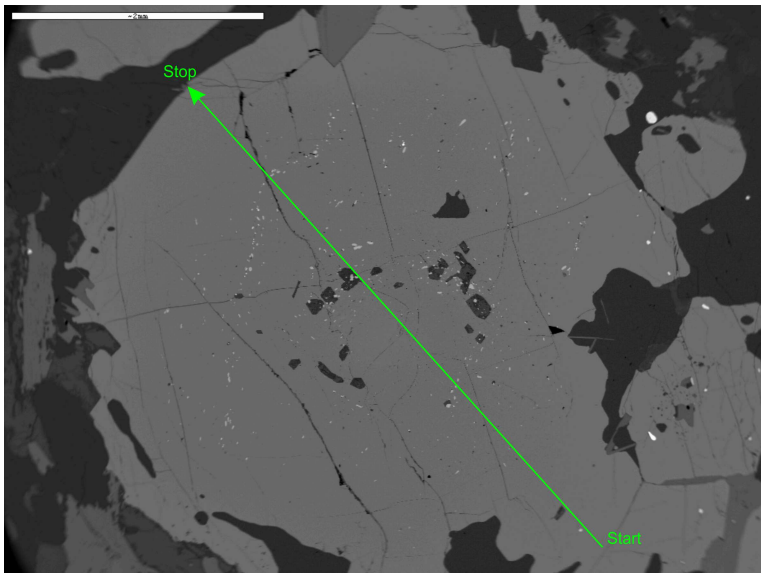

Figure 41: Backscatter electron (BSE) image of a ca. 6mm large garnet porphyroblast. (ML05-16). (the scale bar represents 2mm)

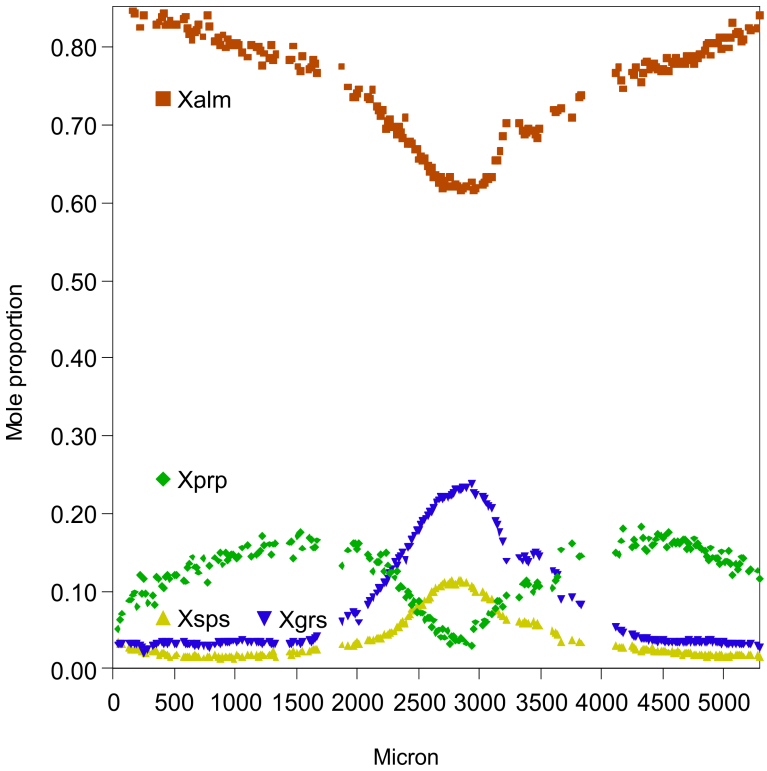

Figure 42: Profile trough the 6mm garnet porphyroblast (ML05-16) in Figure 41, showing an unusual chemical zoning.

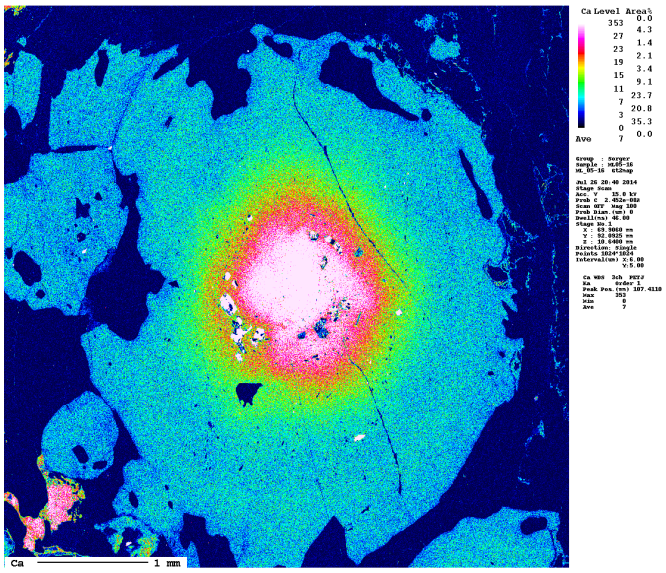

Figure 43: Element distribution mapping of calcium of the ca. 6mm large garnet porpyhroblast in Figure 41. (the scale bar represents 1mm)

3.3 Homogeneous Garnets

Most garnet grains, especially the smaller ones, generally have a homogeneous iron-rich composition. Their chemical zoning shows as single-phase growth and just a slight increase of iron and decrease of magnesium at the rim caused by retrograde diffusion during cooling (Figure 44). A ca. 2.5mm representative garnet porphyroblast is shown in Figure 45. The observed zoning patterns are similar in Grt-Crd-migmatite as well as Opx-Grt-Bt-gneiss and Grt-Crd-Bt-gneiss.

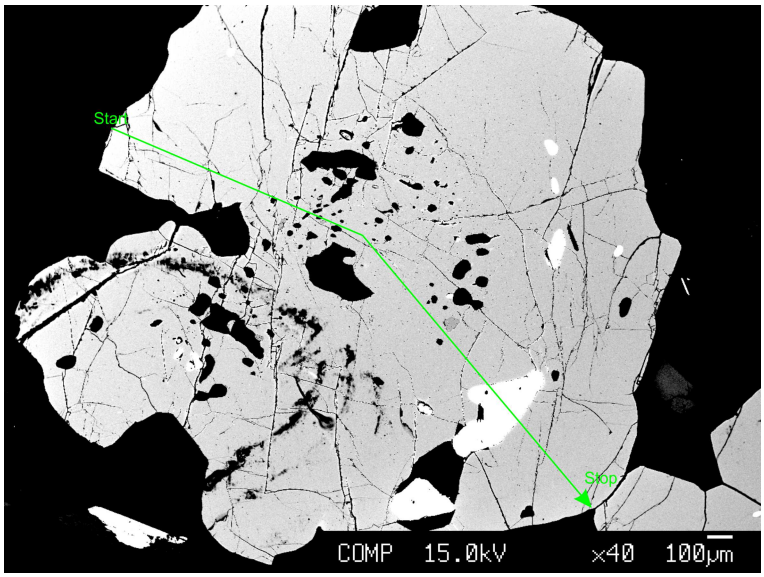

Figure 45: Backscatter electron (BSE) image of a ca. 2.5mm large garnet porphyroblast. (MA1). (high contrast, the scale bar represents 100µm)

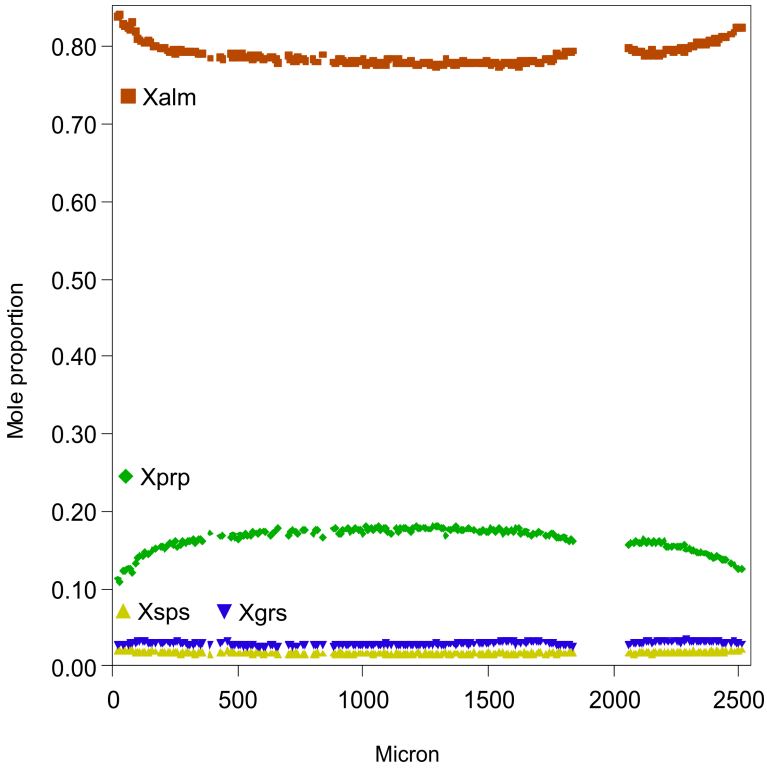

Figure 44: Profile trough the 2.5mm garnet porphyroblast (MA1) in Figure 45, showing a homogeneous composition.

4 Geothermobarometry

Thermobarometric calculations were applied to several samples to constrain metamorphic *P*–*T* conditions for the different lithologies. Multi equilibrium thermobarometry using winTWQ version 2.34 (Berman, 1991) allowed to constrain metamorphic conditions for samples with suitable mineral assemblage. For samples with less suitable mineral assemblages the titanium in biotite thermometer calibrated by Henry et al. (2005) was used to obtain the temperature of metamorphism while pressure could not be constrained. Furthermore two-feldspar thermometry (Benisek et al., 2004) was used for several samples containing plagioclase and K-feldspar.

4.1 Garnet-Cordierite-Spinel-Sillimanite Thermobarometry

Al-rich migmatite/restite represents the metamorphic peak assemblage garnet (rim) + cordierite + olive-green/ brown spinel + sillimanite + K-feldspar + quartz for a thermal peak. The minerals garnet, cordierite, spinel, sillimanite and quartz were used for multi equilibrium thermobarometry with winTWQ version 2.34 (Berman, 1991) and thermodynamic activity models from Berman and Aranovich (1996). Average conditions and their standard deviation was calculated with winTERSX version 2.34 (Berman, 1991). Calculations using the reaction of cordierite formation as well as the garnet-cordierite Fe^{2+}/Mg exchange thermometer were applied:

$$Grt_{(Fe, Mg)} + Sil + Qz = Crd_{(Fe, Mg)} \qquad (1)$$

$$Alm + Crd = Prp + Fe\text{-}Crd \qquad (3)$$

The garnet-spinel Fe^{2+}/Mg exchange thermometer:

$$Alm + Spl = Prp + Hc \qquad (4)$$

As well as three further reactions including garnet cordierite and spinel:

$$\text{Sil + Alm + = Fe-Crd + Hc} \qquad (5)$$

$$\text{Sil + Prp + Alm = Crd + Hc} \qquad (6)$$

$$\text{Fe-Crd + Prp + Sil = Hc + Crd} \qquad (7)$$

These calculations yielded conditions of 870–910°C and 0.6–0.7 GPa (Figure 46). The majority of Al-rich migmatite/restite type1 as well as type 2 show similar *P–T* conditions. Analyses used for calculations are listed in 35.

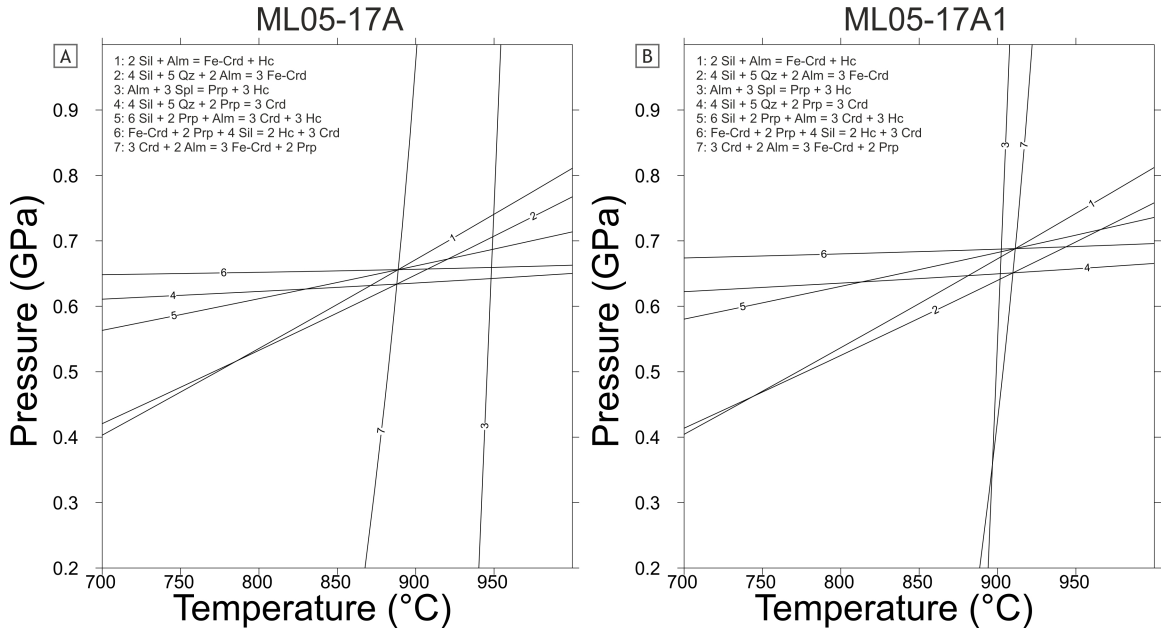

*Figure 46: Geothermobarometric calculations of two samples of **A, B** Al-rich migmatite/restite obtained metamorphic conditions of 892 ± 10°C and 0.64 ± 0.01 GPa (ML05-17A) and 910 ± 5°C and 0.66 ± 0.02 GPa (ML05-17A1) for the thermal peak assemblage. The used reactions are listed in the upper left corner of each diagram.*

Table 35: Analyses used for thermobarometric calculations in Figure 46. ***A1-gt40, A1-cd17, A1-sp29*** *(ML05-17A1),* ***A-gt54, A-cd17, A-sp5*** *(ML05-17A)*

Analysis	**A1-gt40**	**A1-cd17**	**A1-sp29**	**A-gt54**	**A-cd17**	**A-sp5**
Mineral	grt	crd	spl	grt	crd	spl
SiO2	37.51	47.76	<0.1	37.22	47.16	<0.1
TiO2	<0.1	<0.1	<0.1	<0.1	<0.1	0.39
Al2O3	20.90	33.29	51.84	20.72	33.07	53.95
Cr2O3	<0.1	<0.1	6.08	<0.1	<0.1	4.92
V2O3	n.d.	n.d.	1.25	n.d.	n.d.	<0.1
FeO	36.18	11.35	34.58	35.77	11.07	34.44
MnO	0.97	0.15	<0.1	1.00	<0.1	<0.1
MgO	4.07	6.17	2.45	4.06	6.39	1.78
CaO	1.09	<0.1	<0.1	1.14	<0.1	<0.1
ZnO	n.d.	n.d.	3.34	n.d.	n.d.	4.43
Na2O	n.d.	0.13	n.d.	n.d.	0.09	n.d.
Total	**100.72**	**98.85**	**99.54**	**99.91**	**97.79**	**99.91**
Si	2.987	4.960	0.000	2.987	4.945	0.000
Ti	0.000	0.000	0.000	0.000	0.000	0.009
Al	1.962	4.075	1.798	1.960	4.087	1.861
Cr	0.000	0.000	0.141	0.000	0.000	0.114
V	0.000	0.000	0.029	0.000	0.000	0.000
Fe3	0.064	0.000	0.031	0.065	0.000	0.008
Fe2	2.346	0.986	0.820	2.335	0.971	0.835
Mn	0.065	0.013	0.000	0.068	0.000	0.000
Mg	0.483	0.955	0.107	0.486	0.999	0.078
Ca	0.093	0.000	0.000	0.098	0.000	0.000
Zn	0.000	0.000	0.073	0.000	0.000	0.096
Na	0.000	0.026	0.000	0.000	0.018	0.000
Sum	**7.359**	**10.021**	**2.926**	**7.347**	**10.003**	**2.905**
Xalm	0.785	-	-	0.782	-	-
Xprp	0.162	-	-	0.163	-	-
Xgrs	0.031	-	-	0.033	-	-
Xsps	0.022	-	-	0.023	-	-
Xmg	0.171	0.492	0.115	0.172	0.507	0.085
Xspl	-	-	0.125	-	-	0.087
Xhc	-	-	0.789	-	-	0.805
Xghn	-	-	0.085	-	-	0.107
Xchr	-	-	0.073	-	-	0.058

Crd-Grt-Bt-gneiss contain a lot of biotite and small relic garnets which may represent a post peak stage. Investigated samples contain more or less the same mineral assemblage as Al rich migmatite/restite samples, but with smaller amounts of garnet and spinel and higher amounts of biotite. The same reactions were used for *P–T* calculations and conditions of about 755°C and 0.58 GPa were obtained (Figure 47).

Grt-Crd-migmatite shows the lowest *P–T* conditions of garnet and cordierite bearing samples (Figure 47). These samples contain no spinel, thus only the cordierite forming reactions and the garnet-cordierite Fe^{2+}/Mg exchange thermometer were used. *P–T* conditions of 665°C and 0.44 GPa were obtained. Analyses used for calculations are listed in 36.

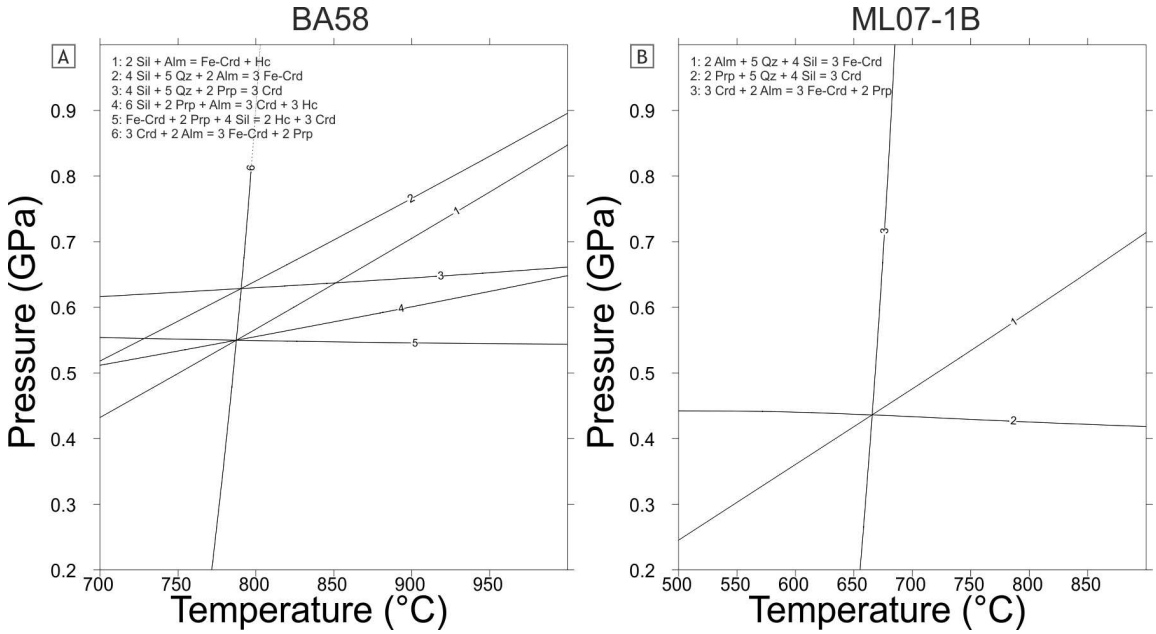

*Figure 47: Geothermobarometric calculations of **A** a Grt-Crd-Bt-gneiss yielded conditions of 755 ± 52°C and 0.58 ± 0.04 GPa (BA58). **B** Calculations of a Grt-Crd-migmatite obtained metamorphic conditions of 665°C and 0.44 GPa. (ML07-1B) The used reactions are listed in the upper left corner of each diagram.*

Table 36: Analyses used for thermobarometric calculations in Figure 47. ***ba58gt28, ba58cd51, ba58sp41*** *(BA58),* ***7-1bgt49, 7-1bcd59*** *(ML07-1B)*

Analysis	**ba58gt28**	**ba58cd51**	**ba58sp41**	**7-1bgt49**	**7-1bcd59**
Mineral	grt	crd	spl	grt	crd
SiO2	38.42	49.27	0.40	36.46	48.19
Al2O3	21.19	32.66	57.73	20.50	32.86
Cr2O3	<0.1	<0.1	0.17	<0.1	<0.1
FeO	32.46	7.67	32.28	34.66	9.68
MnO	1.77	<0.1	0.15	4.57	0.34
MgO	5.38	8.56	4.14	2.89	7.65
CaO	0.96	<0.1	<0.1	0.88	<0.1
ZnO	n.d.	n.d.	3.76	n.d.	n.d.
Na2O	n.d.	0.09	n.d.	n.d.	0.14
Total	**100.18**	**98.25**	**98.63**	**99.96**	**98.86**
Si	3.033	5.052	0.011	2.954	4.974
Al	1.972	3.947	1.951	1.958	3.997
Cr	0.000	0.000	0.004	0.000	0.000
Fe3	0.000	0.000	0.023	0.134	0.000
Fe2	2.143	0.658	0.751	2.215	0.836
Mn	0.118	0.000	0.004	0.314	0.030
Mg	0.633	1.309	0.177	0.349	1.177
Ca	0.081	0.000	0.000	0.076	0.000
Zn	0.000	0.000	0.080	0.000	0.000
Na	0.000	0.018	0.000	0.000	0.028
Sum	**7.148**	**9.657**	**2.910**	**7.261**	**9.807**
Xalm	0.720	-	-	0.750	-
Xprp	0.213	-	-	0.118	-
Xgrs	0.027	-	-	0.026	-
Xsps	0.040	-	-	0.106	-
Xmg	0.228	0.665	0.191	0.136	0.585
Xspl	-	-	0.176	-	-
Xhc	-	-	0.744	-	-
Xghn	-	-	0.080	-	-
Xchr	-	-	0.002	-	-

4.2 Geothermobarometric calculations using cores from poly phase garnets

Garnet porphyroblasts in Al rich migmatite/restite show discontinuous chemical zoning, which represents different stages of garnet growth and probably different metamorphic events. The outermost rim is equilibrated with the matrix and was used for thermobarometric calculations in combination with cordierite and spinel (Figure 46). The inner core represents the first stage of growth and has inclusions of Zn bearing hercynitic spinel which allowed the calculation of the garnet-spinel Fe^{2+}/Mg exchange thermometer with winTWQ version 2.34 (Berman, 1991). Temperature of 740–780°C (Figure 48) was obtained. In order to constrain the *P–T*-field where the garnet cores crystallized, pseudosections were calculated and the observed composition compared with the calculated garnet composition. Conditions of 750–825°C and 1.1–1.3 GPa were estimated for sample ML05-17A1. Details of calculations and used thermodynamic models/data will be described in chapter Pseudosections (pp. 84–93). The outer core represents a second stage of growth with inclusions of biotite + plagioclase + staurolite + sillimanite + quartz. Metamorphic conditions were obtained by using the garnet-biotite Fe^{2+}/Mg exchange thermometer and the garnet-sillimanite-plagioclase-quartz (GASP) barometer with winTWQ version 2.34 (Berman, 1991) and yielded conditions of 580–610°C and 0.46–0.54 GPa (Figure 48). Analyses used for calculations are listed in 39.

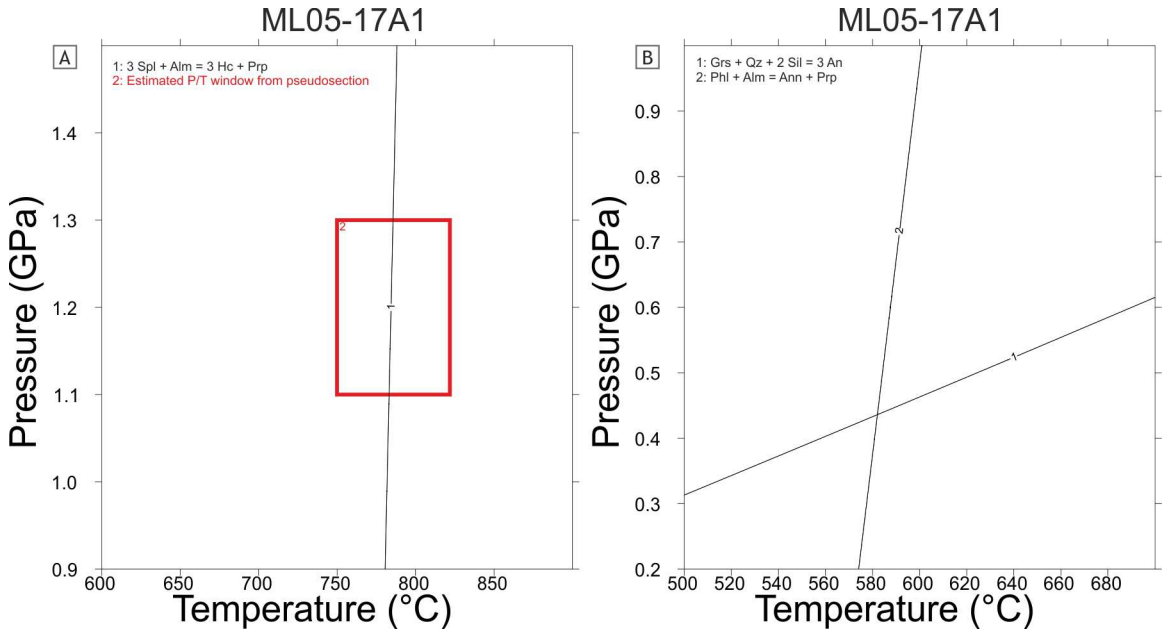

Figure 48: Geothermobarometric calculations of garnet cores. ***A*** *Calculations of the inner core obtained conditions of 750–825°C and 1.1–1.3 GPa (ML05-17A1), whereas the pressure was only estimated from pseudosections.* ***B*** *Calculations of the outer core yielded conditions of 582°C and 0.44 GPa (ML05-17A1). The used reactions are listed in the upper left corner of each diagram.*

Table 37: Analyses used for thermobarometric calculations in Figure 48. ***A1-gt39, A1-sp12*** *(ML05-17A1, inner core);* ***A-gt41, A1-bt32, A1-fs38*** *(ML05-17A1, outer core)*

Analysis	**A1-gt39**	**A1-sp12**	**A1-gt41**	**A1-bt32**	**A1-fs38**
Mineral	grt	spl	grt	bt	pl
SiO2	37.68	<0.1	37.68	35.47	64.00
TiO2	<0.1	<0.1	<0.1	1.30	<0.1
Al2O3	20.89	58.98	21.13	20.34	22.37
Fe2O3	0.00	0.00	0.00	0.00	0.33
FeO	34.10	34.25	35.58	17.44	n.d.
MnO	1.71	<0.1	1.29	<0.1	n.d.
MgO	4.23	4.01	4.30	11.17	<0.1
CaO	1.88	<0.1	0.40	<0.1	2.29
ZnO	n.d.	2.42	n.d.	n.d.	n.d.
BaO	n.d.	n.d.	n.d.	n.d.	<0.1
Na2O	n.d.	n.d.	n.d.	0.17	10.25
K2O	<0.1	<0.1	<0.1	9.49	0.10
F	n.d.	n.d.	n.d.	0.48	n.d.
Total	**100.49**	**99.66**	**100.38**	**95.86**	**99.34**
Si	2.997	0.000	3.006	2.667	2.839
Ti	0.000	0.000	0.000	0.074	0.000
Al	1.958	1.969	1.987	1.802	1.169
Fe3	0.048	0.031	0.001	0.000	0.011
Fe2	2.220	0.780	2.373	1.097	0.000
Mn	0.115	0.000	0.087	0.000	0.000
Mg	0.502	0.169	0.511	1.252	0.000
Ca	0.160	0.000	0.034	0.000	0.109
Zn	0.000	0.051	0.000	0.000	0.000
Ba	0.000	0.000	0.000	0.000	0.000
Na	0.000	0.000	0.000	0.025	0.881
K	0.000	0.000	0.000	0.910	0.006
F	0.000	0.000	0.000	0.114	0.000
Sum	**7.840**	**3.000**	**7.965**	**6.917**	**4.019**
Xalm	0.741	-	0.790	-	-
Xprp	0.168	-	0.170	-	-
Xgrs	0.053	-	0.011	-	-
Xsps	0.038	-	0.029	-	-
Xspl	-	0.174	-	-	-
Xhc	-	0.773	-	-	-
Xghn	-	0.053	-	-	-
Xchr	-	0.016	-	-	-
Xmg	0.184	0.178	0.177	0.533	-
Xab	-	-	-	-	0.885
Xan	-	-	-	-	0.109
Xor	-	-	-	-	0.006
Xcls	-	-	-	-	0.000

4.3 Titanium in Biotite thermometry

Most of the samples from the northern part of the investigated area do not contain garnet but high amounts of titanium-rich biotite. The titanium content in biotite can be used as a geothermometer for peraluminous metapelites that have equilibrated at 480–800°C and 0.4–0.6 GPa (Henry et al. 2015). Further requirements are the presence of another titanium bearing phase (ilmenite or rutile), aluminous minerals such as cordierite, staurolite or an Al_2SiO_5 polymorph and graphite to restrict the Fe^{3+} in biotite due to low and constant f_{O2}. The Ti in biotite thermometer is based on the non-linear function of decreasing Ti with increasing X_{Mg} in biotite. Biotite formula has to be calculated on the basis of 22 oxygen atoms, before using X_{Mg} (Mg/(Mg+Fe) and Ti (a.p.f.u.) for temperature calculations.

The application of the Ti in biotite thermometer (Henry et al. 2015) to a Grt-Crd-migmatite (ML07-1B) indicates temperatures of 694 ± 18°C, which is conform with temperatures calculated with winTWQ version 2.34 (Berman, 1991), another one from the Lichtenberg area (DS24) yields similar temperature of 684 ± 20°C. A Opx-Grt-Bt-gneiss (BA7) shows somewhat higher temperatures of about 729 ± 20°C. Calculations of several Crd-Bt-migmatite/anatexite samples from the Lichtenberg area yields temperatures of 650–705°C, from the Bad Leonfelden area 630–725°C and 710–735°C from the Sauwald area. The detailed results are listed in 38 with annotation of corresponding regions. Some of these may not accurate due to the absence of graphite in some samples, which can produce reasonable temperatures but also can underestimate the calibrated temperatures (Henry et al. 2015). Analyses used for calculations are listed in 39.

Table 38: Results of the Ti in biotite thermometry of different lithologies from different locations. Temperatures are mean values ± standard deviation of several biotite analyses in each sample.

Sample	Lithologie	Region	Temperature ± σ (°C)
ML07-1B	Grt-Crd-Migmatite	Danube Valley	694 ± 18
BA7	Opx-Grt-Bt-Gneiss	Danube Valley	729 ± 20
BA58	Grt-Crd-Bt-gneiss	Lichtenberg area	702 ± 10
BA62	Crd-Bt-Migmatite/Anatexite	Lichtenberg area	672 ± 29
DS5	Crd-Bt-Migmatite/Anatexite	Lichtenberg area	684
DS24	Grt-Crd-Migmatite	Lichtenberg area	684 ± 20
DS35	Grt-Bt-Gneiss	Lichtenberg area	666 ± 18
DS42	Bt-Gneiss	Lichtenberg area	682 ± 20
BA76	Crd-Bt-Mmigmatite/Anatexite	Bad Leonfelden area	647 ± 22
DS6	Crd-Bt-Mmigmatite/Anatexite	Bad Leonfelden area	672 ± 16
DS8	Crd-Bt-Mmigmatite/Anatexite	Bad Leonfelden area	685 ± 16
DS14	Bt-Gneiss	Bad Leonfelden area	695 ± 15
DS66	Crd-Bt-Mmigmatite/Anatexite	Bad Leonfelden area	702 ± 23
DS70	Bt-Gneiss	Bad Leonfelden area	692 ± 32
BA31	Crd-Bt-Mmigmatite/Anatexite	Sauwald area	723 ± 12

Table 39: Analyses used for Ti in biotite thermometry. ***7-1bbt30*** *(ML07-1B),* ***ba7bt16*** *(BA7),* ***ba58bt38*** *(BA58),* ***ds5bt7*** *(DS5),* ***ds42bt5*** *(DS42),* ***76bt15*** *(BA76),* ***ds6bt15*** *(DS6),* ***ba31bt6*** *(BA31). Formula calculated on the basis of 22 oxygen atoms.*

Analysis	**7-1bbt30**	**ba7bt16**	**ba58bt38**	**ds5bt7**	**ds42bt5**	**76bt15**	**ds6bt15**	**ba31bt6**
Mineral	bt	bt	bt	bt	bt	bt	bt	bt
SiO2	34.55	36.33	36.10	34.33	34.34	35.47	35.21	34.67
TiO2	3.33	3.69	3.24	3.17	3.61	2.49	2.85	4.46
Al2O3	19.30	15.83	18.18	17.57	18.41	19.85	19.30	17.67
FeO	21.22	18.35	17.22	20.64	22.09	20.49	19.46	21.25
MnO	<0.1	<0.1	<0.1	0.47	<0.1	0.23	<0.1	<0.1
MgO	8.08	11.59	10.15	7.99	6.72	8.73	8.53	8.68
Na2O	0.29	0.15	0.11	0.08	0.10	0.15	0.10	0.28
K2O	9.47	9.26	9.64	9.93	9.62	9.54	9.77	9.41
F	0.65	0.41	0.30	0.53	1.24	0.49	0.58	0.35
Total	**96.89**	**95.61**	**94.94**	**94.71**	**96.13**	**97.44**	**95.80**	**96.77**
Si	5.266	5.517	5.477	5.377	5.344	5.332	5.374	5.287
Ti	0.382	0.421	0.370	0.373	0.423	0.282	0.327	0.511
Al	3.467	2.833	3.251	3.243	3.376	3.517	3.472	3.176
Fe2	2.705	2.330	2.185	2.703	2.874	2.576	2.484	2.709
Mn	0.000	0.000	0.000	0.062	0.000	0.029	0.000	0.000
Mg	1.836	2.624	2.296	1.866	1.559	1.956	1.941	1.974
Na	0.086	0.044	0.032	0.024	0.030	0.044	0.030	0.081
K	1.841	1.794	1.866	1.984	1.910	1.829	1.902	1.831
F	0.313	0.197	0.144	0.262	0.610	0.233	0.280	0.168
Sum	**15.895**	**15.761**	**15.621**	**15.895**	**16.126**	**15.798**	**15.809**	**15.738**
Xmg	0.404	0.530	0.512	0.408	0.352	0.432	0.439	0.422

4.4 Two-feldspar thermometry

The presence of K-feldspar as well as plagioclase in most of the investigated samples, enables the use of a two-feldspar thermometer. High grade metamorphic rocks cooling down slowly under dry conditions suffer from a retrograde diffusional resetting due to intercrystalline Na-K exchange. Whereas the original anorthite content is preserved due to the slow progress of the Ca + Al ⇌ (Na, K) + Si exchange vector. So if the anorthite content is set to a constant value, a mathematical reversing of the Na-K exchange yields the temperature of the original coexisting of both feldspars (Benisek et al., 2004). The endmember composition (X_{ab}, X_{an}, X_{or}, X_{cls}) of analysed feldspar pairs as well as interaction parameters obtained by Benisek et al. (2010) were used for calculations. The problem of perthitic K-feldspar were solved by reintegration of plagioclase exsolution lamellae to restore the original composition of K-feldspars. The estimated pressure for calculations was assumed to be 0.6 GPa ± 0.2 GPa. Only Crd-Bt-migmtites/anatexites were calculated with an estimated pressure of 0.4 GPa ± 0.2 GPa. Temperature was calculated for the estimated pressure including uncertainties and then a mean and a standard deviation of temperature were determined following Benisek et al. (2010).

The two-feldspar thermometer was applied to several lithologies (40) and resulted in temperatures similar to obtained values with winTWQ version 2.34 (Berman, 1991), or the Ti in biotite thermometer. In some cases the calculated temperatures are slightly higher compared to Ti in biotite temperatures, maybe due to the absence of graphite in some samples and the error caused thereby. Analyses used for calculations of three selected samples are listed in 41.

Table 40: Results of the two-feldspar thermometry of different lithologies from different locations. Temperatures are mean values ± standard deviation, calculated with assumed pressure error of ± 0.2 GPa.

Sample	Lithologie	Region	Temperature ± σ (°C)
ML05-17A1	Al-rich Migmatite/Rrestite	Danube Valley	906 ± 19
ML07-1B	Grt-Crd-Migmatite	Danube Valley	659 ± 22
BA58	Grt-Crd-Bt-Gneiss	Lichtenberg area	753 ± 21
DS24	Grt-Crd-Migmatite	Lichtenberg area	689 ± 21
DS35	Grt-Bt-Gneiss	Lichtenberg area	738 ± 22
BA76	Crd-Bt-Mmigmatite/Anatexite	Bad Leonfelden area	681 ± 37
DS6	Crd-Bt-Mmigmatite/Anatexite	Bad Leonfelden area	695 ± 23
DS66	Crd-Bt-Mmigmatite/Anatexite	Bad Leonfelden area	653 ± 16

Table 41: Analyses used for two-feldspar thermometry. ***A1-fs18*** *matrix plagioclase,* ***A1-fs36*** *K-feldspar host,* ***A1-fs37*** *exsolution lamella ((ML05-17A1)),* ***ds35fs10*** *matrix plagioclase,* ***ds35fs8*** *K-feldspar host,* ***ds35fs8*** *exsolution lamella (DS35),* ***ds6fs7*** *matrix plagioclase,* ***ds6fs11*** *K-feldspar host,* ***ds6fs12*** *exsolution lamella (DS6).*

Analysis	**A1-fs18**	**A1-fs36**	**A1-fs37**	**ds35fs10**	**ds35fs7**	**ds35fs8**	**ds6fs7**	**ds6fs11**	**ds6fs12**
Mineral	pl	kfs	pl	pl	kfs	pl	pl	kfs	pl
SiO2	60.44	64.32	65.15	63.60	64.73	69.56	62.25	64.31	69.57
Al2O3	25.84	19.31	22.73	24.06	18.85	20.02	24.60	18.81	19.89
CaO	6.69	<0.1	3.59	4.55	0.11	0.41	5.38	<0.1	0.37
BaO	<0.1	0.64	0.17	0.10	0.48	<0.1	<0.1	0.60	<0.1
Na2O	7.71	1.49	9.94	8.45	1.05	10.00	8.51	1.93	11.05
K2O	0.34	14.73	0.39	0.11	14.89	0.38	0.20	14.23	<0.1
Total	**101.02**	**100.49**	**101.97**	**100.87**	**100.11**	**100.37**	**100.94**	**99.88**	**100.88**
Si	2.665	2.959	2.828	2.782	2.983	3.010	2.734	2.973	3.002
Al	1.343	1.047	1.163	1.240	1.024	1.021	1.273	1.025	1.011
Ca	0.316	0.000	0.167	0.213	0.005	0.019	0.253	0.000	0.017
Ba	0.000	0.012	0.003	0.002	0.009	0.000	0.000	0.011	0.000
Na	0.659	0.133	0.837	0.717	0.094	0.839	0.725	0.173	0.924
K	0.019	0.865	0.022	0.006	0.875	0.021	0.011	0.839	0.000
Sum	**5.002**	**0.864**	**5.020**	**4.960**	**4.990**	**4.910**	**4.996**	**5.021**	**4.954**
Xab	0.663	0.132	0.813	0.764	0.096	0.954	0.733	0.169	0.982
Xan	0.318	0.000	0.162	0.227	0.005	0.022	0.256	0.000	0.018
Xor	0.019	0.856	0.021	0.006	0.890	0.024	0.011	0.820	0.000
Xcls	0.000	0.012	0.003	0.002	0.009	0.000	0.000	0.011	0.000

5 Pseudosections

In order to model the metamorphic evolution and metamorphic history, pseudosections were calculated for selected samples. Perple_X version 6.7.0 (Connolly, 2005, updated in 2014) and the internally consistent thermodynamic data set hp04ver.dat (Holland and Powell, 1998, revised in 2004) were used. For some samples the Matlab splitting tool Paralyzer version 1.5 (Caddick, 2014) was applied for a better compositional resolution and to avoid some typical Perplex artefacts. Isopleths of mineral compositions or modes were plotted with PyWerami version 2.0.1. (Lexa, 2011). Calculations were performed in the chemical system MnO–Na_2O–CaO–K_2O–FeO–MgO–Al_2O_3–SiO_2–H_2O–TiO_2 (MnNCKFMASHT) using the following solid-solution models: garnet (Ganguly et al., 1996), biotite (Tajcmanova et al., 2009), cordierite (Baumgartner, 2003), feldspar (Benisek et al., 2010), mica (Coggon and Holland, 2002; Auzanneau et al., 2010), orthopyroxene (Holland and Powell, 1999), spinel (Holland and Powell, 1998), staurolite (Holland and Powell, 1998) and melt phase (Holland and Powell, 2001; White et al., 2001). For all calculations an empirical correction for ferric iron (15% of total iron) content was applied. Water content was assumed to be 1 wt% based on observed mineralogy and phase relations in an T–wt% pseudosection diagram.

5.1 Al-rich Migmatite/Restite

Zoned garnet porphyroblasts in Al-rich migmatite/restite allow the reconstruction of a possible *P–T* path based on pseudosection modelling and use of mineral isopleths and classical thermobarometry. The measured bulk rock composition represents the composition at the first stage of garnet growth and was used to model metamorphic conditions for the innermost relic garnet cores (Figure 49). Intersections of calculated isopleths of garnet endmembers yield a *P–T* window of 750–825°C and 1.1–1.3 GPa. Similar *P–T* conditions can be obtained with the garnet-spinel Fe/Mg exchange thermometer (750–800°C). However, spinel was not observed in pseudosection calculations which is probably due to the fact that spinel is stabilized by a significant gahnite component. Since the used composition space does not consider ZnO we could only consider the endmembers hercynite and Mg-spinel. Tajcmanova et al. (2003) demonstrated in the system KFMZnASH that the incorporation of a Zn component in spinel increases its stability field towards lower temperature and higher pressures, which is

also confirmed by experimental work (Nichols et al., 1992; Hensen, 1986; Shulters, 1989). Because of the absence of any other inclusion phases which might allow to constrain a field in *P–T* space the garnet composition isopleths are the only possibility to define the metamorphic conditions of the garnet core.

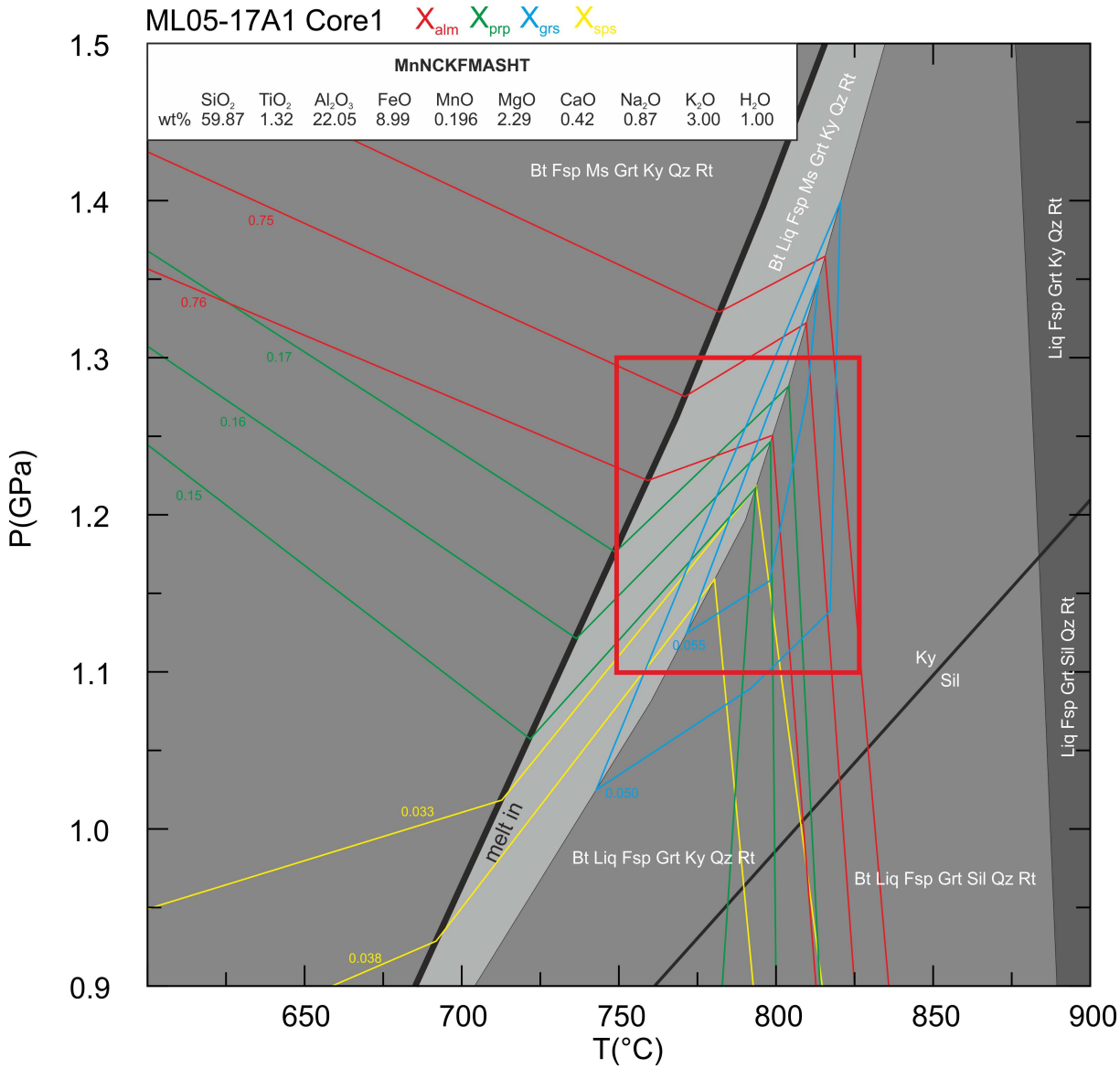

Figure 49: Calculated pseudosection of bulk-rock composition representing the first stage of garnet growth. Isopleth match in a P–T window of 750–825°C and 1.1–1.3 GPa (ML05-17A1).

In order to model the phase relations and stability fields of mineral assemblages in equilibrium with the outer core and rim zone of garnet the garnet core composition, which is not part of the reaction volume has to be subtracted from the whole rock composition. Several authors have applied this correction for specific samples (Gaidies et al., 2011; Evans, 2004; Spear et al., 1998). Evans (2004) used Mn partitioning between whole rock and garnet as a proxy for fractionation. Since garnet compositions are usually modified by diffusion during granulite facies metamorphism the volume of garnet cores was subtracted from a defined sample volume. The garnet core volume was obtained by counting of garnet cores on thinsection and assuming a 10mm thick layer as reaction volume, depending on the garnet size. However, the small changes in composition do not have a dramatic effect on mineral stability and calculated mineral composition with the exception of spessartine component in garnet.

The outer core of garnet is characterized by a lower grossular component and numerous inclusions of Bt + St + Pl + Sil + Qz + Ilm. *P–T* conditions of this sector, obtained by thermobarometric calculations with winTWQ version 2.34 (Berman, 1991) are 580–610°C and 0.46–0.54 GPa. The calculated pseudosection field containing the observed mineral assemblage defines a similar *P–T* region (Figure 50).

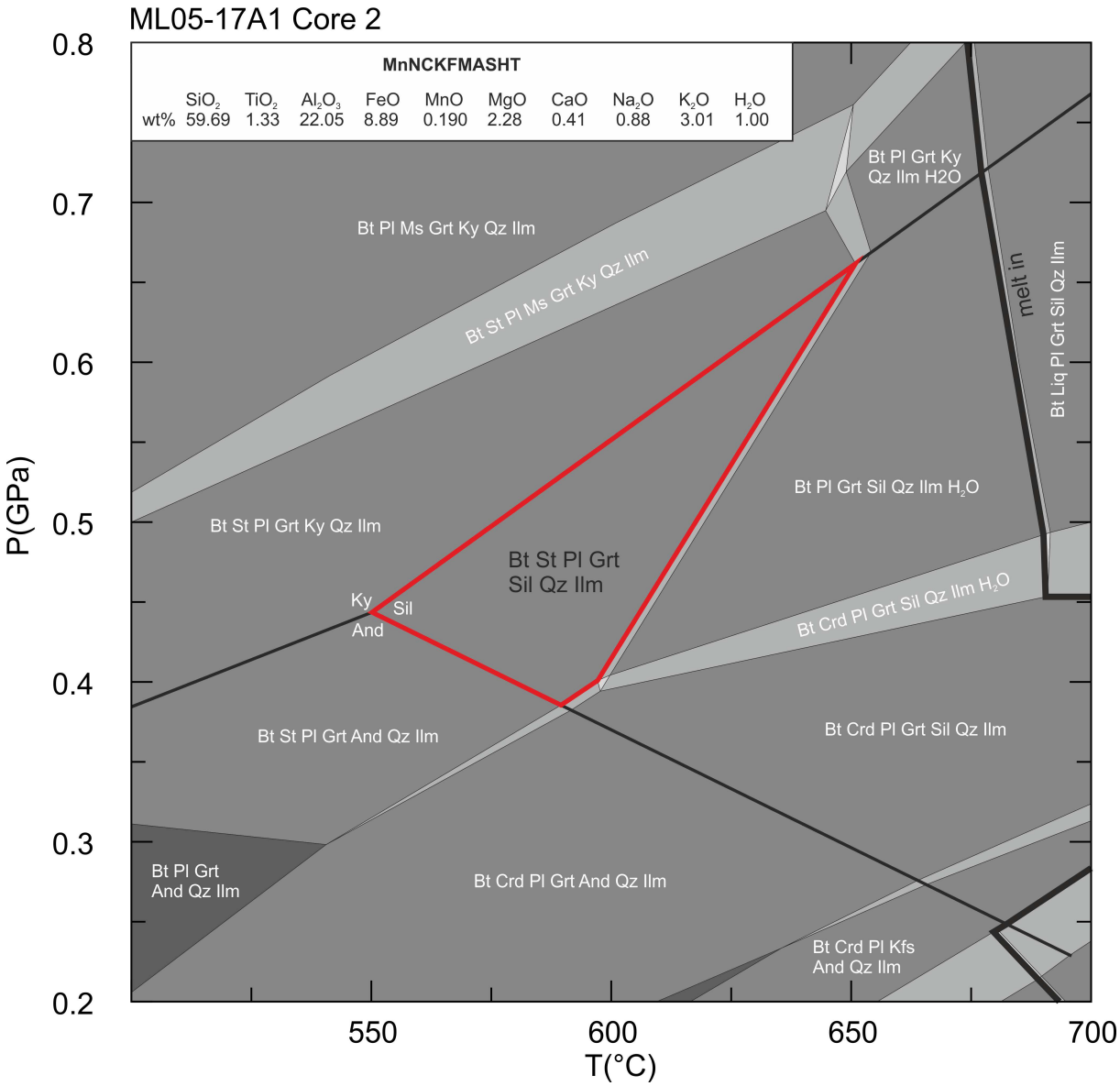

Figure 50: Calculated pseudosection of adapted bulk-rock composition representing the second stage of garnet growth. The suitable mineral assemblage lie within the marked field. (ML05-17A1). Used bulk composition is in the upper left corner of the diagram.

Effective bulk composition for the rim zone, which represents the last stage of crystallisation was also corrected by considering garnet fractionation. The calculated pseudosection (Figure 51) represents the last stage of garnet growth. Intersections of calculated isopleths of garnet endmembers as well as X_{Mg} in cordierite yields conditions of 820–870°C and 0.4–0.6 GPa which are similar to conditions obtained with winTWQ version 2.34 (Berman, 1991). The observed mineral assemblage is Liq + Crd + Pl + Kfs + Grt + Sil + Qz + Ilm. Again, stability field of spinel does not correspond to observations in thinsection because of Cr and Zn content in spinel. Spinel occurs only as a minor phase and is thus not important for the reconstruction of the metamorphic history and thus calculations including Cr_2O_3 and ZnO omitted.

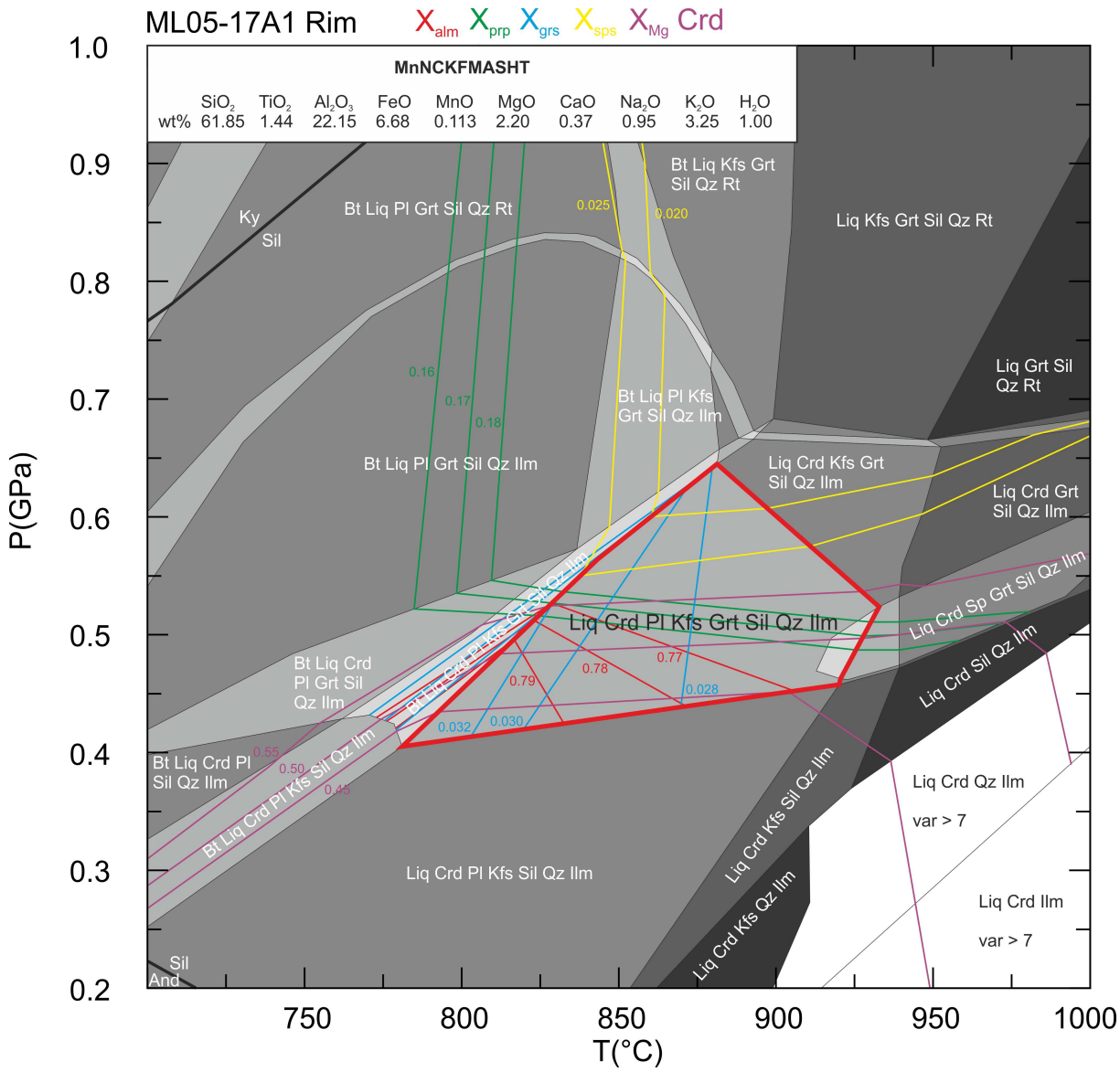

Figure 51: Calculated pseudosection of adapted bulk-rock composition representing the last stage of garnet growth. Isopleth match in a P–T window of 820–870°C and 0.4–0.6 GPa (ML05-17A1).Used bulk composition is in the upper left corner of the diagram.

5.2 Crd-Grt-Bt-Gneiss

Crd-Grt-Bt-gneiss contains relic single-phase garnet grains, lots of biotite some cordierite as well as plagioclase, K-feldspar, quartz, spinel and sillimanite. Isopleths of garnet endmembers as well as X_{Mg} in cordierite and biotite define a field within the observed mineral assemblage and yields conditions of 750–800°C and 0.5–0.6 GPa (Figure 52) which are similar to values obtained with winTWQ version 2.34 (Berman, 1991), Ti in biotite and two-feldspar thermometry.

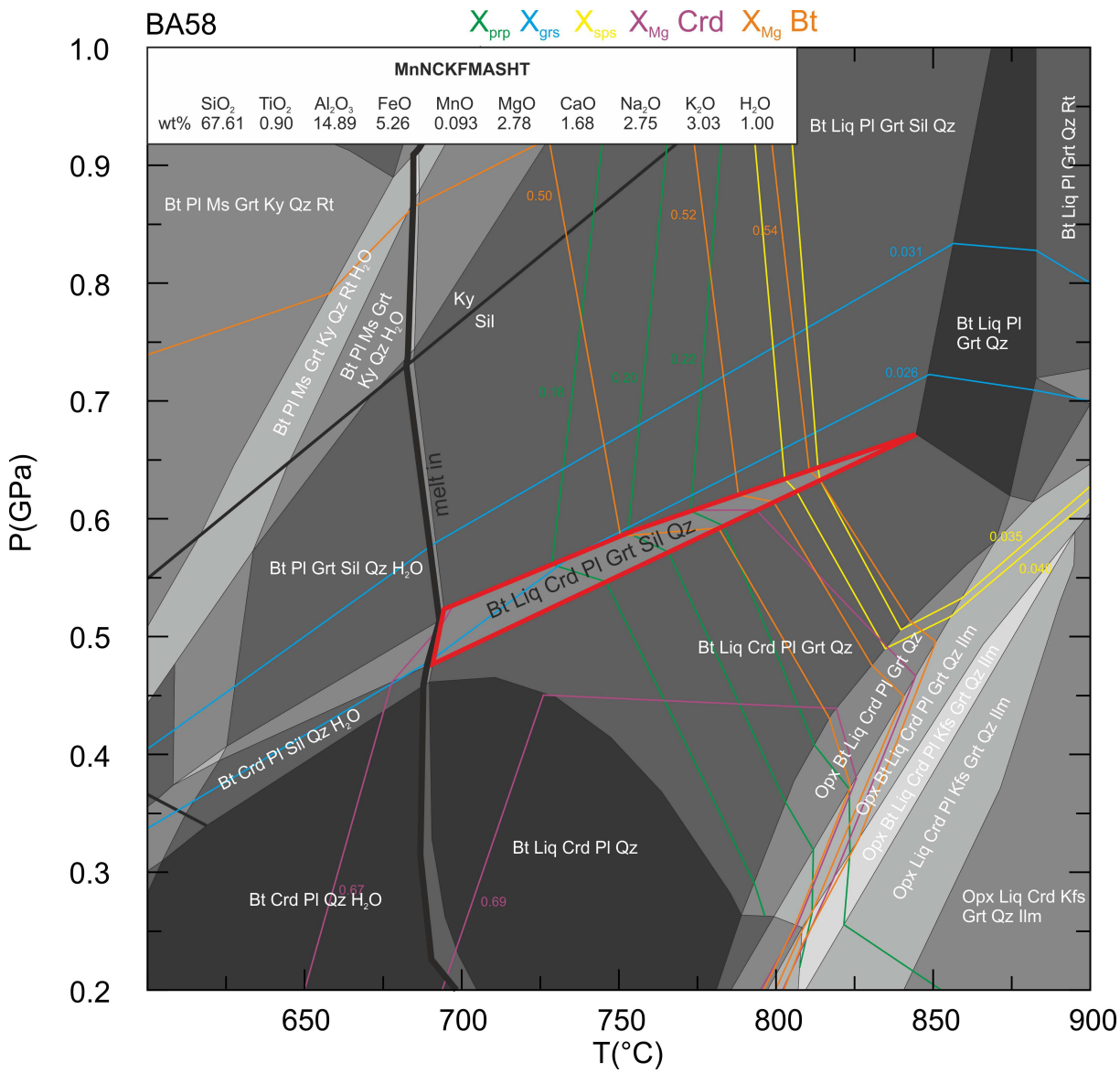

Figure 52: Calculated pseudosection of a Crd-Grt-Bt-gneiss. Isopleth match in a P–T window of 750–800°C and 0.5–0.6 GPa (BA58). Used bulk composition is in the upper left corner of the diagram.

5.3 Opx-Grt-Bt-Gneiss

Opx-Grt-Bt-gneiss contains single phase grown garnet, orthopyroxene, biotite, plagioclase, quartz and ilmenite. Although texturally no evidence is found that garnet and orthopyroxene are in disequilibrium, thermobarometry and calculated stability fields in pseudosections indicate this. Isopleths were calculated for garnet endmembers as well as X_{Mg} in orthopyroxene, but they fall into different *P–T* windows. Orthopyroxene composition shows higher grade conditions of 850–900°C and 0.5–0.8 GPa, garnet displays lower conditions of 650–750°C and 0.5–0.7 GPa (Figure 56). The absence of cordierite defines a minimum pressure above the cordierite stability fields.

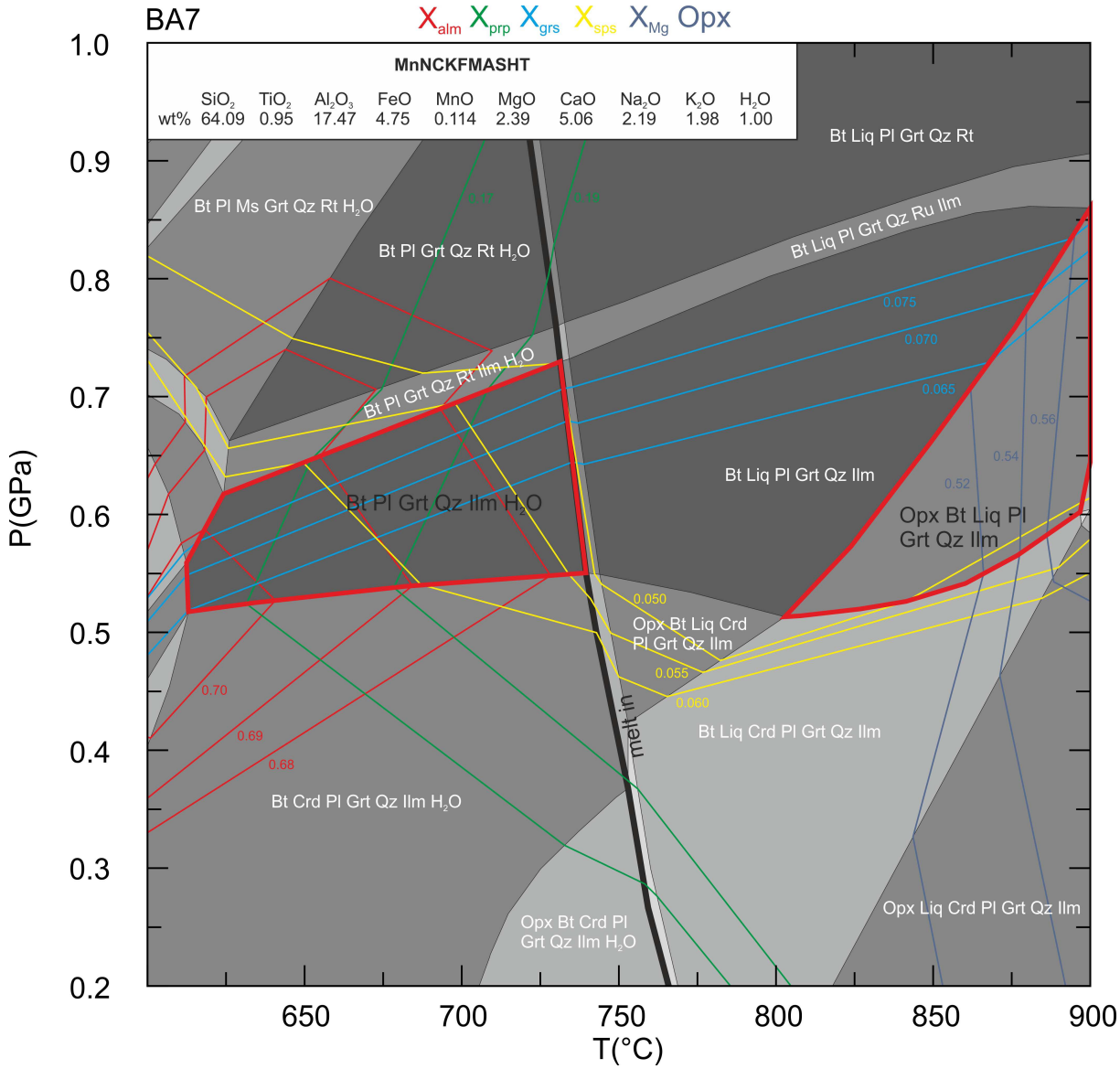

Figure 53: Calculated pseudosection of a Opx-Grt-Bt-gneiss. Garnet isopleth match in a P–T window of 650–750°C and 0.5–0.7 GPa, orthopyroxene leads to higher temperatures of 850–900°C and 0.5–0.8 GPa (BA7). Used bulk composition is in the upper left corner of the diagram.

5.4 Crd-Bt-Migmatite/Anatexite

These samples do not contain any garnet, which complicates a reconstruction of metamorphic conditions. The presence of cordierite and absence of garnet allows to constrain maximum pressure, which has to be below the stability field of garnet. In case of sample DS6 (west of Bad Leonfelden area) (Figure 54) a maximum pressure of 0.45 GPa is obtained. Calculated isopleth of X_{Mg} of cordierite and biotite as well as X_{an} run more or less parallel and show only intersections at very low angles and thus not allowing an accurate intersection point. All of them are found in a field containing the observed mineral assemblage Crd + Bt + Pl + Kfs + Sil + Qz, which indicates conditions of 670–780°C and 0.25–0.45 GPa

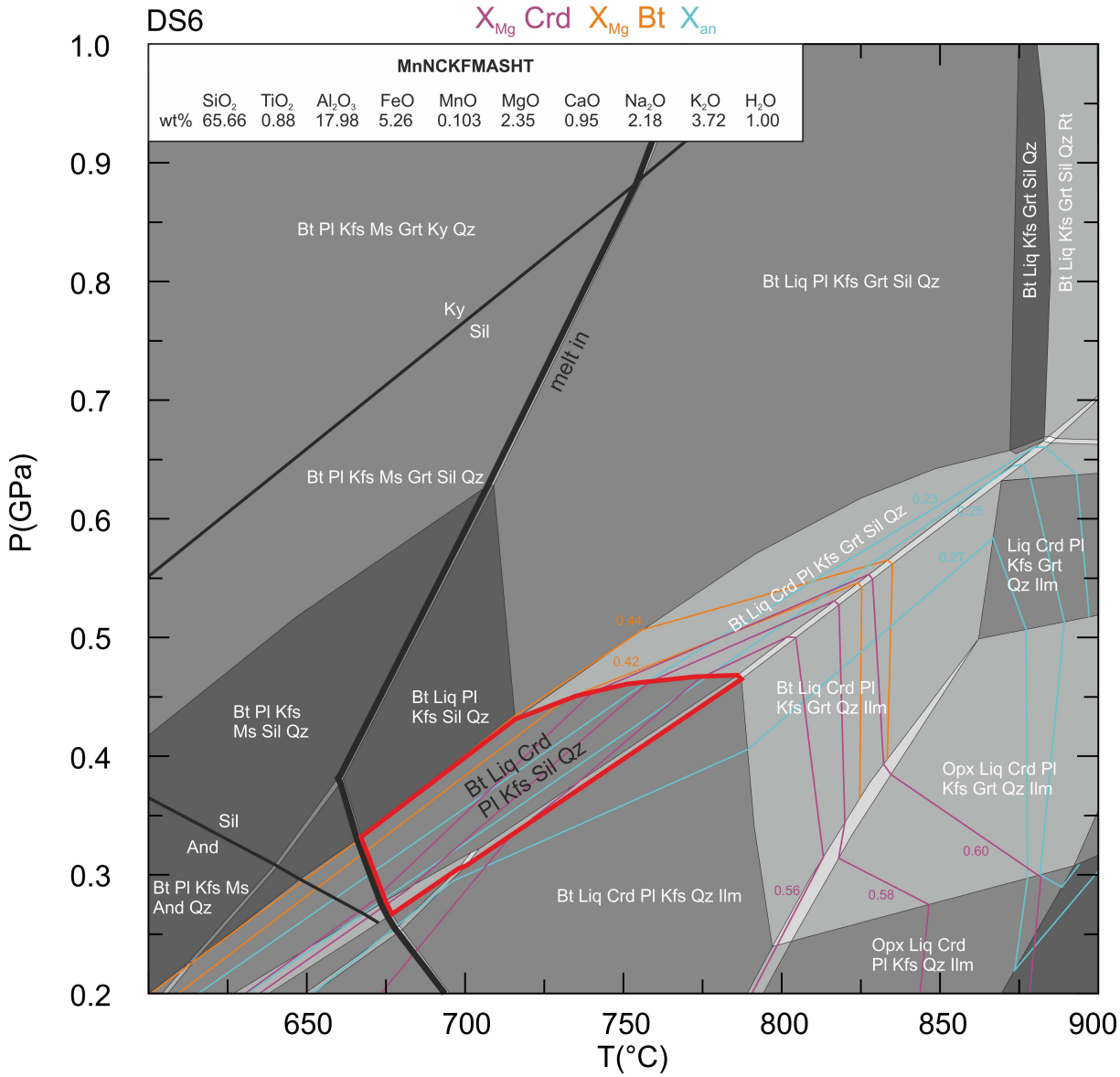

Figure 54: Calculated pseudosection of a Crd-Bt-migmatite/anatexite. Isopleth match in a P–T window of 670–780°C and 0.25–0.45 GPa (DS6). Used bulk composition is in the upper left corner of the diagram.

Sample BA76 from the east of Bad Leonfelden area contains a similar mineral assemblage as DS6. Calculated isopleths of X_{Mg} of cordierite and biotite do not show any intersections, but both are found in a field containing the observed paragenesis Crd + Bt + Pl + Kfs + Sil + Qz (Figure 55). The determined field is within the range of temperatures obtained with Ti in biotite and two feldspar thermometry.

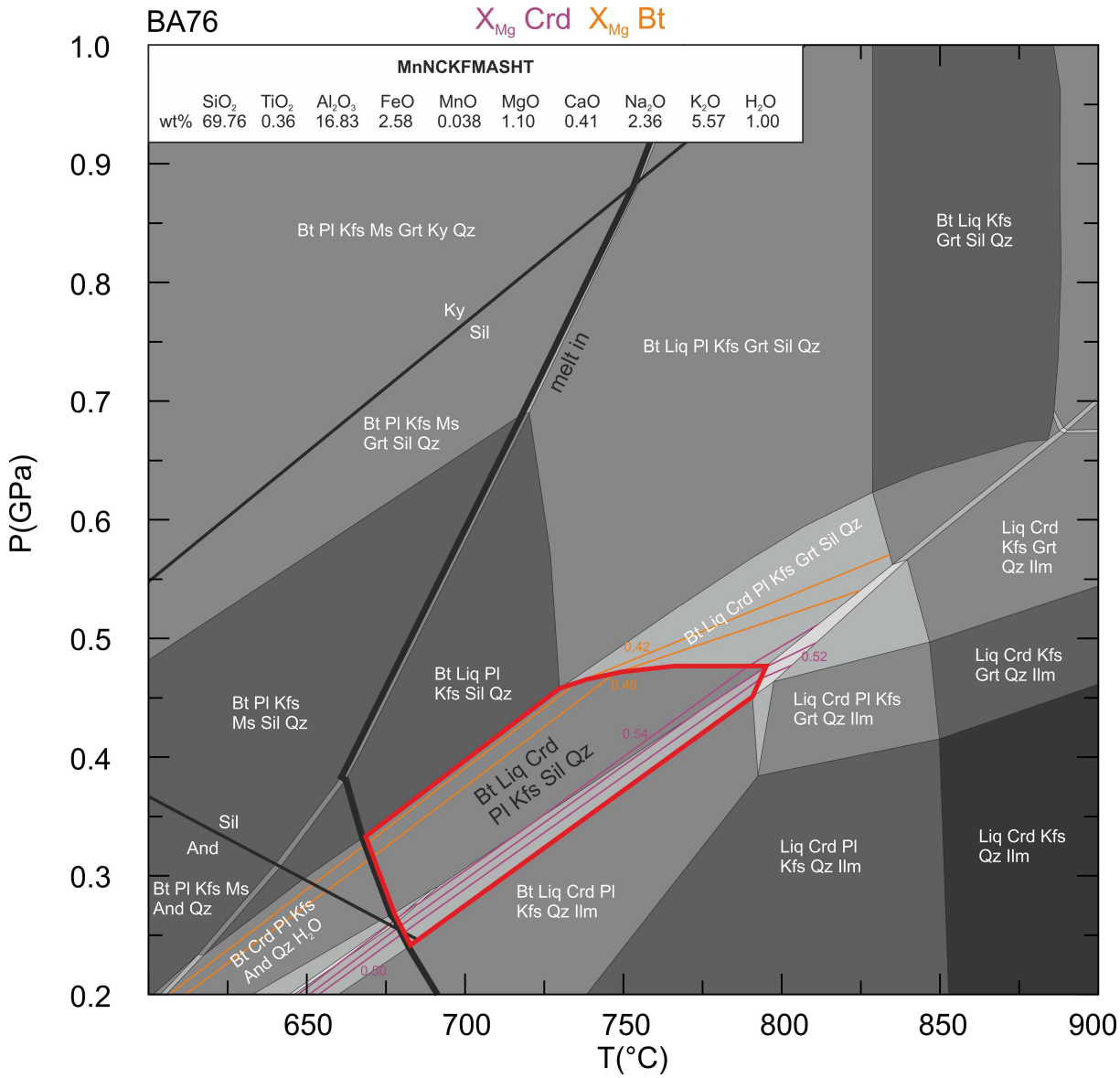

Figure 55: Calculated pseudosection of a Crd-Bt-migmatite/anatexite. Observed mineral assemblage lie within a P–T window of 670–790°C and 0.25–0.45 GPa (BA76). Used bulk composition is in the upper left corner of the diagram.

A calculated pseudosection of sample DS5 (in the north-east of Lichtenberg area) shows similar phase relations (Figure 56). Remnants of cordierite are present but cannot be analysed and thus no chemical parameters for mineral isopleths are available. Composition of biotite falls into a field with the observed mineral assemblage Crd + Bt + Pl + Kfs + Sil + Qz, which indicates conditions of 670–770°C and 0.25–0.45 GPa.

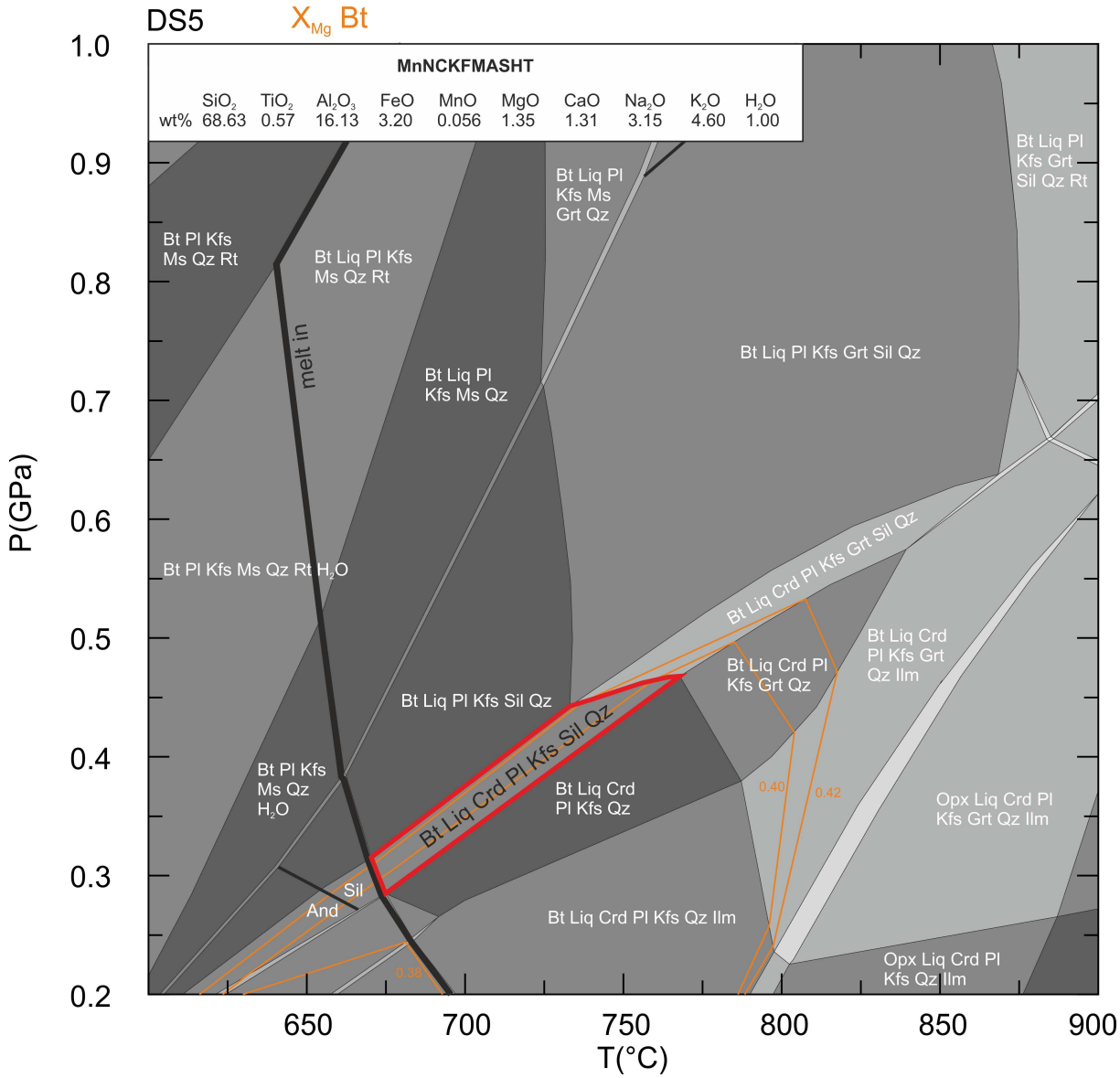

Figure 56: Calculated pseudosection of a Crd-Bt-migmatite/anatexite. Observed mineral assemblage lie within a P–T window of 670–770°C and 0.25–0.45 GPa (DS5). Used bulk composition is in the upper left corner of the diagram.

6 Discussion and Interpretation

The investigated low-pressure granulite facies rocks from the Danube valley (1), the Lichtenberg area (2), the Bad Leonfelden area (3) and the Sauwald area (4) represent characteristic migmatitic paragneisses of the Bavarian Unit, part of the Moldanubian Superunit with a late Variscan (post 330 Ma) LP–HT overprint (Gerdes et al. 2006). Garnet + cordierite + sillimanite bearing granulite samples were used for multiequilibrium geothermobarometry using winTWQ version 2.34 (Berman, 1991). Two-feldspar thermometry (Benisek et al., 2004) was applied on several samples containing plagioclase and K-feldspar. Titanium in biotite thermometry (Henry et al., 2005) was used primary for garnet free samples. Furthermore several samples were used to calculate pseudosections for better constraining metamorphic conditions and metamorphic history.

P–T of the Danube valley and Southern Lichtenberg area

Al-rich migmatite/restite samples found along the Danube Valley, represent the metamorphic peak assemblage garnet + cordierite + spinel + sillimanite + K-feldspar + quartz. Calculations of metamorphic peak conditions yield 830–910°C and 0.60–0.66 GPa (42) which is similar to conditions obtained in the Bavarian Forest (850°C and 0.50–0.70 GPa) by Kalt et al. (1999) and slightly higher compared to peak conditions obtained in the Sauwald zone (750–840°C and 0.29–0.53 GPa) by Tropper et al. (2006). Large garnets in some samples show chemical zoning with calcium-rich inner cores (core 1), calcium-poorer outer cores (core 2) and intermediate calcium rims. Thermobarometric calculations combined with pseudosections determined 740–825°C and 1.1–1.3 GPa for the inner core and 580–610°C and 0.44–0.54 GPa for the outer core (42).

Table 42: Geothermobarometric calculations of Al-rich migmatite/restite samples.

Sample	Region	Method	T ± σ (°C)	P ± σ (GPa)
MA1	Danube Valley	winTWQ	827 ± 28	0.60 ± 0.03
ML05-16	Danube Valley	winTWQ	913 ± 40	0.66 ± 0.03
ML05-17A Rim	Danube Valley	winTWQ	892 ± 10	0.64 ± 0.01
ML05-17A1 Rim	Danube Valley	winTWQ	910 ± 5	0.66 ± 0.02
ML05-17A1 Rim	Danube Valley	two-fsp thermometry	906 ± 19	-
ML05-17A Core1	Danube Valley	winTWQ	740	-
ML05-17A1 Core1	Danube Valley	winTWQ	780	-
ML05-17A Core2	Danube Valley	winTWQ	607	0.54
ML05-17A1 Core2	Danube Valley	winTWQ	582	0.44

Grt-Crd-Bt-gneiss is mainly found in the southern part of the Lichtenberg area and contains high amounts of biotite, some cordierite and small relic garnet as well as plagioclase, K-feldspar, quartz, spinel and sillimanite. Garnet in most cases is surrounded by cordierite and most likely consumed by the reaction:

$$Grt + Sil + Qz = Crd \qquad (1)$$

Metamorphic conditions were obtained with winTWQ version 2.34 (Berman, 1991), Ti in biotite thermometry (Henry et al., 2005) and two-feldspar thermometry (Benisek et al., 2004) and yielded results of 700–800°C and 0.4–0.6 GPa with different methods (43), which are similar to conditions determined with calculated pseudosections.

Table 43: Geothermobarometric calculations of Grt-Crd-Bt-gneiss samples.

Sample	Region	Method	T ± σ (°C)	P ± σ (GPa)
BA58	Lichtenberg area	winTWQ	755 ± 52	0.58 ± 0.04
BA58	Lichtenberg area	two-fsp thermometry	753 ± 21	-
BA58	Lichtenberg area	Ti in biotite thermometry	702 ± 10	-
DS35	Lichtenberg area	two-fsp thermometry	738 ± 22	-
DS35	Lichtenberg area	Ti in biotite thermometry	666 ± 18	-

The same methods were applied to Grt-Crd-migmatite samples, which occur along the Danube valley as well as in southern parts of the Lichtenberg area. Geotheromobarometric calculations yielded *P–T* values of 650–750°C and 0.5–0.6 GPa, which represent the lowest conditions of garnet bearing samples. Grt-Crd-migmatite samples from the Danube valley and from the southern Lichtenberg area yield similar values (44).

Table 44: Geothermobarometric calculations of Grt-Crd-migmatite samples.

Sample	Region	Method	T ± σ (°C)	P ± σ (GPa)
ML07-1B	Danube Valley	winTWQ	665	0.44
ML07-1B	Danube Valley	two-fsp thermometry	659 ± 22	-
ML07-1B	Danube Valley	Ti in biotite thermometry	694 ± 18	-
DS24	Lichtenberg area	two-fsp thermometry	689 ± 21	-
DS24	Lichtenberg area	Ti in biotite thermometry	684 ± 20	-

P–T of the Northern Lichtenberg, Bad Leonfelden and Sauwald area

Crd-Bt-migmatite/anatexite is a common rock type occurring all over the investigated area while the above mentioned types only occur in the south along the Danube valley and the southern Lichtenberg area. Samples vary in their chemical composition but have generally a similar mineral assemblage of Crd + Bt + Pl + Kfs + Sil + Qz. Temperature conditions were determined with Ti in biotite thermometry (Henry et al., 2005) and two-feldspar thermometry (Benisek et al., 2004) from samples containing plagioclase and K-feldspar. Obtained temperatures from different regions range from 650–720°C (45). Pressure could only be estimated from calculated pseudosections which is 0.25–0.45 GPa.

Table 45: Geothermobarometric calculations of Crd-Bt-migmatite/anatexite samples.

Sample	Region	Method	T ± σ (°C)	P ± σ (GPa)
BA62	Lichtenberg area	Ti in biotite thermometry	672 ± 29	-
DS5	Lichtenberg area	Ti in biotite thermometry	684	-
BA76	Bad Leonfelden area	two-fsp thermometry	681 ± 37	-
BA76	Bad Leonfelden area	Ti in biotite thermometry	647 ± 22	-
DS6	Bad Leonfelden area	two-fsp thermometry	695 ± 23	-
DS6	Bad Leonfelden area	Ti in biotite thermometry	672 ± 16	-
DS66	Bad Leonfelden area	two-fsp thermometry	653 ± 16	-
DS66	Bad Leonfelden area	Ti in biotite thermometry	702 ± 23	-
DS8	Bad Leonfelden area	Ti in biotite thermometry	685 ± 16	-
BA31	Sauwald area	Ti in biotite thermometry	723 ± 12	-

Regional distribution of *P–T* estimates

Determined conditions of samples from several locations were used to prepare a regional distribution map of P and T (Figure 57). Highest grade metamorphism (830–910°C and 0.60–0.66 GPa) was obtained in the Danube valley, south of the river Danube. In the southern part of the Lichtenberg area garnet is common, but becomes rare to the north. Calculated metamorphic conditions decline towards the north as well. Approximately close to the small town Lichtenberg the northernmost garnet bearing samples were observed. In the northern part of the investigated area, east and west of the Rodl Fault outcrops are scarce. Investigated Crd-Bt-migmatite/anatexite samples of this sector show similar conditions of 650–700°C and 0.25–0.45 GPa. Conspicuous is the decreasing temperature and pressure gradient from the Danube valley in the south to the northern parts of the Lichtenberg and Bad Leonfelden area. Samples investigated in the Sauwald area gave *P–T* conditions of 720°C which are slightly lower (750–840°C and 0.29–0.53 GPa) than reported by Tropper et al. (2006).

Polymetamorphic history from large garnet porphyroblasts

Large garnet porphyroblasts in Al-rich migmatite/restite samples have preserved polymetamorphic history. Chemical zoning, especially seen in the grossular component, allows the reconstruction of a possible *P–T* path. Figure 58 shows a calculated pseudosection with marked *P–T* windows of the inner core (C1), the outer core (C2) and the rim (R) of these zoned garnets. The coloured lines represent vol% of garnet which were used to demonstrate that garnet growth occurred during the inferred *P–T* path which is a prerequisite for validating the proposed *P–T* path. The inner core (C1) has grown during prograde HP–HT (750–825°C and 1.1–1.3 GPa) metamorphism, temperature was estimated by garnet–spinel Fe/Mg exchange thermometer using composition if spinel inclusions in garnet cores. While pressure conditions could only be estimated with calculated isopleths of garnet core (C1) composition. Between the stages C1 and C2 garnet may have been slightly resorbed due to predicted garnet consumption during decompression and cooling, but may have also been metastable preserved. No textural nor chemical evidence is observed in samples. The growth of C2 has started with increasing temperatures, after cooling and decompression to 580–610°C and 0.44–0.54 GPa. Above 800°C the rate of growth increases and the rim (R) zone has grown up to the calculated LP–HT peak conditions of 830–910°C and 0.60–0.66 GPa.

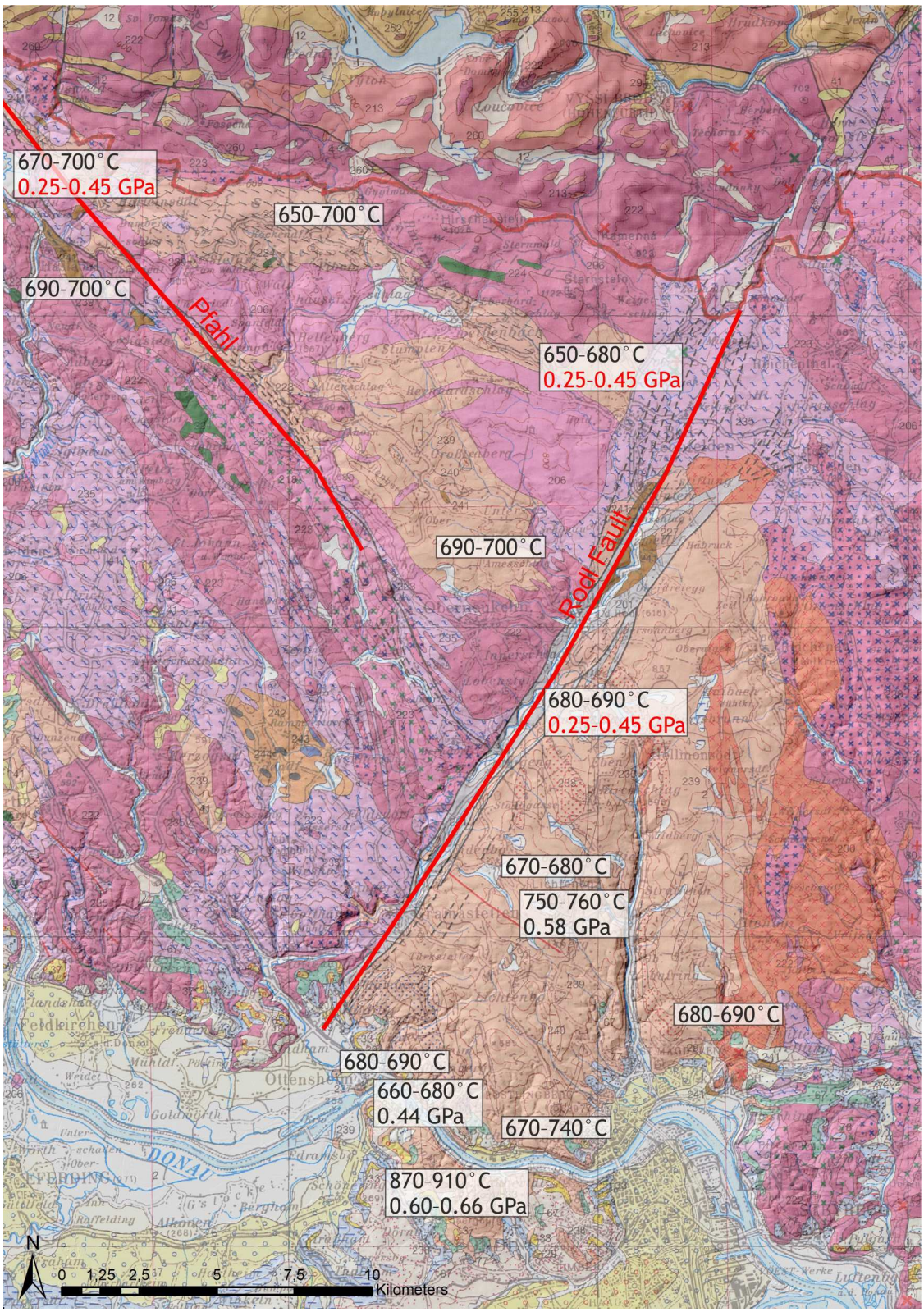

Figure 57: Regional P–T distribution map showing the highest grade metamorphic conditions in the south and a gradient of decreasing conditions towards the north. Red pressure values are only estimated from pseudosections and not calculated. Modified after Geological Map of Upper Austria 1:200000 (Geological Survey of Austria, 2006)

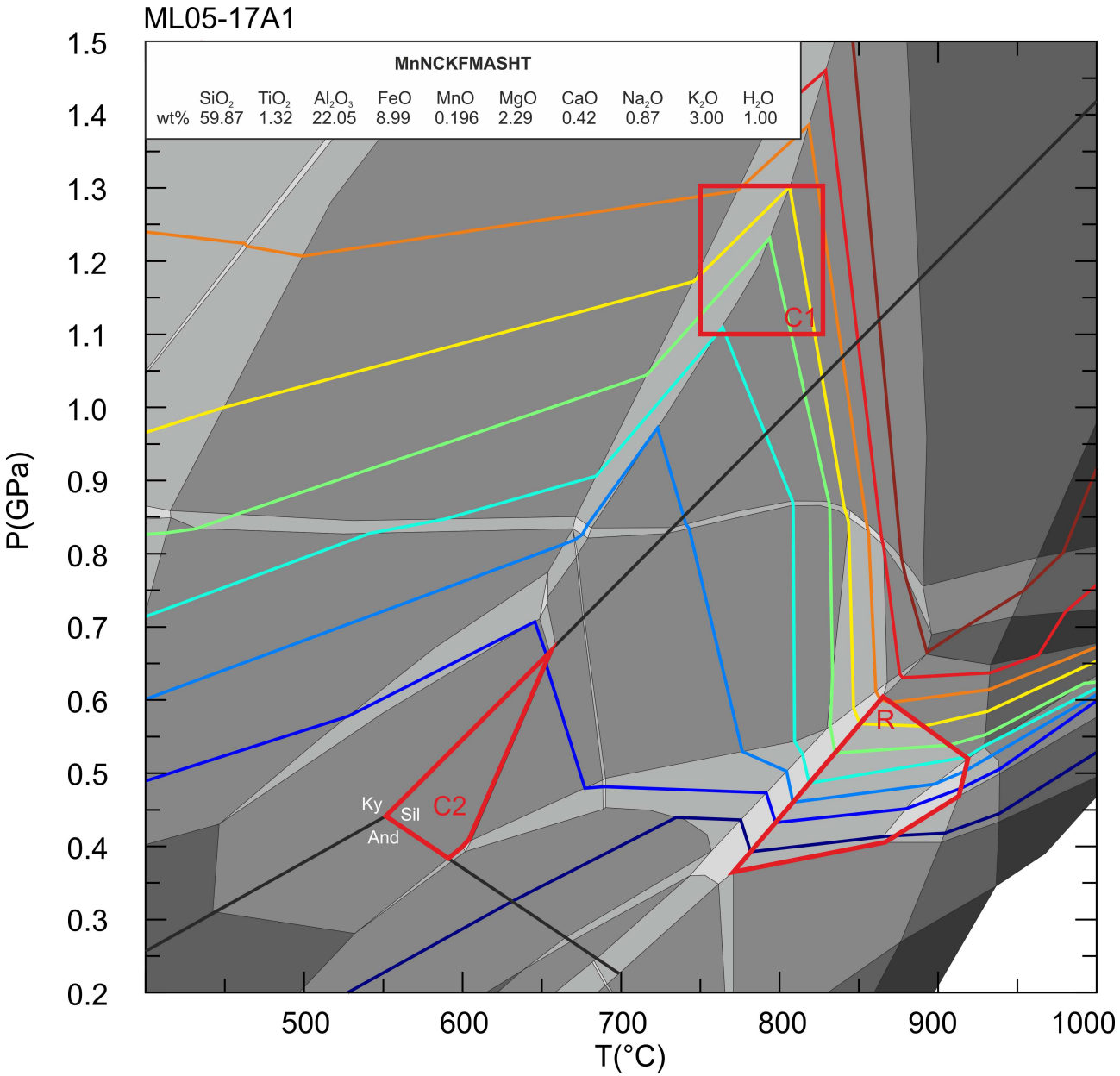

Figure 58: Pseudosection calculated to show the three stages of garnet growth in Al-rich migmatite/restite garnet porphyroblasts.C1 representing the HP–HT innermost core, C2 the outer core and R the LP–HT rim zone.

Pseudosections used in addition with geothermobarometric calculations allows the reconstruction of a possible *P–T* path (Figure 59) for the southern part of the investigated area. A first HP–HT stage at conditions of 750–825°C and 1.1–1.3 GPa was followed by exhumation, decompression and cooling to conditions of 580–610°C and 0.44–0.54 GPa. Late Variscan reheating which is postulated to be the result of mantle delamination and asthenospheric upwelling (Henk et al., 2000) increased temperatures considerably at near constant pressures which lead to the LP–HT overprint and widespread melting of a mid-crustal segment, now seen as migmatites, anatexites and even granitoids in the Bavarian unit.

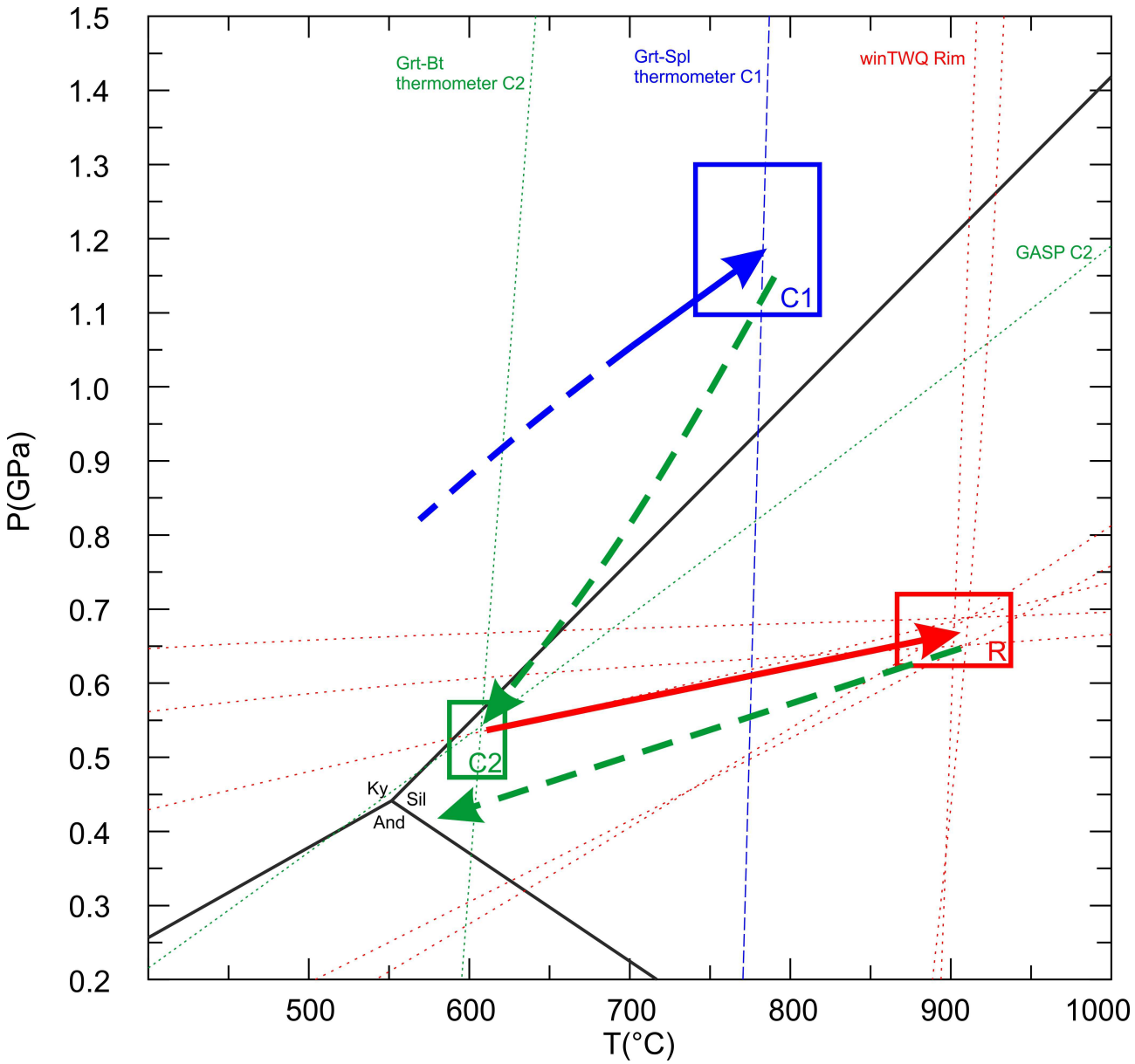

Figure 59: Possible P–T path of rocks from the Danube valley. A first HP–HT stage (740–825°C and 1.1–1.3 GPa) and a subsequently exhumation stage (580–610°C and 0.44–0.54 GPa) are followed by the well-established LP–HT stage (830–910°C and 0.60–0.66 GPa). Dashed lines are the results of calculations with winTWQ version 2.34 (Berman, 1991) from inner core (blue) (pressure estimated from pseudosection), outer core (green) and rim (red).

From the northern section no *P–T* data were available so far. We made an attempt to determine the grade of metamorphism and to reconstruct a possible *P–T* path (Figure 60). The observed conditions of 650–700°C and 0.25–0.45 GPa represent the LP–HT Bavarian phase, but at significant lower conditions compared to the Danube valley. The *P–T* conditions for this area was estimated by Ti in biotite (Henry et al., 2005) and two-feldspar thermometry (Benisek et al., 2004), pressure was estimated from several calculated pseudosections. Samples do not show any relics indicating that they have been involved in a former high pressure stage. However, since minerals such as garnet, which are able to record earlier phases, are missing, a former metamorphic overprint is possible.

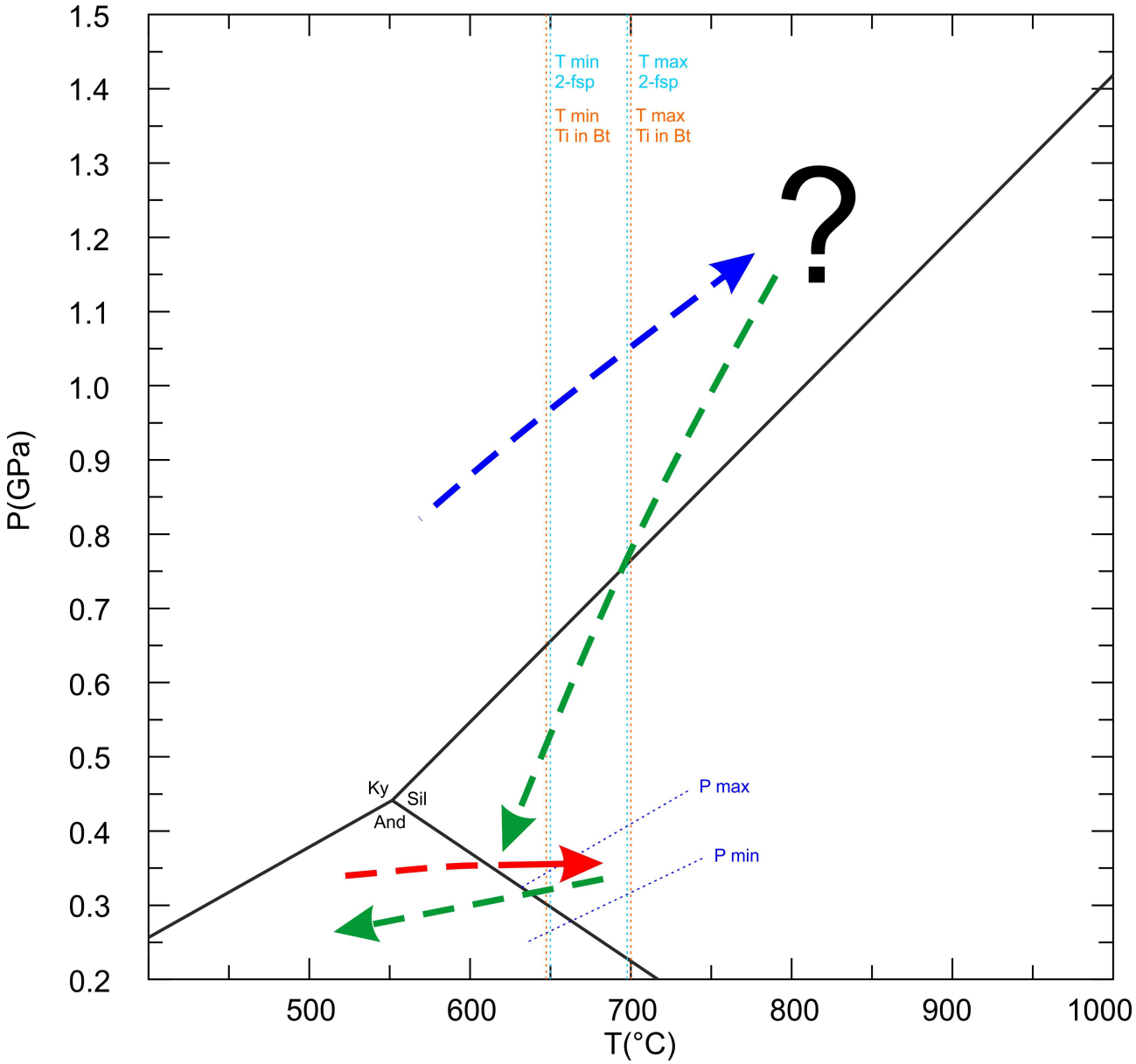

Figure 60: Possible P–T path of rocks from northern Lichtenberg and Bad Leonfelden area. Well established is the last LP–HT stage at conditions of 650–700°C and 0.25–0.45 GPa. Dashed lines are the results of calculations with Ti in biotite (Henry et al., 2005) (orange), two-feldspar thermometry (Benisek et al., 2004) (light blue) and pressure estimated from pseudosection (dark blue). *A former HP–HT stage* could not be documented.

7 Conclusion

The Austrian part of the Bavarian Unit was formed by late Variscan (post 330 Ma, Gerdes et al., 2006) LP–HT overprint triggered by delamination of mantle lithosphere and asthenospheric upwelling (Henk et al., 2000). Most of these rocks underwent high degrees of melting and have formed meta- and diatexites. For this study samples were taken along the (1) Danube valley (west of Linz), from the (2) Lichtenberg area (north of Linz), the (3) Bad Leonfelden area (west of the Rodl Fault) and the (4) Sauwald area (south of the river Danube). After detailed investigation, can conclude the following:

- Al-rich granulite facies migmatite/restite samples from the Danube valley have formed at metamorphic conditions of 830–910°C and 0.60–0.66 GPa, which is slightly lower compared to conditions obtained in the Sauwald area by Tropper et al. (2006). Observed garnet bearing migmatite and gneiss samples from the southern part of the Lichtenberg area reached conditions of 650–800 and 0.4–0.6 GPa. In the northern part of the investigated area (northern Lichtenberg and Bad Leonfelden area) garnet free migmatite/anatexite is the predominant lithology. *P–T* values of 650–720°C and 0.25–0.45 GPa were determined for these rock type. Sauwald area samples were treated only marginally and show a temperature (720°C) slightly lower than obtained by Tropper et al. (2006).

- Geothermobarometric calculations allowed the preparation of a regional distribution map of P and T. A gradient with decreasing conditions from high grade Danube valley samples in the south (830–910°C and 0.60–0.66 GPa) to lower grade migmatite/anatexite samples from Lichtenberg and Bad Leonfelden area in the north (650–700°C and 0.25–0.45 GPa) can be observed.

- Furthermore Al-rich migmatite/restite samples contain large polyphase grown garnet porphyroblasts with distinct chemical zoning in their grossular component, which allows the reconstruction of a 2 stage *P–T* path for the southern region of the investigated area. A first HP–HT stage at conditions of 750–825°C and 1.1–1.3 GPa, was followed by decompression and cooling to conditions of 580–610°C and 0.44–0.54 GPa and a final LP–HT overprint of 830–910°C and 0.60–0.66 GPa.

- Samples from the northern areas show a LP–HT path at lower conditions of 650–720°C

and 0.25–0.45 GPa, a former high pressure overprint is possible but could not be documented.

8 References

Auzanneau E, Schmidt MW, Vielzeuf D, Connolly JAD (2010) Titanium in phengite: A geobarometer for high temperature eclogites: Contributions to Mineralogy and Petrology 159: 1–24

Becker H, Altherr R (1992) Evidence from ultra-high-pressure marbles for recycling of sediments into the mantle. Nature 358: 745–748

Benisek A, Kroll H, Cemič L (2004) New developments in two-feldspar thermometry. American Mineralogist 89: 1496–1504

Benisek A, Dachs E, Kroll H (2010) A ternary feldspar-mixing model based on calorimetric data: development and application. Contributions to Mineralogy and Petrology 160: 327–337

Berman RG (1991) Thermobarometry using multi-equilibrium calculations: a new technique, with petrological applications. Canadian Mineralogist 29: 833–855

Berman RG, Aranovich LY (1996) Optimized standard state and mixing properties of minerals: I. Model calibration for olivine, orthopyroxene, cordierite, garnet, and ilmenite in the system $FeO–MgO–CaO–Al_2O_3–SiO_2–TiO_2$. Contributions to Mineralogy and Petrology 126: 1–24

Carswell DA (1991) Variscan high P–T metamorphism and uplift-history in the Moldanubian Zone of the Bohemian Massif in Lower Austria. European Journal of Mineralogy 3: 323–342

Coggon R, Holland TJB (2002) Mixing properties of phengitic micas and revised garnet phengite thermobarometers: Journal of Metamorphic Geology 20: 683–696

Connolly JAD (2005) Computation of phase equilibria by linear programming: A tool for geodynamic modeling and its application to subduction zone decarbonation: Earth and Planetary Science Letters 236: 524–541

Dachs E (1998) PET: Petrological elementary tools for Mathematica. Computers & Geoscience 24/3: 219–235

Dallmeyer RD, Franke W, Weber K (eds) (1995) Pre-Permian Geology of central and eastern Europe. Springer-Verlag, Berlin, pp 1–593

Evans TP (2004) A method for calculating effective bulk composition modification due to crystal fractionation in garnet-bearing schist: Implications for isopleth thermobarometry. Journal of Metamorphic Geology 22: 547–557

Fiala J, Fuchs G, Wendt JI (1995) Stratigraphy of the Moldanubian Zone. In: Dallmeyer RD, Franke W, Weber K (eds) Pre-Permian Geology of Central and Eastern Europe. Springer-Verlag, Berlin, pp 417–428

Finger F, Gerdes A, Janoušek V, René M, Riegler G (2007) Resolving the Variscan evolution of the Moldanubian sector of the Bohemian Massif: the significance of the Bavarian and the Moravo–Moldanubian tectonometamorphic phases. Journal of Geoscience 52: 9–28

Friedl G (1997) U/Pb Datierungen an Zirkonen und Monaziten aus Gesteinen vom österreichischen Anteil der Böhmischen Masse. Unpublished PhD. thesis, Universität Salzburg, pp 1–242

Fritz H, Neubauer F (1993) Kinematics of crustal stacking and dispersion in the south-eastern Bohemian Massif. Geologische Rundschau 82: 556–565

Gaidies F, Pattison DRM, de Capitani C (2011) Toward a quantitative model of metamorphic nucleation and growth. Contributions to Mineralogy and Petrology 162: 975–993

Ganguly J, Cheng W, Tirone M (1996) Thermodynamics of aluminosilicate garnet solid solution: new experimental data, an optimized model, and thermometric applications. Contributions to Mineralogy and Petrology 126: 137–151

Gerdes A, Finger F, Parrish RR (2006) Southwestward progression of a late-orogenic heat front in the Moldanubian Zone of the Bohemian Massif and formation of the Austro-Bavarian anatexite belt. Geophysical Research Abstract 8: 10698

Grauert B, Hänny R, Soptrajanova G (1974) Geochronology of a polymetamorphic and anatectic gneiss region: the Moldanubicum of the area Lam–Deggendorf, Eastern Bavaria, Germany. Contributions to Mineralogy and Petrology 45: 37–63

Henry DJ, Guidotti CV, Thomson JA (2005) The Ti-saturation surface for low-to-medium pressure metapelitic biotites: Implications for geothermometry and Ti-substitution mechanisms. American Mineralogist 90: 316–328

Henk A, von Blanckenburg F, Finger F, Schaltegger U, Zulauf G (2000) Syn-convergent high temperature metamorphism and magmatism in the Variscides: a discussion of

potential heat sources. In: Franke W, Haak V, Oncken O, Tanner D (eds) Orogenic Processes: Quantification and Modelling in the Variscan Belt. Geological Society, London, Special Publication 179: 387–399

Hensen BJ (1986) Theoretical phase relations involving cordierite and garnet revisited: the influence of oxygene fugacity on the stability of sapphirine and spinel in the system Mg–Fe–Al–Si–O. Contributions to Mineralogy and Petrology 92: 362–367

Holland TJB, Powell R (1998 revised by authors in 2004) An internally consistent thermodynamic data set for phases of petrological interest. Journal of Metamorphic Geology 16: 309–343

Holland TJB, Powell R (1999) Relating formulations of the thermodynamics of mineral solid solutions: Activity modeling of pyroxenes, amphiboles, and micas. American Mineralogist 84: 1–14

Holland TJB, Powell R (2001) Calculation of phase relations involving haplogranitic melts using an internally consistent thermodynamic solid solutions: American Mineralogist 81: 1425–1437

Janoušek V, Farrow CM, Erban V (2006) Interpretation of whole-rock geochemical data in igneous geochemistry: introducing Geochemical Data Toolkit (GCDkit). Journal of Petrology 47: 1255–1259

Kalt A, Berger A, Blümel P (1999): metamorphic evolution of cordierite bearing migmatites from the Bayerische Wald (Variscan belt, Germany). Journal of Petrology 40: 601–627

Kalt A, Corfu F, Wijbrams JR (2000) Time calibration of a P–T path from a Variscan high temperature low-pressure metamorphic complex (Bayerische Wald, Germany), and the detection of inherited monazite. Contributions to Mineralogy and Petrology 138: 143–163

Kotková J, Harley SL, Fišera M (1997) A vestige of very high-pressure (ca. 28 kbar) metamorphism in the Variscan Bohemian Massif, Czech Republic. European Journal of Mineralogy 9: 1017–1033

Linner M, Mandl GW, Rupp C (2011) Geographischer Überblick. Erläuterungen zu Geologische Karte von Oberösterreich 1:200000, pp 9–13

Nichols GT, Berry RF, Green DH (1992) Internally consistent gahnitic spine-cordierite-garnet equilibria in the FMASHZn system: geothermobarometry and applications. Contributions to Mineralogy and Petrology 111: 362–377

O'Brien PJ (2000) The fundamental Variscan problem: high-temperature metamorphism at different depths and high-pressure metamorphism at different temperatures. In: Franke W, Haak V, Oncken O, Tanner D (eds) Orogenic Processes: Quantification and Modelling in the Variscan Belt. Geological Society, London, Special Publication 179: 369–386

Petrakakis K (1997) Evolution of Moldanubian rocks in Austria: review and synthesis. Jornal of Metamorphic Geology 15: 203–222

Propach G, Baumann A, Schultz-Schmalschläger M, Grauert B (2000) Zircon and monazite U-Pb ages of Variscan granitoid rocks and gneisses in the Moldanubian Zone of eastern Bavaria, Germany. Neues Jahrbuch fur Geologie und Paläontologie-Monatshefte 6: 345–377

Schulmann K (1990) Fabric and kinematic study of the Bíteš orthogneiss (southwestern Moravia) – result of largescale northeastward shearing parallel to the Moldanubian boundary. Tectonophysics 177: 229–244

Schulmann K, Ledru P, Autran A, Melka R, Lardeaux JM, Urban M, Lobkowicz M (1991) Evolution of nappes in the eastern margin of the Bohemian Massif: a kinematic interpretation. Geologische Rundschau 80: 73–92

Schulmann K, Kröner A, Hegner E, Wendt I, Konopásek J, Lexa O, Štípská P (2005) Chronological constraints on the pre-orogenic history, burial and exhumation of deep-seated rocks along the eastern margin of the Variscan Orogen, Bohemian Massif, Czech Republic. American Journal Science 305: 407–448

Shulters JC, Bohlen SR (1989) The stability of hercynite and hercynite-gahnite spinels in corundum- or quartz-bearing assemblages. Journal of Petrology 30: 1017–1031

Spear FS, Daniel CG (1998) Three-dimensional imaging of garnet porphyroblast sizes and chemical zoning: nucleation and growth history in the garnet zone. Geological Material Research 1: 1–44

Suess FE (1926) Intrusionstektonik und Wandertektonik im variszischen Grundgebirge. Bornträger, Berlin, pp 1–156

Tajčmanová L, Konopásek J (2003) The Role of zinc in stabilization of spinel-bearing mineral assemblages – examples from the Bohemian Massif and NW Namibia. Geolines 16: 102–103

Tajčmanová L, Connolly JAD, Cesare B, (2009) A thermodynamic model for titanium and ferric iron solution in biotite: Journal of Metamorphic Geology 27: 153–164

Tropper P, Deibl I, Finger F, Kaindl R (2006) P–T–t evolution of spinel-cordierite-garnet gneisses from the Sauwald Zone (Southern Bohemian Massif, Upper Austria): is there evidence for two independent late-Variscan low-P/high-T events in the Moldanubian Unit? International Journal of Earth Sciences 95: 1019–1037

Vrána S, Frýda J (2003) Ultrahigh-pressure grossular-rich garnetite from the Moldanubian Zone, Czech Republic. European Journal of Mineralogy 15: 43–54

White RW, Powell R, Holland TJB (2001) Calculation of partial melting equilibria in the system Na2O–CaO–K2O–FeO–MgO–Al2O3–SiO2–H2O (NCKFMASH): Journal of Metamorphic Geology 19: 139–153

Whitney DL, Evans BW (2010) Abbreviations for names of rock-forming minerals. American Mineralogist 95: 185–187

Programms:

Paralyzer (version 1.5, downloaded from the website http://www.metamorphism.geos.vt.edu /Paralyzer_files/paralyzer_version.html)

PyWerami (version 2.0.1, downloaded from the website http://petrol.natur.cuni.cz/~ondro/ pywerami:home)

Maps:

Geological map of Upper Austria 1:200000, Geological Survey of Austria (GBA) 2006

Cartographic model 1:500000, Geological Survey of Austria (GBA) 2013

OpenStreetMap, © OpenStreetMap contributors (openstreetmap.org)